

Graphical Structures for Design and Verification of Quantum Error Correction

Nicholas Chancellor¹, Aleks Kissinger², Stefan Zohren³, Joschka Roffe¹, and Dominic Horsman¹

¹Department of Physics, Durham University, UK

²Radboud University, Nijmegen, Netherlands

³Department of Materials, University of Oxford, UK

January 15, 2018

Abstract We introduce a high-level graphical framework for the design, analysis, and verification of quantum error correcting codes. The coherent parity check construction for stabilizer codes allows us to construct a broad range of quantum codes based on classical codes, and gives a framework in which large classes of such codes can be both analytically and numerically discovered. Using graphical tools based on the ZX calculus, we explicitly construct small distance 3 and 5 codes with high code rates using this framework. We also show how this framework can be used to represent CSS codes and conversely how to compute stabilisers for a CPC code. We give a construction turns (almost) any pair of classical $[n, k, 3]$ codes into a $[[2n - k + 2, k, 3]]$ CPC code, and give a straightforward technique for machine search which yields thousands of potential codes, and demonstrate its operation for distance 3 and 5 codes. Finally we use the graphical tools we introduce to demonstrate how Clifford computation can be performed within CPC codes.

Nicholas Chancellor: nicholas.chancellor@gmail.com

Aleks Kissinger: aleks@cs.ru.nl

Stefan Zohren: stefan.zohren@materials.ox.ac.uk

Joschka Roffe: joshua.roffe@durham.ac.uk

Dominic Horsman: dom.horsman@gmail.com

Contents

1	Introduction	3
2	Background: quantum and classical error correction	4
3	Background: the ZX-calculus	6
4	Operation of a coherent parity check	8
4.1	The coherent parity check	8
4.2	Coherent parity checking in the ZX calculus	10
4.3	Error propagation through a CPC	11
4.4	Stabilizers and the CPC operation	12
4.5	Continuous CPC operation	13
4.6	A first CPC code: detecting and correcting one type of error	13
5	Single-error correcting CPC codes	15
5.1	Bit- and phase- parity checks	15
5.2	Box-code representation in the ZX calculus	17
5.3	A full ring code	21
5.4	Finding the cross-check matrix C	23
5.4.1	Cross-checks for the ring code	23
5.4.2	Cross checks for distance 3 codes Hamming codes	24
5.4.3	Cross check matrices for general distance 3 codes	27
5.5	Numerical test of the [[11,3,3]] code	28
6	Tripartite CPC codes	29
6.1	Stabilizers and logical operators	29
6.2	CPC construction for CSS codes	32
6.3	CPC codes and fault tolerance	33
7	Generalised CPC codes	34
7.1	Combined parity checking	34
7.2	Automated design and search	36
7.2.1	Matrix representation of errors	36
7.2.2	Matrix representation for syndrome extraction	36
7.2.3	Small codes from random search	37
7.3	Stabilizers for generalised codes	37
8	Encoded computation	39
8.1	Modifying the encoder	39
8.2	Error propagation through the decoder or stabilizer measurement	43
9	Outlook and conclusions	44
A	Fidelity analysis of an elementary three-qubit CPC gadget	47
B	Verification and analysis of the ring code	47
B.1	Verification	48
B.2	Fidelity analysis	49
B.3	Numerical performance of the code in ion traps	50
C	Source code for finding distance 3 CPC codes	51
D	Source code for finding arbitrary distance CPC codes	53

E Source code for converting CPC matrices to stabilizer tables	54
F Additional Codes	55
F.1 Numerically discovered codes	55
F.2 Other codes	57
G Encoded CNOT with Quantomatic	58
References	60

1 Introduction

Quantum computers of an appreciable size that run for any significant amount of time will need to be error corrected [6, 12]. Quantum error correction expands the Hilbert space in which logical qubits live by adding more physical resources to make a larger, typically entangled state. The additional degrees of freedom are used to detect and correct errors, without disturbing the logical information held non-locally in the larger state.

One leading form of error correction includes topological codes such as the surface code [19]. A logical qubit is distributed over a large number of physical qubits. Each block contains a single logical qubit, and higher error tolerances are obtained by expanding the size of the block. These codes are well-studied, conceptually straightforward, flexible, and have high thresholds (the maximum error rate of the underlying components that can be tolerated – for surface codes, around 1% [42]). Such codes are powerful, but need too many physical qubits to support a single logical qubit to make them viable for the first generation of quantum computers currently being developed.

On the other hand, using Calderbank-Shor-Steane (CSS) codes [5, 41] or extensions thereof, it is possible to obtain much higher code densities by encoding many logical qubits in a single code block. However, this added efficiency comes at the expense of losing the high-level structure which makes topological codes so appealing, such as localised stabiliser measurements, efficient decoding algorithms, and the ability to implement fault-tolerant computations via topolgical manipulations [4, 11, 20, 24].

Finding the best code for a given hardware device, which is also easy to work with conceptually (as the topological codes are) but efficient in terms of qubit resources (as many CSS codes are) is a hard problem. What is needed is a high-level language for stabiliser codes that enables them to be constructed intuitively and easily. With a flexible construction, codes can be tailored to the needs of different devices, enabling e.g. automated search for codes that are implementable with certain constraints on qubit connectivity.

The *coherent parity check* (CPC) construction gives a new way of interpreting classical error correcting codes as quantum codes. Rather than re-interpreting classical parity checks as stabiliser measurements (as in e.g. CSS codes), they are interpreted as a direct description of the encoder (or equivalently, decoder) circuit. For our first family of codes, called *tripartite CPC codes*, we do this by making an explicit partition into data, bit-check, and phase-check qubits. Then, a pair of classical error correcting codes are used to determine how the bit- and phase-check qubits interact with the data qubits, respectively. The classical codes can be arbitrary, and need not, for example, yield commuting stabilisers. There is a price to pay for this extra flexibility: such an encoder may yield a quantum code with a lower code distance than its classical constituents. To correct this, a third, *cross-check* matrix is employed to enable bit- and phase-check qubits to ‘check each other’ for otherwise undetectable errors.

In this paper we present a graphical toolkit for constructing and reasoning about CPC codes, based on the *zx-calculus*. This tensor-network-based language originated as a means of studying the interaction of complementary observables [8], but also gives a very powerful tool for representing and transforming circuits [9]. For example, it has been shown that any two Clifford circuits describe the same unitary if and only they can be transformed into each other using the four core rules of the zx-calculus [1, 9]. Recently by considering extensions to the calculus, this has been extended to Clifford+T circuits [16] and an exact-universal family of circuits [34].

We will show how the zx-calculus enables a visual representation of CPC codes and, through re-writing, the generation error syndrome and stabilizer tables. This present paper aims to be accessible to researchers in both quantum error correction and quantum diagrammatic languages, introducing the core concepts of both. We hope this will encourage the further fruitful expansion of the dialogue between error correction and the zx-calculus, initiated by, e.g. [10, 13, 14, 23].

An alternative exposition of CPC codes, using standard circuit notation, is given in [39]. That paper also shows how CPC codes can be adapted to specific hardware, including a full run of a $[[4, 2, 2]]$ CPC detection code on the

IBM Q device.

In this paper, after giving an explicit construction of an $[[11,3,3]]$ tripartite CPC code in section 5, we give two more general constructions for distance-3 codes: one that turns any $[n, k, 3]$ Hamming code into a $[[2n-k+1, k-1, 3]]$ code, and another that turns almost any pair of $[n, k, d \geq 3]$ codes into a $[[2n-k+2, k, 3]]$ code, subject to the relatively minor restriction that the codes must not have a ‘global’ parity check. That is, they admit a standard-form generator matrix $[\mathbb{1}|A]$ where A does not contain a row of all 1’s.

We show in section 6 any CSS code can be represented as a tripartite CPC code and show conversely how to compute logical operators and stabilisers for tripartite CPC codes. In section 7, we generalise tripartite codes to *mixed CPC codes*, which enable qubits to act as mixed bit- and phase- parity checks. This in turn allows for encoding and numerical search for both cross-check matrices and optimisation of codes. By search we are able to find many thousands of small quantum codes. Optimising over parameters such as circuit depth then enables us to find codes optimised to potential devices. These include a structurally straightforward $[[11,3,3]]$ code, a more compressed $[[10,3,3]]$ code, and a dense $[[9,4,3]]$ code. We have also used machine search to identify distance-5 codes, giving explicit check matrices for $[[16,4,5]]$ and $[[18,4,5]]$ codes. For codes of this size the optimization is relatively computationally easy; for example, using a simple search program of < 100 lines on a single core of a desktop machine we can generate around 2500 $[[9,4,3]]$ codes in ten minutes.

We conclude by describing initial investigations into performing computation as well as memory tasks in these codes. As many logical data qubits are located on the same space of physical qubits, operations between them can be performed within the code block by altering the exact configuration of the encoder. The ZX graphical tools enable the configuration of the modified encoder to be found easily for Clifford-group gates, using the automated diagram re-writing tool Quantomatic [28].

2 Background: quantum and classical error correction

The job of error correction is to detect that an error has occurred, pinpoint which data carriers have become errored, and correct the error back to the original state. In general this is done using probabilistic inference: measurements on the data give the most likely error, which is then corrected for. Error correction protocols expand the number of data carriers, with the extra degrees of freedom used to perform the error correction. Exactly how a message (or a computation) is re-written into the larger space defines the particular *error correction code*.

Classical high-performance codes work on a straightforward basis. The simplest situation is a message string of n bits communicated over a channel. Errors are considered as changes to bit values: a 0 can flip to a 1, and *vice versa*. To detect if this has occurred, different bit values in the string are compared to each other at the start of the communication. These measurements are then communicated along with the string, and the comparisons performed again. If there are changes, then a bit value has changed during transit. With suitable choice of which bit-value comparisons are sent, the position of the error can be found.

Quantum error correction differs from classical error correction in two important respects. First, quantum data (qubits) can suffer more than one form of error. Even on the simplest error model, both bit- and phase- values of a qubit can flip during transit: $|0\rangle \leftrightarrow |1\rangle$ and $(\alpha|0\rangle + \beta|1\rangle) \leftrightarrow (\alpha|0\rangle - \beta|1\rangle)$. Secondly, measurement of qubits, unlike bits, generally disturbs the system, with the state after measurement being an eigenstate of the measurement operator rather than the original state. To compensate for this, the most typical method of quantum error correction expands the qubit space so that the only operators that are measured are so-called “stabilizers”: the expanded state is a joint eigenstate of these operators, and therefore measuring them will not disturb the state. The particular stabilizer subspaces of the expanded state give the quantum error correction code.

The difference can be seen most straightforwardly in basic three-system examples. In the classical case, consider the fundamental parity check of figure 1. A and B are the ‘data’ bits, and P is a parity checking bit. At the beginning of the protocol, the joint bit-parity of A, B is measured and stored in P : $[[P(0)]] = [[A(0)]] \oplus [[B(0)]]$. After a time in which errors can occur, the procedure is repeated: $[[P(t)]] = [[A(0)]] \oplus [[B(0)]] \oplus [[A(t)]] \oplus [[B(t)]]$. If there were no errors then $[[P(t)]] = 0$. An outcome 1 shows that an error has occurred (but not, at this stage, where).

Now we consider the quantum case, figure 2. A single data qubit $|A\rangle = a|0\rangle + b|1\rangle$ is supplemented with two ‘code’ qubits P, Q initialised in the state $|0\rangle$. The three are entangled using the encoder given, creating the three-qubit state $a|000\rangle + b|111\rangle$. The state is now in an eigenstate of the two Pauli operators $S_1 = Z_A \otimes Z_P$ and $S_2 = Z_A \otimes Z_Q$. These can therefore be measured without disturbing the data encoded in the state. If at a subsequent point the operators are measured and found not to return the value +1 then an error has occurred.

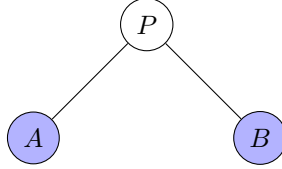


Figure 1: A classical three-bit error detection code: two bits of data, A and B , have their mutual parity encoded into the bit-value of P .

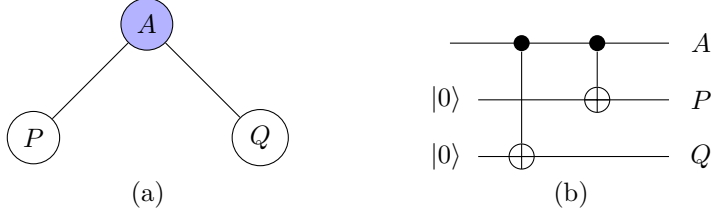


Figure 2: Quantum three-qubit code: (a) A single qubit of data $|A\rangle = a|0\rangle + b|1\rangle$ is supplemented by two additional code qubits P, Q ; (b) Encoding circuit, resulting a single logical qubit supported on all three physical qubits, $a|000\rangle + b|111\rangle$.

More specifically, a bit-flip error has occurred; this encoding detects only a single type of error. Unlike the classical case, this is an error correction code as the two ‘syndromes’ (outcomes ± 1 of measuring the two stabilizers S_1 and S_2) give enough information to pinpoint the source of the error: if $S_1(S_2)$ flips to -1 then $P(Q)$ has an error, and if both are measured as -1 then it is A that is errored.

The use of additional ‘code’ qubits in the quantum case therefore serve a dual purpose. Firstly they expand the space so that some of the operators that stabilize it are known; these then can be measured without disturbing the encoded data. Secondly, the pattern of these measurements needs to be such that, as in the classical case, it gives enough information to decode whether there is an error and (if it is a correction code not just a detection one) where it has occurred.

More additional qubits are needed if a quantum code is to correct both phase- and bit- errors. One method is to concatenate, nesting a bit-correction code in a phase-correction code (the three-qubit code can be concatenated into a nine-qubit code capable of detecting and correcting one of both types of error). Another way is used in CSS quantum codes: two classical codes, sharing a property of duality, are used together, one correcting bit- and one correcting phase- information. For example, the CSS Steane code is formed from two copies of the classical Hamming code, encoding one qubit of information with six additional code qubits. The stabilizers are (with the tensor product understood):

$$\begin{array}{lll} Z_1Z_3Z_5Z_7 & Z_2Z_3Z_6Z_7 & Z_4Z_5Z_6Z_7 \\ X_1X_3X_5X_7 & X_2X_3X_6X_7 & X_4X_5X_6X_7 \end{array}$$

Quantum codes are described using $[[n, k, d]]$ terminology: k qubits of information are carried using n total qubits, with the code capable of correcting $d - 1/2$ (or $d/2$ if integer) errors. The Steane code is a $[[7, 1, 3]]$ code.

By comparison with classical codes, not many quantum codes are known. The various constraints in terms of specifying stabilizer subspaces, error decoding, and (in the case of CSS codes) finding dual classical codes, has proven prohibitive so far in constructing large number of codes from which to chose the best for given hardware and use-cases. The most flexible in terms of expanding easily to any desired distance are the topological codes. However, they have huge overheads in terms of qubit resources compared to the more information-dense CSS codes. This would make CSS codes seem the obvious choice, in particular for first-generation quantum technologies where the efficient use of qubit resources is paramount. However, CSS codes often lack the desirable properties of topological codes, such as sparsity and efficient decoding algorithms.

3 Background: the ZX-calculus

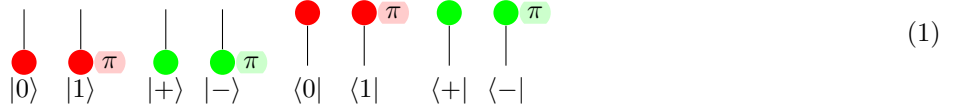
The ZX -calculus is a language for quantum diagrammatic reasoning based on interacting complementary observables [8, 9]. In the standard model of the calculus, the observables are given by the Pauli X and Z operators. The ZX -calculus is a high-level language for reasoning about quantum systems which generalises quantum circuit language. However, unlike quantum circuits, they exhibit of well-understood algebraic structure (based on so-called ‘commutative Frobenius algebras’) which enable one to easily prove many identities between ZX -diagrams.

In particular, equality of ZX -diagrams is captured by a small number of diagrammatic equations (i.e. equations between certain small, equivalent tensor networks). Thus, reasoning about equality for ZX -diagrams becomes an exercise in diagram transformation. This joins an important line of graphical equational tools in physics, where diagrams are not only aids to understanding but also have equational power, such as Feynman diagrams [17] and the Penrose tensor notion [37] (which is a direct ancestor of the ZX calculus [26, 40]).

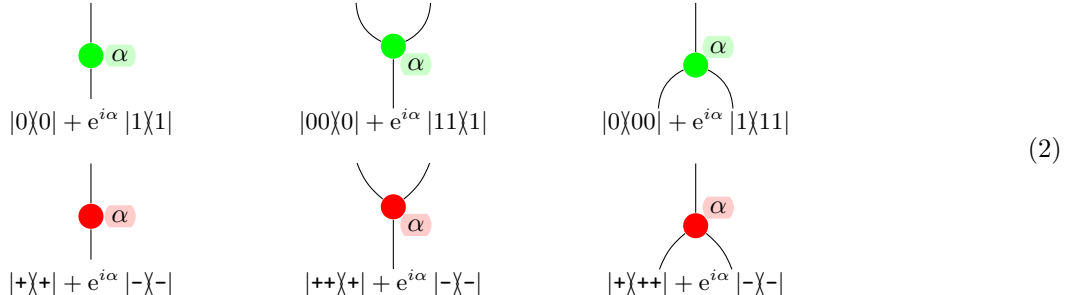
As with circuit diagrams, ZX -diagrams consist of compositions and tensor products of linear maps. Plugging two diagrams together represents composition and putting them side-by-side represents tensor product. However, unlike circuit diagrams, the components need not be unitary, so we can have components with more or fewer wires as inputs then outputs. As a result, wires need not correspond to individual qubits.

In the diagrams here, the ‘time’ axis runs vertically from bottom to top of the page – this is not, however, a necessary part of the calculus, and later on when looking at the translation from circuits we will rotate some diagrams to run left-right.

A diagram starts with the input at the bottom, often state preparation, and terminates with measurements. These are given in the calculus by



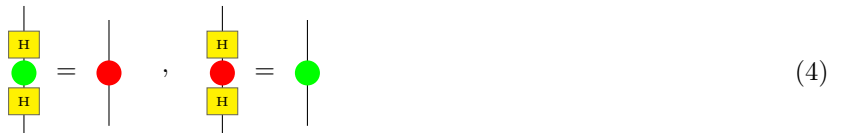
(where each diagram fragment represents the operator written below it, which is not a standard part of a diagram). Further basic operations in the calculus are the nodes



These nodes come in adjoint pairs, as follows (blank nodes denote either colour):

$$\left[\begin{array}{c} \text{blank} \\ \text{blank} \end{array} \alpha \right]^\dagger = \begin{array}{c} \text{blank} \\ \text{blank} \end{array} -\alpha ; \quad \left[\begin{array}{c} \text{blank} \\ \text{blank} \end{array} \alpha \right]^\dagger = \begin{array}{c} \text{blank} \\ \text{blank} \end{array} -\alpha ; \quad \left[\begin{array}{c} \text{blank} \\ \text{blank} \end{array} \alpha \right]^\dagger = \begin{array}{c} \text{blank} \\ \text{blank} \end{array} -\alpha \quad (3)$$

Finally, we have the Hadamard box that swaps colours:



The Hadamard box has the decomposition into Euler angles [9, 9.4.4]

$$\begin{array}{c} \text{H} \\ | \end{array} = \begin{array}{c} \text{red circle} \quad \pi/2 \\ \text{green circle} \quad \pi/2 \\ \text{red circle} \quad \pi/2 \end{array} \quad (5)$$

When using the ZX calculus for describing processes in quantum computing, they are generally composed of multiple nodes wired together. A good example to see how this works is the CNOT gate (those familiar with the calculus will note we are neglecting scalar factors for the sake of clarity of presentation):



$$\begin{aligned}
 &= |0\rangle\langle 0| \otimes |0\rangle\langle +| \otimes |+\rangle\langle +| + |0\rangle\langle 0| \otimes |0\rangle\langle -| \otimes |-\rangle\langle -| \\
 &\quad + |1\rangle\langle 1| \otimes |1\rangle\langle +| \otimes |+\rangle\langle +| + |1\rangle\langle 1| \otimes |1\rangle\langle -| \otimes |-\rangle\langle -| \\
 &= |0\rangle\langle 0| \otimes I + |1\rangle\langle 1| \otimes X = \text{CNOT.}
 \end{aligned} \tag{6}$$

Another standard gate is the controlled-phase (cz) operation, which is written

$$\text{H} \quad (7)$$

The ZX calculus is not, however, merely just another way of writing quantum processes. In addition to being provably **universal** (any set of gates can be written as a diagram [8]), it is also equational: like other types of graphical tensor notation, it's a graphical language we can actually calculate using. This is done through graph rewriting, following set rules, called axioms of the calculus. Following the rules to re-write one diagram into another is equivalent to equational reasoning. The ZX calculus is proved to be **sound**: any equivalence of diagrams guarantees that the interpretations of the diagrams in terms of Hilbert space matrices are equal (up to global phase) [8]. Very recently the calculus has also been proved to be fully complete for all of quantum mechanics (previous completeness proofs being restricted to stabilizer [1] or Clifford+T fragments [16]) [34]. Full axiom lists can be found in these papers (and [9]), but we give the important re-writes for our purposes here.

One of the most useful re-write rules is the π copy rule, $n \in \{0, 1\}$:

$$\begin{array}{c} \text{Diagram 1} \\ \text{Diagram 2} \end{array} = \begin{array}{c} \text{Diagram 3} \\ \text{Diagram 4} \end{array} \quad (8)$$

In other words, red and green nodes copy basis operators of the opposite colour. Next we have the topological re-writing rules:

$$\text{Diagram 1} = \text{Diagram 2} = \text{Diagram 3} = \text{Diagram 4} ; \quad \text{Diagram 5} = \text{Diagram 6} ; \quad \text{Diagram 7} = \text{Diagram 8} = \text{Diagram 9} . \quad (9)$$

(where a white node means either red or green, as long as the colour choice is consistent in the same diagram). We can combine the nodes with one or two inputs/outputs that we have seen so far into much larger nodes using the *spider rule*:

$$\begin{array}{c} \text{Diagram showing two green circles with radii } \alpha \text{ and } \beta \text{ meeting at a point, with a green shaded region between them.} \\ = \end{array} \begin{array}{c} \text{Diagram showing a single green circle with radius } \alpha + \beta \text{ meeting the same set of lines.} \\ \dots \end{array} \quad (10)$$

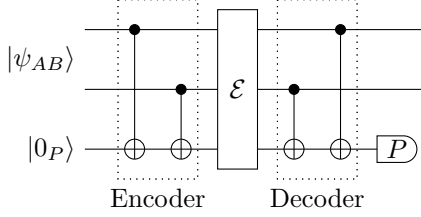


Figure 3: The fundamental coherent parity check. A bit-flip error on any of the three qubits is picked up by the measurement P .

where the notation “...” stands for arbitrary numbers of wires, with the only proviso that the number of inputs and outputs match on both sides of the equation.

This is now the basic language for transforming and calculating with the tensors of quantum theory, and it is a system that is self-contained and well-suited to automation. The software tool Quantomatic automates the process of re-writing, to automatically generate true equations, and to output verified proofs [28].

The zx calculus, dealing as it does with interacting Z and X Pauli observables, has previously proved attractive for analysing stabilizer codes [10, 13, 14, 23]. This present work builds on that foundation to present a full graphical toolkit for a large class of quantum stabilizer codes, and we now present the framework in which the graphical tools will show their full expressive use.

4 Operation of a coherent parity check

The coherent parity check (CPC) is a simple way to check for errors on pairs (or more) of qubits over time that is analogous with parity checking in classical error correction in a more direct way than standard presentations of quantum error correction. In this section we introduce the basic gadget on two qubits, showing how it checks for errors while being non-disturbing. After introducing it in terms of circuit notation and Dirac notion, we give the operation in terms of the zx calculus, and show how this simplifies calculations. We begin to make contact with the usual format for quantum error correction by showing how the gadget essentially constructs stabilizers across qubits, and deal graphically with errors propagating in the gadget. We end the section by constructing a first CPC code that uses six qubits to detect and correct one error of a single type on three qubits of information. This section concerns only a handful of qubits and error detection; in subsequent sections we build full error correction codes in the CPC construction.

4.1 The coherent parity check

The basic coherent parity check is a three-stage circuit on three qubits that detects an error of a single type (Pauli X or Z) on one of the qubits. As with classical error correction, Figure 1, we use one of the qubits (a “parity qubit”) to detect errors, and the other two (“data qubits”) to store information¹. The circuit for the basic operation is shown in Figure 3. The data qubits A and B are in the state $|\psi_{AB}\rangle = \sum_{ij} a_{ij} |ij\rangle$ where $i, j \in 0, 1$. The parity qubit P starts in the state $|0\rangle$, and then is entangled with the data qubits through two CNOT gates. Measuring the parity qubit now gives a measurement of the Pauli $Z_A \otimes Z_B$ operator – the joint bit parity of A and B . In qubits, as we noted in the Introduction, such a measurement would be disturbing. We therefore do not measure P but let the system evolve.

Using a simple error model in which error ε occurs in a specific time window t during which the system is evolving, we then repeat the encoding step at the end of the gadget to unentangle the parity check qubit from the data qubits. By measuring the parity qubit, it is possible to deduce whether an error has occurred during time t on either A , B , or P , while not disturbing the information $|\psi_{AB}\rangle$ held in AB . Importantly, nothing need be known about the state of A or B – it does not have to be a stabilizer state.

To see how this simple gadget works, we walk through its mathematical action on the three qubit system $|\psi_{AB}\rangle \otimes |0_P\rangle$. To this end, it is useful to re-express the CPC circuit in the form shown in Figure 4 by making the

¹It is worth noting at the outset that in the CPC construction, the term “data qubits” refers to a subset of what are termed data qubits in standard presentations of stabilizer codes. In the CPC framework, both data and parity qubits together make up what are in other presentations called simply data qubits. We will deal with syndrome qubits later on.

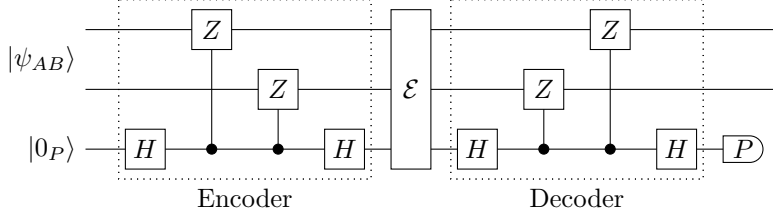


Figure 4: The fundamental CPC gadget re-written as controlled-phase operations.

substitution

$$\text{CNOT}_{a,b} \rightarrow H_a \circ \text{CZ}_{a,b} \circ H_a. \quad (11)$$

where H_i is the single-qubit Hadamard operator, and ‘ \circ ’ denotes sequential gate composition. In this form, it can be seen that the action of the encoder is to perform the parity check Z_AZ_B on the data register, conditional on the value of the parity check qubit which is prepared in the conjugate basis by a Hadamard gate.

Following the encode stage, the state of the three-qubit system is given by

$$U_{\text{encode}} |\psi_{AB}\rangle |0_P\rangle = (I + Z_AZ_B) |\psi_{AB}\rangle |0_P\rangle + (I - Z_AZ_B) |\psi_{AB}\rangle |1_P\rangle. \quad (12)$$

We now have a three-party entangled state, where the two terms of the superposition correspond to the $+1$ and -1 eigenstates of the Z_AZ_B operator respectively.

During the wait stage, the system is subject to a single-qubit operation from the set $\mathcal{E} = \{I, X_A, X_B, X_P\}$. The state of the CPC gadget is then given by

$$\mathcal{E}U_{\text{encode}} |\psi_{AB}\rangle |0_P\rangle = \mathcal{E}(I + Z_AZ_B) |\psi_{AB}\rangle |0_P\rangle + \mathcal{E}(I - Z_AZ_B) |\psi_{AB}\rangle |1_P\rangle, \quad (13)$$

Following the wait stage, the parity qubit is disentangled from the register by the decoder. The decoder, U_{decode} , is the unitary inverse of the encoder and transforms the system as follows,

$$\begin{aligned} U_{\text{decode}} \mathcal{E}U_{\text{encode}} |\psi_{AB}\rangle |0_P\rangle = \\ (I + Z_AZ_B)\mathcal{E}(I + Z_AZ_B) |\psi_{AB}\rangle |0_P\rangle + (I - Z_AZ_B)\mathcal{E}(I + Z_AZ_B) |\psi_{AB}\rangle |1_P\rangle \\ + (I - Z_AZ_B)\mathcal{E}(I - Z_AZ_B) |\psi_{AB}\rangle |0_P\rangle + (I + Z_AZ_B)\mathcal{E}(I - Z_AZ_B) |\psi_{AB}\rangle |1_P\rangle. \end{aligned} \quad (14)$$

The above simplifies to

$$\begin{aligned} U_{\text{decode}} \mathcal{E}U_{\text{encode}} |\psi_{AB}\rangle |0_P\rangle = \\ (\mathcal{E} + Z_AZ_B\mathcal{E}Z_AZ_B) |\psi_{AB}\rangle |0_P\rangle + (\mathcal{E} - Z_AZ_B\mathcal{E}Z_AZ_B) |\psi_{AB}\rangle |1_P\rangle. \end{aligned} \quad (15)$$

The final step in the CPC gadget is to measure the parity qubit P . In the event that no error occurred, $\mathcal{E} = I$, the second term in the above goes to zero and the measured syndrome is 0. Intuitively we would expect this as the encoder is the unitary inverse of the decoder and

$$U_{\text{decode}} \mathcal{E}U_{\text{encode}} |\psi_{AB}\rangle |0_P\rangle = I |\psi_{AB}\rangle |0_P\rangle, \quad (16)$$

when $\mathcal{E} = I$. If a bit-flip error did occur, $\mathcal{E} \in \{X_A, X_B, X_P\}$, the first term goes to zero and the measured syndrome is 1. More generally, the output of the CPC gadget can be written as follows

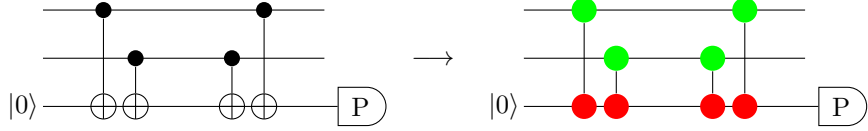
$$U_{\text{decode}} \mathcal{E}U_{\text{encode}} |\psi_{AB}\rangle |0_P\rangle = \begin{cases} |\psi_{AB}\rangle |0_P\rangle, & \text{if } [\mathcal{E}, Z_AZ_B]_- = 0 \\ |\psi_{AB}\rangle |1_P\rangle, & \text{if } [\mathcal{E}, Z_AZ_B]_- \neq 0. \end{cases} \quad (17)$$

From the above we see that the parity qubit is no longer entangled with the register at the end of the CPC cycle. The final syndrome measurement will therefore not decohere the register: the output depends only upon whether the error operator \mathcal{E} commutes with the parity check operator Z_AZ_B .

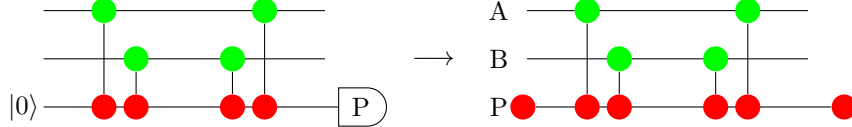
This elementary operation is a very simple error detection code (there is not yet enough information to correct the error) for a single error of a single qubit. In Appendix A we give the full $|\psi_{AB}\rangle$ analysis showing how many errors it can detect, and we calculate the error suppression to be $\varepsilon^2 \rightarrow \varepsilon^4$. The result also generalises to other parity checks. For example, replacing the Z_AZ_B parity check with X_AX_B gives a CPC gadget that can detect phase-flip errors.

4.2 Coherent parity checking in the ZX calculus

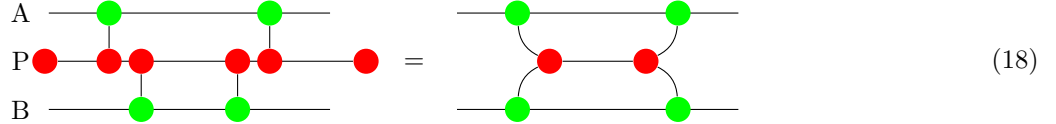
The action of the coherent parity check is even clearer when considered diagrammatically. To show how the CPC operation looks in the ZX calculus, we will give a step-by-step translation from the circuit notation². We start by replacing the CNOT gates in figure 4 with their ZX representation, given in (6). Controls map to green nodes, targets to red, and edges replace wires:



Now we replace the state creation and measurement of the parity-check qubit with the relevant (here red) nodes, as in (1):

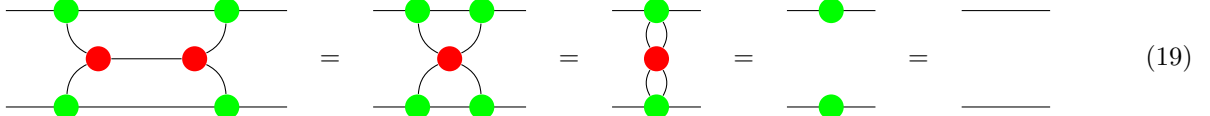


Now we re-arrange the order of the qubits for clarity from A-B-P to A-P-B, and then apply the spider rules to merge the red nodes :

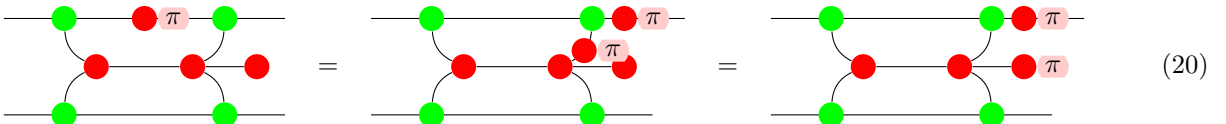


This last re-write is now entirely within the calculus, and so truly is an equation.

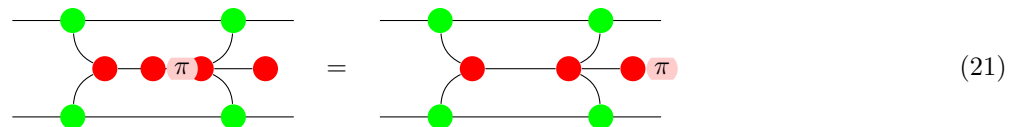
We term this the normal form of the basic CPC operation. The space in the middle of the diagram is where errors occur (under the particular simplified model we are dealing with at the moment), and we will see shortly how they interact with the CPC diagram. First, however, we use the algebraic power of the calculus to demonstrate that the CPC encoding-decoding cycle does not disturb the information contained in qubits A and B . This is demonstrated by proving through re-writes that the diagram of (18) is equivalent to the identity operations on qubits A and B . This verification of the operation is simple in the calculus:



We now show how this basic operation detects errors on the three qubits. We use an extended normal form, pulling out the measurement of the parity qubit, for clarity. We see how a Pauli Z error occurring during time t on qubit A propagates forward through the decoder to the measured qubit using re-writing (remembering that these are full equations):



This represents the error remaining on qubit A , and also propagating to qubit P (the red- π s). The error propagating onto P then causes the measurement outcome to switch to 1 (that is, the measurement projects onto $|1\rangle$). By symmetry, the same is true for an error on B . The error on P is even more straightforward, and it is immediately clear in the calculus that it does not propagate onto the other qubits:



²Note this translation is not in itself equational reasoning/graph rewriting, and should be viewed as purely illustrative.

These equations prove the functionality of the basic CPC operation simply, intuitively, and rigorously.

4.3 Error propagation through a CPC

If we look at equations (20) and (21), we see that they do more for us than proving how the CPC functions: they are also an immediate method of visualising how errors propagate through the parity check. The basic rules are simple in ZX terms: Pauli Z errors (bit flips) are red π nodes. These are copied by green nodes, and propagate unchanged through red nodes. A CPC for Pauli X errors (green π s) is identical, with all colours in the diagram reversed. Combining the re-write rules of the calculus with temporal flow, therefore enables us to see immediately and clearly the flow of errors.

We can get a further way of modelling error propagation by making the transformation to controlled- Z gates as in the previous section, and in Figure 11. We first note that, in the ZX calculus, the transformation given in (11) is easy to prove by a simple re-write (rather than a somewhat tedious matrix calculation) as:

$$\begin{array}{c} \text{Diagram 1} \\ \text{Diagram 2} \end{array} = \begin{array}{c} \text{Diagram 3} \\ \text{Diagram 4} \end{array} \quad (22)$$

where we can identify the central structure as a controlled- Z gate, (7). The CPC now becomes

$$\begin{array}{c} \text{Diagram 1} \\ \text{Diagram 2} \end{array} = \begin{array}{c} \text{Diagram 3} \\ \text{Diagram 4} \end{array} \quad (23)$$

(note we do not cancel out the central pair of Hadamard boxes as error can occur in between them). In this way of viewing the action, the Hadamard boxes can be seen as switching the colour of an error as it goes through. Green errors on A and B go through unaffected, but a green error on P will propagate through both Hadamard boxes and nodes until it is on all qubits. However, it will not be picked up at the measurement as it is a different colour from the measurement projection, showing that in this form of the basic operation, phase errors are undetectable:

A CPC that does detect such phase errors will be the colour-inverse of this one (compare to (23)).

$$\begin{array}{c} \text{Diagram 1} \\ \text{Diagram 2} \end{array} = \begin{array}{c} \text{Diagram 3} \\ \text{Diagram 4} \end{array} \quad (25)$$

4.4 Stabilizers and the CPC operation

We can now start to make contact between codes based on the CPC gadget, as presented here, and the usual understanding of quantum error correction in terms of stabilizer subspaces and syndrome measurement. General stabilizer codes encode quantum information by ‘spreading’ the state of the data qubits in a non-specific way over a space of codewords. In contrast, CPC codes retain a clear distinction between qubits which encode data and qubits which encode parity information. To see this, consider two data qubits A and B which are in the state

$$|\psi_{AB}\rangle = \alpha_{00} |0_A 0_B\rangle + \alpha_{01} |0_A 1_B\rangle + \alpha_{10} |1_A 0_B\rangle + \alpha_{11} |1_A 1_B\rangle. \quad (26)$$

The action of the CPC encoder is to replicate the parity value given by the operator $Z_A Z_B$ into a parity check qubit P such that,

$$|\psi_{ABP}\rangle_{\text{enc}} = U_{\text{encode}} |\psi_{AB}\rangle |0_P\rangle, \quad Z_A Z_B |\psi_{ABP}\rangle_{\text{enc}} = p_{AB} |\psi_{ABP}\rangle_{\text{enc}}, \quad (27)$$

$$Z_P |\psi_{AB}\rangle_{\text{enc}} = p_p |\psi_{ABP}\rangle_{\text{enc}}, \quad p_{AB} = p_p \forall \{A, B\}, \quad (28)$$

where $p_{\{AB, P\}} = \pm 1$ are the parity check outcomes. Applied to the two qubit state, the full output of the CPC encoder is therefore

$$|\psi_{ABP}\rangle_{\text{enc}} = \alpha_{00} |0_A 0_B\rangle |0_P\rangle + \alpha_{01} |0_A 1_B\rangle |1_P\rangle + \alpha_{10} |1_A 0_B\rangle |1_P\rangle + \alpha_{11} |1_A 1_B\rangle |0_P\rangle. \quad (29)$$

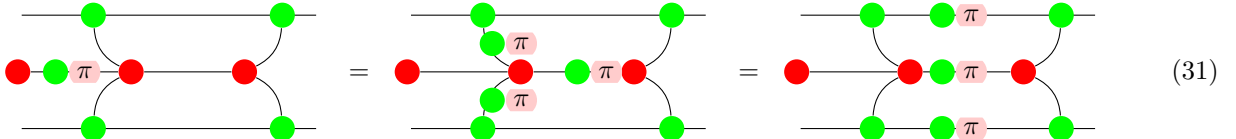
The encode stage projects the $|\psi_{AB}\rangle$ state into a $4D$ subspace of the expanded 3-qubit Hilbert space \mathcal{H}_{ABP} . In the language of conventional stabilizer codes, this partitioning of the Hilbert space can be thought of in terms of a code space $\mathcal{C}_{\text{code}}$ and an error space $\mathcal{C}_{\text{error}}$ as shown below

$$\mathcal{C}_{\text{code}} = \left[\begin{array}{c} |0_A 0_B\rangle |0_P\rangle, \\ |0_A 1_B\rangle |1_P\rangle, \\ |1_A 0_B\rangle |1_P\rangle, \\ |1_A 1_B\rangle |0_P\rangle \end{array} \right], \quad \mathcal{C}_{\text{error}} = \left[\begin{array}{c} |0_A 0_B\rangle |1_P\rangle, \\ |0_A 1_B\rangle |0_P\rangle, \\ |1_A 0_B\rangle |0_P\rangle, \\ |1_A 1_B\rangle |1_P\rangle \end{array} \right]. \quad (30)$$

In each of the four element of $\mathcal{C}_{\text{code}}$, the bit values of the first two qubits correspond to the basis states in unencoded state $\{|0_A 0_B\rangle, |0_A 1_B\rangle, |1_A 0_B\rangle, |1_A 1_B\rangle\}$. As a result it remains possible to distinguish qubits A and B as the data qubits even after encoding. Carrying the parity information forward coherently, in a qubit rather than a classical measurement outcome, allows arbitrary such joint parity measurements to be made, rather than having to measure a known stabilizer of the data qubits.

The duplication of parity information into the parity check qubits gives rise to stabilizers across the combined system of data+parity qubits. The code space of the CPC gadget $\mathcal{C}_{\text{code}}$, defined in Equation 30, is stabilized by the operator $Z_A Z_B Z_P$. This is the case, regardless of the values of A and B , as the encoder ensures that $Z_A Z_B |\psi_{AB}\rangle_{\text{enc}} = Z_P |\psi_{AB}\rangle_{\text{enc}}$ and therefore $Z_A Z_B Z_P |\psi_{AB}\rangle_{\text{enc}} = (+1) |\psi_{AB}\rangle_{\text{enc}}$. The decode step of the CPC gadget can be viewed as measuring the $Z_A Z_B Z_P$ stabilizer. While the identification of stabilizers becomes more complicated as we move to CPC codes that detect both bit and phase errors, we will see that the conclusion carries through, and that CPC constructed codes are stabilizer codes.

While supporting this way of viewing how the CPC encoding constructs a stabilizer across the state, a ZX calculation gives a further insight into how the stabilizer is formed. To construct a stabilizer, we re-write from a known stabilizer at the start of the diagram. Here, what we know is that the parity qubit is initialised as a red node ($|0\rangle$). A green π operations (Pauli Z , a phase flip) does nothing to this state. Using an extended normal form where we extend out the preparation of the parity qubit this time, we obtain a stabilizer by ‘pushing’ this operation through the encoding operations:



We will make use of this later as the general method for computing stabilizers for CPC codes, starting from the known stabilizers of the parity-check qubits.

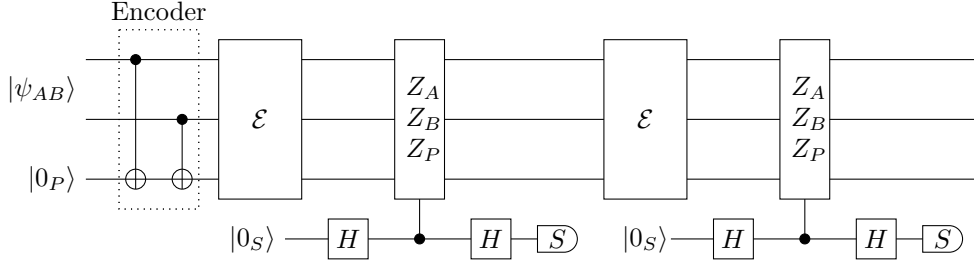


Figure 5: The CPC gadget with continuous error protection using stabilizer measurements.

4.5 Continuous CPC operation

As presented so far, the CPC gadget has been described in terms of an *encode-error-decode* structure. Whilst this approach is good for demonstrating the fundamental operation of the CPC framework, the disadvantage is that there are gaps in protection during the encode and decode stages of the cycle. We can use the understanding of the CPC as constructing stabilizers to switch instead to a situation standard in quantum error correction: qubits A, B and P remain continuously encoded, and a separate syndrome qubit S is brought in to measure the stabilizer $Z_A Z_B Z_P$, Figure 5. An auxiliary qubit S is introduced to extract the stabilizer value before being measured out to yield a syndrome. This auxiliary qubit could be recycled after each cycle allowing the stabilizer to be measured repeatedly with constant overhead. Formulating CPC codes in this way would allow for continuous protection at all points in the circuit following the initial encode stage.

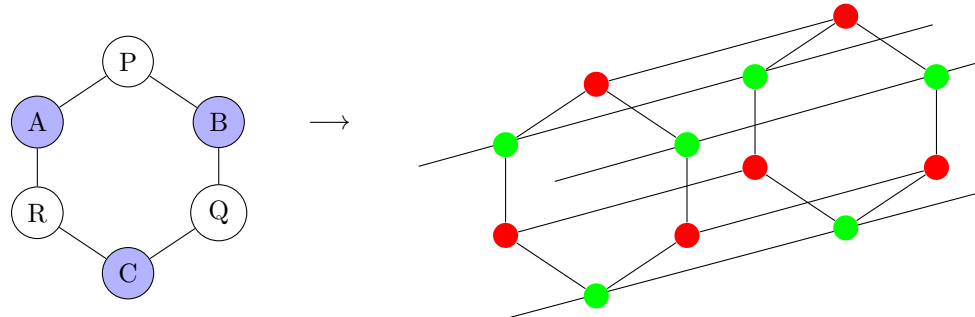
It is worth noting, though, that encode-error-decode codings should not be ruled out of consideration when determining the correct way to implement codes on small- or medium- scale machines. On some devices the error rate may be low enough, and the gate speed high enough, that encoding, decoding, and then re-encoding could be good enough to gain an appreciable degree of error mitigation. For small codes and devices, the reduction in the number of qubits required may well be worth it in some situations.

For completeness, we show the syndrome measurement of Figure 5 in ZX form:

A re-write procedure (either by hand or using the tool Quantomatic) demonstrates that this continues to re-write to the identity operation.

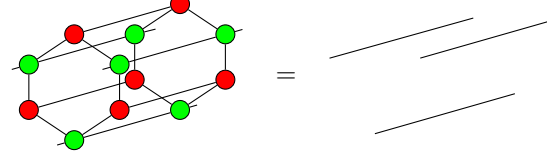
4.6 A first CPC code: detecting and correcting one type of error

We can see how the CPC basic operation combines to form error correction codes by taking a simple example. Considering still only a single type of error (X error), let us take three data qubits, A, B, C , and three parity check qubits, P, Q, R , in a ring formation:



We can now perform three operations on this diagram to verify the code, using the Quantomatic software package to automate derivations.

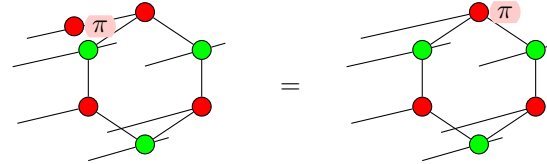
Re-write to the identity. This verifies that, in the absence of errors, the encoder plus decoder in non-disturbing on the data qubits, and hence that the decode reverses the encoder:



(33)

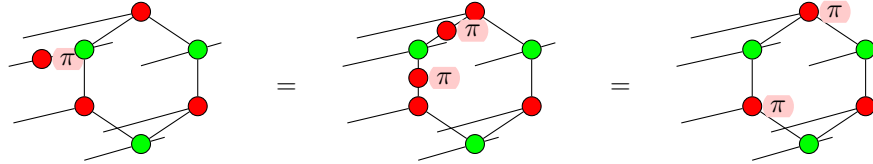
where the full derivation tree is given in Appendix B.

Error propagation on parity qubits. It is trivial to prove using ZX that a Pauli X (red π node) error in between encode and decode on a parity qubit does not propagate, and is picked up as a $+1$ measurement of that qubit at decode. We demonstrate on qubit P ; proofs for Q and R follow by symmetry. We need consider only the decode step:



(34)

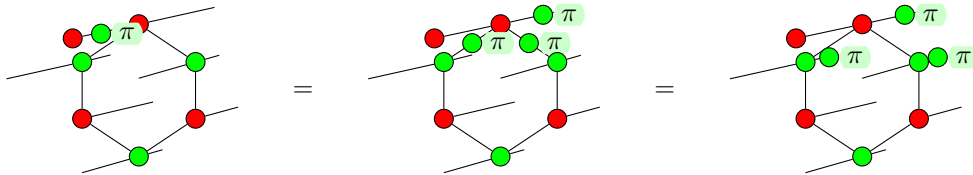
Error propagation on data qubits. It is similarly straightforward to show how errors on data qubits will propagate to a pair of parity measurements. Consider an X error on data qubit A . This will be picked up as $+1$ measurement outcomes on P and R (proofs for B and C follow by symmetry):



(35)

In combination, these three elements show that the code is non-disturbing, detects all single-qubit (bit-flip) errors, and each error leads to a unique syndrome (combination of measurement outcomes). It is a clear demonstration of the power of the ZX approach that it can prove this straightforwardly and intuitively (the equivalent calculation of (33), (34), and (35) in either Dirac or matrix notation is much larger and contains no intuition on error propagation). This three-stage verification, using Quantomatic for larger calculations (and later automating looping over all possible error placements), will be our tools for use with CPC codes.

Extraction of stabilizers. As well as verifying the code, we can also use re-writing to characterise it in terms of its stabilizers. As before, we find stabilizers of the code this by ‘pushing’ a stabilizer on a parity qubit through the encoder. Consider the X (green π node) operator on P :



(36)

That is, the stabilizer Z_P maps through the encoder to the stabilizer of the code $Z_AZ_BZ_P$. Repeating for Q and R gives the full set of stabilizers:

$$Z_AZ_BZ_P, Z_BZ_CZ_Q, Z_AZ_CZ_R \quad (37)$$

In Appendix B we show that the error suppression of this code, for a single type of error, is $\varepsilon^2 \rightarrow \varepsilon^4$. Using an experimentally-motivated Pauli- X error rate of $0.007s^{-1}$ [22], we show numerical simulation results for how the code significantly extends the lifetime of an encoded trio of data qubits.

Finally, we can make the connection with classical error correction. The code we have presented in this section deals only with a single type of error, and so can be viewed straightforwardly classically. However, given the different partitioning of qubits into data+parity that the CPC construction gives compared to standard methods, the connection with classical codes is also different. The coherent parity check replaces the classical parity check.

The ring code can be given using adjacency matrices, as in classical presentations [31]. We will use this formalism along with the ZX calculus when dealing in subsequent sections with quantum codes for all forms of error. An adjacency matrix for n qubits is an $n \times n$ matrix M where each element M_{ij} is 1 if there is a CNOT gate between qubits i and j (in either direction) and zero otherwise. The full adjacency matrix for the ring code is

$$M = \begin{pmatrix} & \begin{matrix} A & B & C & P & Q & R \end{matrix} \\ \begin{matrix} A \\ B \\ C \\ P \\ Q \\ R \end{matrix} & \left(\begin{matrix} 0 & 0 & 0 & 1 & 0 & 1 \\ 0 & 0 & 0 & 1 & 1 & 0 \\ 0 & 0 & 0 & 0 & 1 & 1 \\ 1 & 1 & 0 & 0 & 0 & 0 \\ 0 & 1 & 1 & 0 & 0 & 0 \\ 1 & 0 & 1 & 0 & 0 & 0 \end{matrix} \right) \end{pmatrix} = \left(\begin{array}{c|c} \mathbf{0} & B^T \\ \hline B & \mathbf{0} \end{array} \right) \quad (38)$$

where $\mathbf{0}$ is the zero matrix.

The adjacency matrix is therefore fully described for the ring by the single matrix B , which we term the bit-parity check matrix for the code. By virtue of its operation, all CNOT gates determined by B are in the same direction, from data qubit to parity-check qubit. The matrix for the ring is

$$B = \begin{pmatrix} 1 & 1 & 0 \\ 0 & 1 & 1 \\ 1 & 0 & 1 \end{pmatrix} \quad (39)$$

This is the parity check matrix for a classical [6,3] error correction code.

We now turn to extending the CPC construction from single error type correcting codes to quantum codes capable of detecting and correcting both bit and phase error, and introduce a new set of elements to the ZX calculus that will allow us to operate at the level of logical structures as well as single qubits.

5 Single-error correcting CPC codes

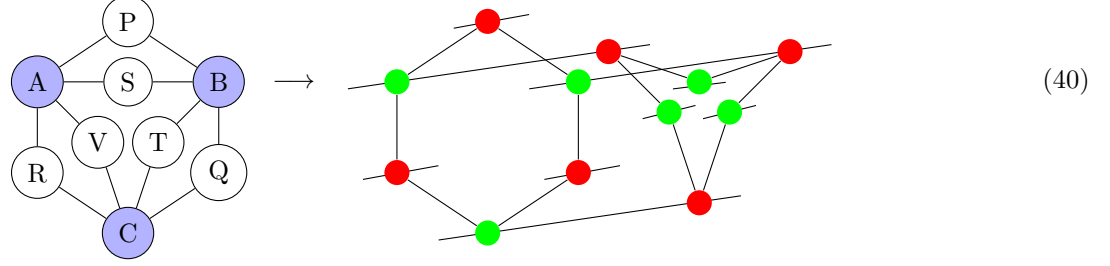
In this section we consider fully quantum codes that are capable of detecting and correcting both types of error – Pauli X (bit-flip) and Pauli Z (phase flip). Again we use the simplified error model where gates are error-free, and errors occur on all qubits with equal probability in the time between operations.

The first code we consider will be an extension of the ring code of the previous section, combining both bit and phase parity checks. We demonstrate how undetectable errors can propagate through the code unless cross-checks are brought in between the parity qubits themselves, and additional qubits measuring overall parity. With these elements in place, the ring code becomes a fully quantum [[11,3,3]] code. We give a generalised formalism for such full codes, and a major proof of this paper: that any distance 3 classical code can be turned into a distance 3 quantum code as $[n, k] \rightarrow [[2n - k + 1, k - 1, 3]]$.

5.1 Bit- and phase- parity checks

The first step in constructing our full ring code is to add a set of qubits that will perform phase parity checking. We do this in exactly the way the bit parity qubits were added. Choosing a scenario where first bit then phase

operations are performed, in diagrammatic form we have

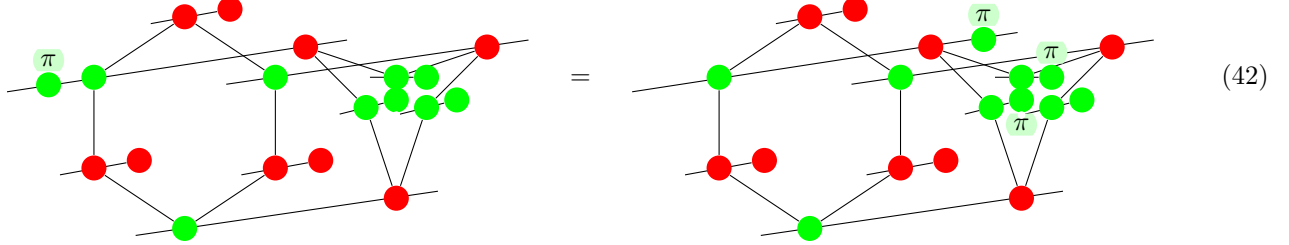


In matrix form, the full adjacency matrix is

$$M = \left(\begin{array}{c|c|c} \mathbf{0} & B^T & P^T \\ \hline B & \mathbf{0} & \mathbf{0} \\ \hline P & \mathbf{0} & \mathbf{0} \end{array} \right) \quad (41)$$

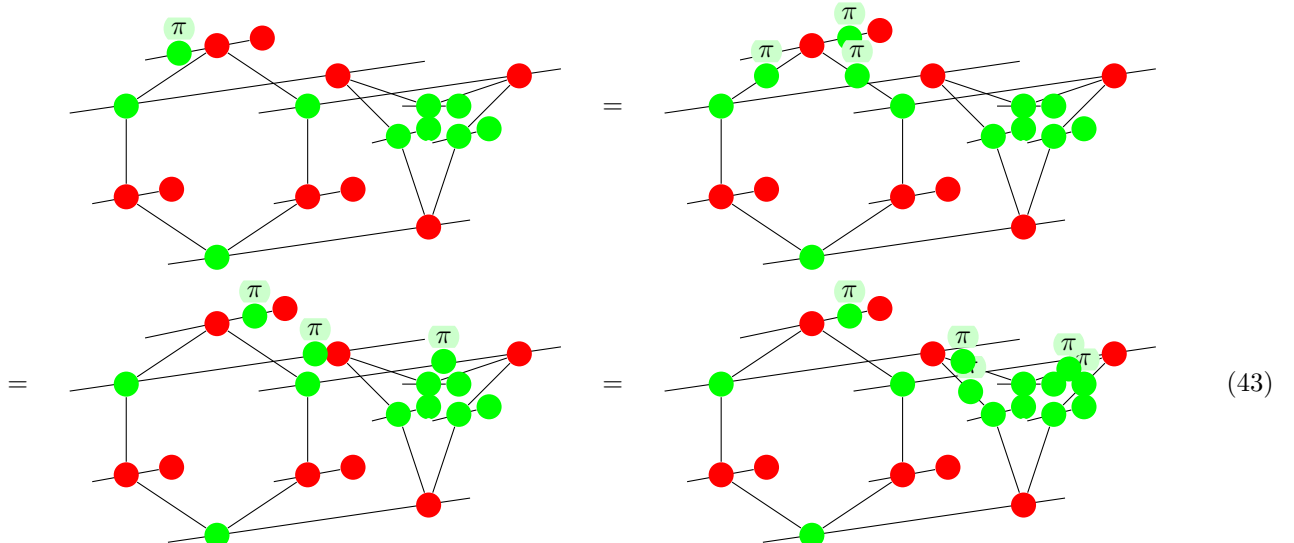
where again $\mathbf{0}$ is the zero matrix, and B is as in equation (39). In this particular example of the ring, we have $B = P$. Recall that the adjacency matrix simply says whether there is a gate between qubits; the direction of the gate will be different if it is given by B or P (to gather bit or phase information).

We can now look at the propagation of individual errors through this as a decoder. For example, a phase error on a data qubit is indeed picked up by the decoder (with the measurements of the parity-check qubits now represented explicitly):



where we recall that a π node as a measurement represents the $+1$ outcome.

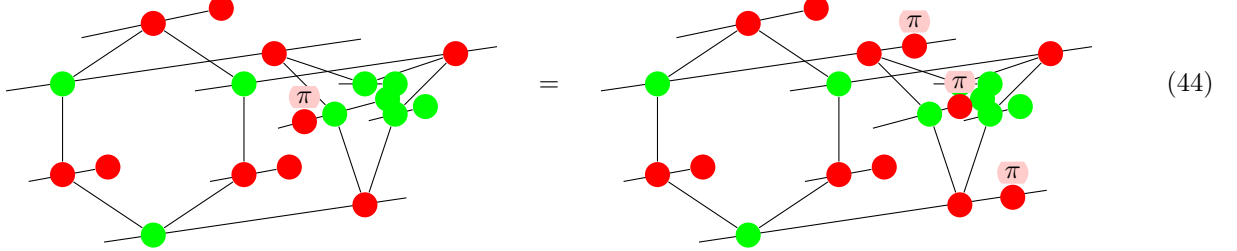
However, we can also find two situations where errors are problematic for this proposed code. Firstly, when there is a phase error on a bit-parity check qubit. This will propagate as



While this error will be picked up on the phase-check (as can be seen from in the final diagram), there is no guarantee that it can be correctly identified. By propagating through the bit checks, the error has spread to more

than one data qubit. As the phase check can only correct single errors, the code will not be able to pinpoint which qubits are in error.

The second problem comes when we consider a bit error on a phase parity-check qubit. In this situation, the error propagates to the data qubit while remaining completely undetected by the decoder:



In considering these errors, and how we might deal with them, the notation we have been using for the ZX calculus becomes significantly unwieldy. To represent the proposed code in a compact form, and to then be able to introduce and verify a correct and full distance 3 code, we introduce new notation that allows us to incorporate adjacency matrix representations into ZX diagrams.

5.2 Box-code representation in the zx calculus

We define a ‘spider box’ on a collection of n nodes as follows:

$$\begin{array}{c} n \\ \square \end{array} := \begin{array}{c} \text{---} \\ \text{---} \\ \vdots \\ \text{---} \end{array} \} n \quad (45)$$

$$\begin{array}{c} n \\ \square \end{array} := \begin{array}{c} \text{---} \\ \text{---} \\ \vdots \\ \text{---} \end{array} \} n \quad (46)$$

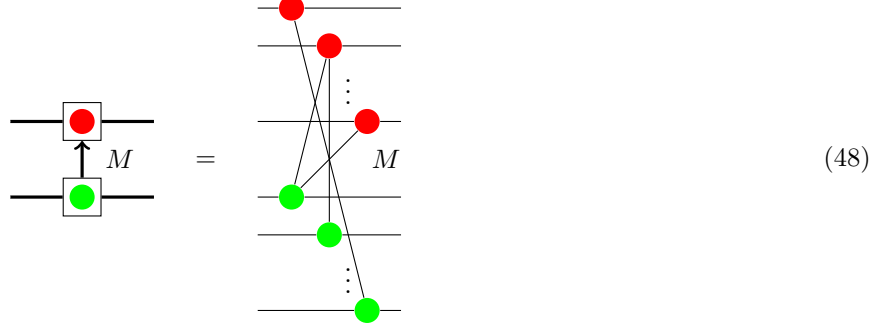
As it is typically clear, we will standardly suppress the n .

Spider boxes can be joined by edges to either single nodes or to other spider boxes. An undecorated (but thick) edge from a spider box to a spider box denotes an edge from the i -th wire of the first box to the i -th wire of the second (the spider boxes must therefore be of the same size, that is contain the same number of nodes):

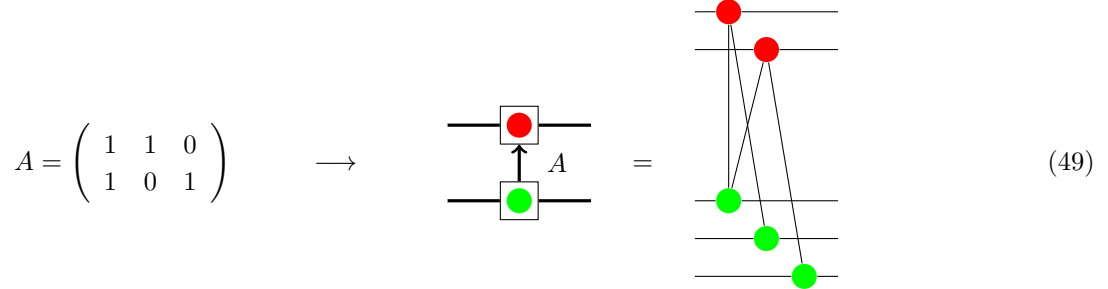
This definition holds for all combinations of coloured spider boxes.

Adjacency matrices may be associated with thick edges joined to spider boxes. In such a case the edge becomes directed. Two spider boxes joined by a directed edge indexed by matrix M , where $M_{ij} \in \{0, 1\}$ stands for an edge between the i -th input node and the j -th output node iff $M_{ij} = 1$, where the directionality of the edge determines

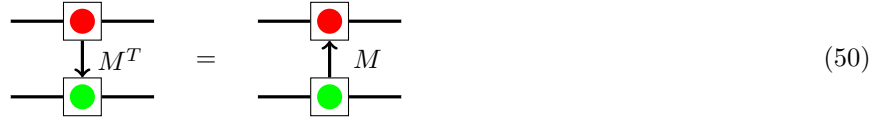
input and output:



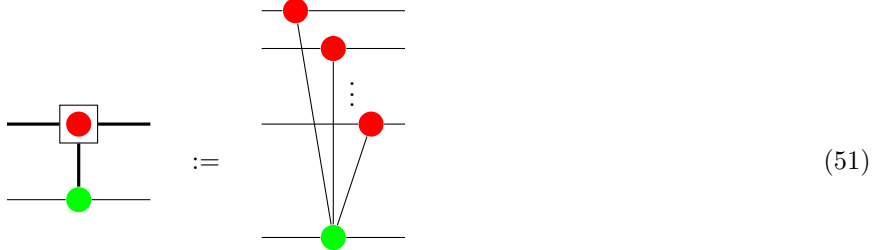
As an example, with the specific adjacency matrix A we have the following:



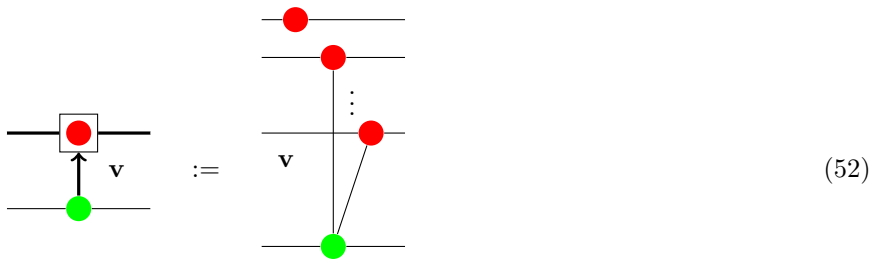
The direction of the edge may be switched by a transpose of the adjacency matrix:



In the case where one spider box has size $n = 1$, this reduces to a single node on a standard wire. A box connected to a node by an unannotated edge stands for an edge between every node in the box and the individual node:



When the edge is annotated with a vector \mathbf{v} , where $v_i \in \{0, 1\}$, an edge is placed between the standalone node and the i -th node in the box iff $v_i = 1$. This edge is properly directed, although in general this is not needed to distinguish inputs and outputs (as long as there is more than a single node in the box):



For example,

$$\omega = \begin{pmatrix} 1 \\ 0 \\ 1 \end{pmatrix} \rightarrow \begin{array}{c} \text{---} \\ \text{---} \\ \text{---} \end{array} \begin{array}{c} \text{---} \\ \text{---} \\ \text{---} \end{array} \begin{array}{c} \text{---} \\ \text{---} \\ \text{---} \end{array} = \begin{array}{c} \text{---} \\ \text{---} \\ \text{---} \end{array} \begin{array}{c} \text{---} \\ \text{---} \\ \text{---} \end{array} \begin{array}{c} \text{---} \\ \text{---} \\ \text{---} \end{array} \quad (53)$$

Transpose is also defined for edges between single nodes and boxes:

$$\begin{array}{c} \text{---} \\ \text{---} \\ \text{---} \end{array} \begin{array}{c} \text{---} \\ \text{---} \\ \text{---} \end{array} \begin{array}{c} \text{---} \\ \text{---} \\ \text{---} \end{array} = \begin{array}{c} \text{---} \\ \text{---} \\ \text{---} \end{array} \begin{array}{c} \text{---} \\ \text{---} \\ \text{---} \end{array} \begin{array}{c} \text{---} \\ \text{---} \\ \text{---} \end{array} \quad (54)$$

All these definitions hold for all combinations of coloured spider boxes.

When considering phases on collections of nodes, we do not use spider-box notation. Instead, a node on a thick wire is automatically assumed to stand for multiple nodes across all n wires thus represented. We term such nodes ‘spider nodes’.

A π -phase on a spider node of any colour stands for that phase on each node, eg:

$$\begin{array}{c} \text{---} \\ \text{---} \\ \text{---} \end{array} \begin{array}{c} \text{---} \\ \text{---} \\ \text{---} \end{array} \begin{array}{c} \text{---} \\ \text{---} \\ \text{---} \end{array} := \begin{array}{c} \text{---} \\ \text{---} \\ \text{---} \end{array} \begin{array}{c} \text{---} \\ \text{---} \\ \text{---} \end{array} \begin{array}{c} \text{---} \\ \text{---} \\ \text{---} \end{array} \quad (55)$$

also for red nodes and boxes. A single π phase on the i -th wire is given by the phase $\mathbf{e}_i\pi$ where \mathbf{e}_i is the unit column vector with 1 in the i -th position and zero elsewhere:

$$\begin{array}{c} \text{---} \\ \text{---} \\ \text{---} \end{array} \begin{array}{c} \text{---} \\ \text{---} \\ \text{---} \end{array} \begin{array}{c} \text{---} \\ \text{---} \\ \text{---} \end{array} := \begin{array}{c} \text{---} \\ \text{---} \\ \text{---} \end{array} \begin{array}{c} \text{---} \\ \text{---} \\ \text{---} \end{array} \begin{array}{c} \text{---} \\ \text{---} \\ \text{---} \end{array} \quad (56)$$

(and for red nodes and phases). For example,

$$\mathbf{e}_1 = \begin{pmatrix} 1 \\ 0 \\ 0 \end{pmatrix} \rightarrow \begin{array}{c} \text{---} \\ \text{---} \\ \text{---} \end{array} \begin{array}{c} \text{---} \\ \text{---} \\ \text{---} \end{array} \begin{array}{c} \text{---} \\ \text{---} \\ \text{---} \end{array} = \begin{array}{c} \text{---} \\ \text{---} \\ \text{---} \end{array} \begin{array}{c} \text{---} \\ \text{---} \\ \text{---} \end{array} \begin{array}{c} \text{---} \\ \text{---} \\ \text{---} \end{array} \quad (57)$$

A number of such phases with weights v_i may be summed, resulting in a phase vector:

$$\sum_i a_i \mathbf{e}_i \pi = \mathbf{v} \pi \quad (58)$$

where $v_i \in \{0, 1\}$. An arbitrary phase α on a spider node represents α on all nodes:

$$\begin{array}{c} \text{---} \\ \text{---} \\ \text{---} \end{array} \begin{array}{c} \text{---} \\ \text{---} \\ \text{---} \end{array} \begin{array}{c} \text{---} \\ \text{---} \\ \text{---} \end{array} := \begin{array}{c} \text{---} \\ \text{---} \\ \text{---} \end{array} \begin{array}{c} \text{---} \\ \text{---} \\ \text{---} \end{array} \begin{array}{c} \text{---} \\ \text{---} \\ \text{---} \end{array} \quad (59)$$

A single phase on node i is given by $\mathbf{e}_i\alpha$ as before. Arbitrary phases sum linearly, as with π :

$$\sum_i a_i \mathbf{e}_i \alpha = \mathbf{v} \alpha \quad (60)$$

where again $v_i \in \{0, 1\}$. A phase $\mathbf{e}_i\pi$ incident on an edge with associated matrix M transforms to a phase $M\mathbf{e}_i\pi$ after the edge if the direction is forward (and $M^T\mathbf{e}_i\pi$ if against):

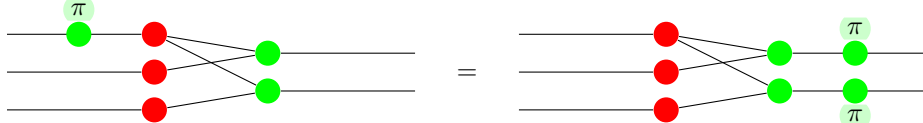


$$(61)$$

For example, if we have

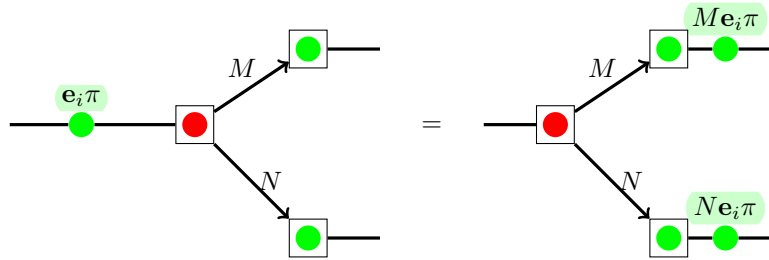
$$\mathbf{e}_i = \begin{pmatrix} 1 \\ 0 \\ 0 \end{pmatrix}, \quad A = \begin{pmatrix} 1 & 1 & 0 \\ 1 & 0 & 1 \end{pmatrix} \quad \rightarrow \quad A\mathbf{e}_i = \begin{pmatrix} 1 \\ 1 \end{pmatrix} \quad (62)$$

then the re-write given by equation (61) is



$$(63)$$

A vector of integer π phase incident on a node of opposite colour copies linearly along the outputs:

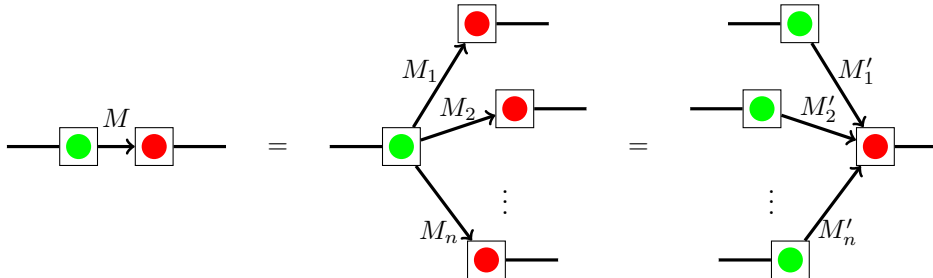


$$(64)$$

Given a partition of an adjacency matrix either over groups of outputs

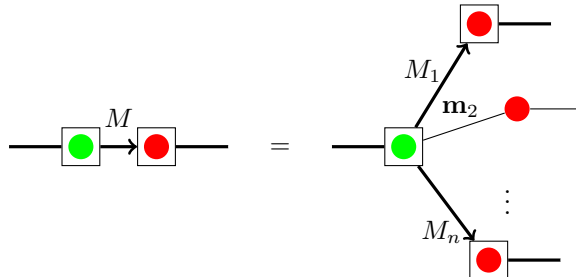
$$\begin{pmatrix} \frac{M_1}{M_2} \\ \frac{M_2}{M_3} \\ \vdots \\ \frac{M_n}{M_n} \end{pmatrix} \quad (65)$$

or groups of inputs, $M = (M'_1 | M'_2 | \dots | M'_n)$. Then a pair of spider boxes can also be partitioned either by input or output boxes:



$$(66)$$

In particular, a single input or output may be extracted. For example,

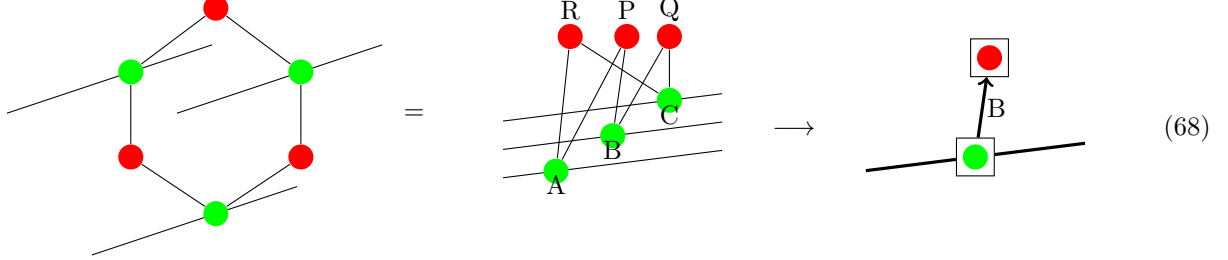


$$(67)$$

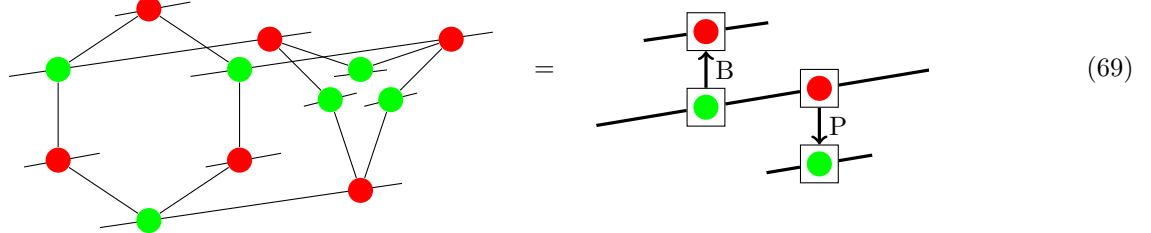
where \mathbf{m}_2 is an adjacency vector.

5.3 A full ring code

Armed with this new notation, we now re-write the ring code using spider boxes and the adjacency matrices. For instance, the bit check ring re-writes as

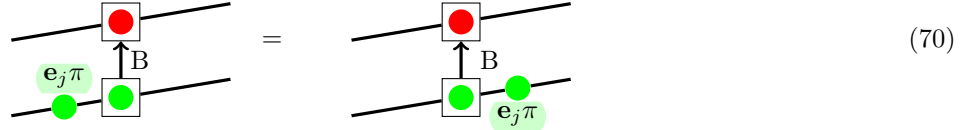


where the code matrix B is given in (39). The ring, before any cross-checks, re-writes from (40) as

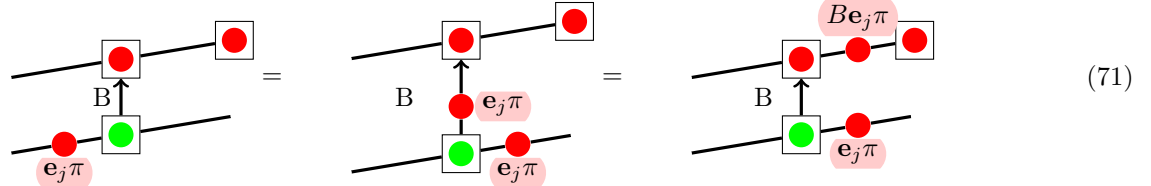


We can now completely characterise the error propagation through this first attempt at a code. In doing so we will see again the two scenarios where the errors cause the code to fail, this time in this much clearer formalism.

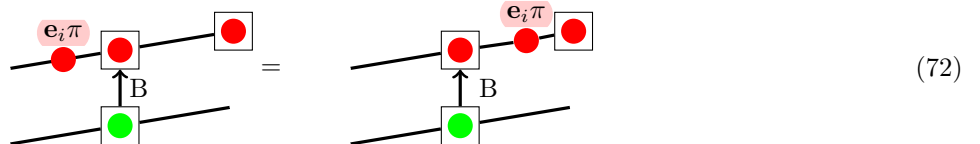
A phase error on the i -th data qubit is represented as



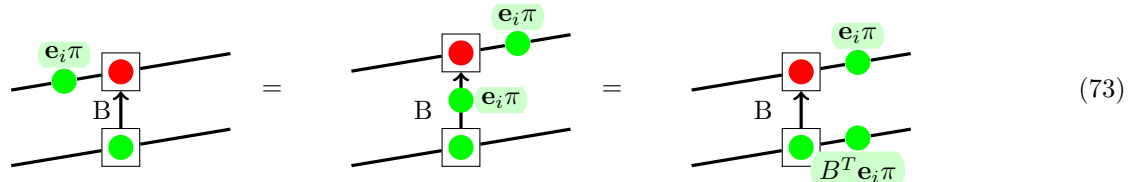
A bit error on a data qubit is picked up by the code, represented as:



Bit errors on the bit-parity check qubit are picked up by the code:

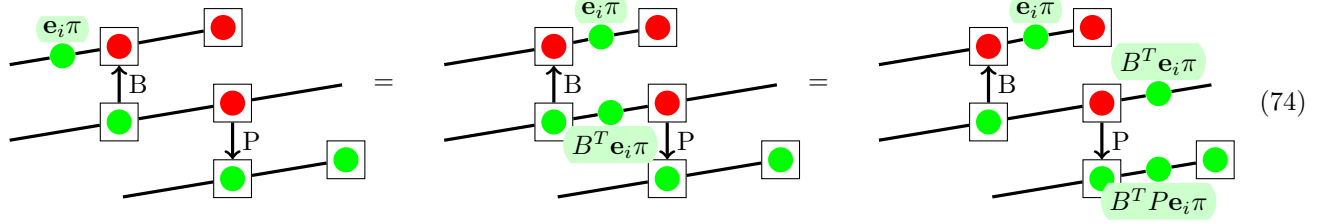


Finally, phase errors on the bit-parity check qubit propagate back through B^T to the data qubits:



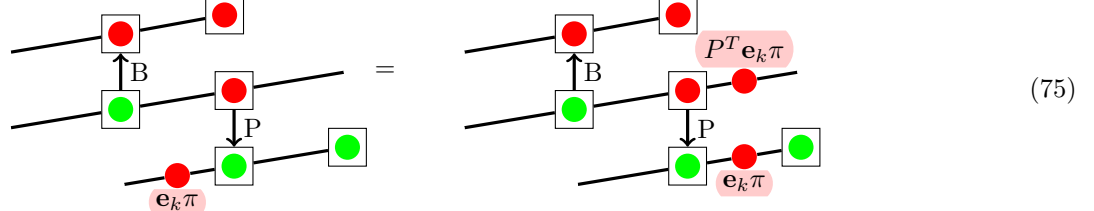
where in all cases the number of wires is determined by the number of qubits in the code. The diagrams for the phase-parity checks with P are identical with colours and arrow direction reversed, and B exchanged for P .

We can now see in detail the problems with the set-up in (40). Firstly, the phase error on a bit-parity check qubit as it comes into the decoder, given originally in (43):



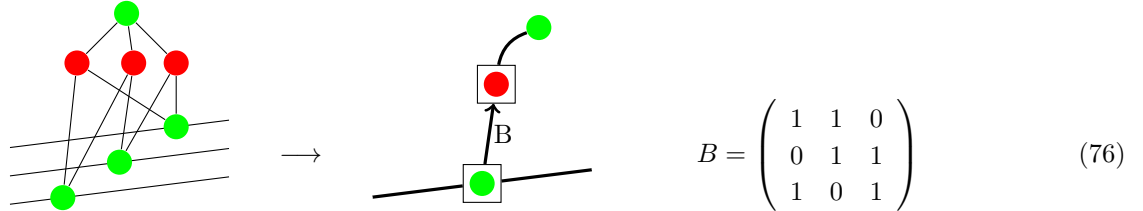
In the new formalism the propagation of the error to (in general) more than one data qubit via B^T is immediately shown. The code will then fail as P can only deal with a single phase error.

The second problem, that of a bit error on a phase parity-check qubit, was shown originally in (44). Here we see much more immediately that the bit error does not propagate at all to the bit parity check, and is therefore undetectable:

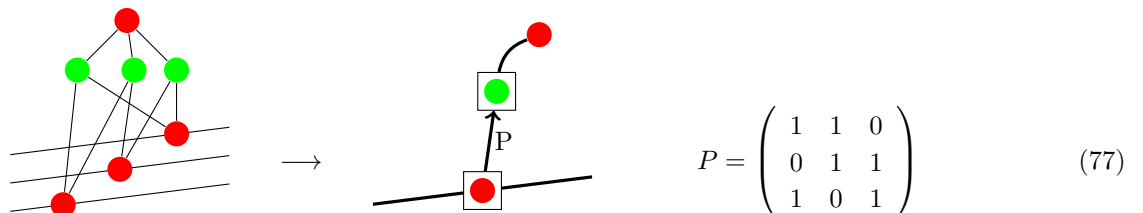


We can now start to solve these issues. We solve them together, and make sure that the solution does not depend on the choice of which type of parity check to perform first. This is done by introducing cross-checking between the bit- and phase- parity qubits: bit-parity check qubits will check for bit errors on phase-parity check qubits, and vice versa.

There are two elements to this cross-checking. Firstly, we add overall-parity checking qubits for each of the bit- and phase- checks. This allows us to tell whether an error originates from the parity check qubits or not. In the ring case we have



and



The second element will be a direct cross-check between the bit- and phase- parity qubits – that is, an addition to the adjacency matrix without additional qubits. There is no guarantee at this point that such a cross-check exists that will make the code work; we investigate this below. Putting both elements together, and using a new

double node for the data qubits, we represent such a full code as



5.4 Finding the cross-check matrix C

We now show how to construct the cross check matrix for the ring code. We then go on to show that this argument in fact generalises for a large set of codes of distance 3. Throughout this section, we restrict to the case where the number of phase check qubits = the number of bit check qubits. Furthermore, the cross-checks are taken as being performed after the other operations of the code.

We introduce some general notation. Let the set of data qubits be $\mathcal{D} = \{\mathcal{D}_i\}$, that of phase-parity check qubits \mathcal{P} , and bit-parity check qubits \mathcal{B} . Furthermore let the overall phase check qubit, (76), be \mathcal{S}_P and the overall bit check qubit, (77), \mathcal{S}_B .

The full adjacency matrix for the code is

$$\begin{array}{cccccc} & \mathcal{D} & \mathcal{B} & \mathcal{P} & \mathcal{S}_B & \mathcal{S}_P \\ \mathcal{D} & \mathbf{0} & B^T & P^T & 0 & 0 \\ \mathcal{B} & B & \mathbf{0} & C^T & 1 & 0 \\ \mathcal{P} & P & C & \mathbf{0} & 0 & 1 \\ \mathcal{S}_B & 0 & 1 & 0 & - & 0 \\ \mathcal{S}_P & 1 & 0 & 0 & 0 & - \end{array} \quad (79)$$

5.4.1 Cross-checks for the ring code

In the ring, $\mathcal{D} = \{A, B, C\}$, $\mathcal{B} = \{P, Q, R\}$, and $\mathcal{P} = \{S, T, V\}$. We now prove the following:

Theorem 1. *For the full ring given by (78), (79), with $P = B$ as in (39), then the addition of cross checks given by the matrix C gives an error correction code of distance $d = 3$, where C is the permutation matrix with no fixed point*

$$\begin{pmatrix} 0 & 1 & 0 \\ 0 & 0 & 1 \\ 1 & 0 & 0 \end{pmatrix} \quad (80)$$

Proof. To prove this we look at the function of the cross-check matrix C . It will enable the \mathcal{B}_i to check the \mathcal{P}_k for bit errors, and vice versa. The action must be two-fold: firstly it must pick up errors directly on the check qubits, as in (75), and secondly it must pick up any errors that have propagated from parity qubits to bit qubits and then back to parity qubits, as in (74).

We take each set of qubits in turn, and show that single errors in each group give a signature of measurements that differs from those of the previous groups.

Data qubits \mathcal{D} . A bit error on a \mathbf{D}_j is detected on the \mathcal{B}_i , as B is a valid classical code by construction. Similarly, a phase error on a \mathbf{D}_j is located by the P_k as P is a valid classical code by construction.

Overall parity check qubits $\mathcal{S}_B, \mathcal{S}_P$. A bit error on \mathcal{S}_B will cause a $+1$ measurement result on \mathcal{S}_B itself. All errors on data qubits cause pairs of $+1$ measurement outcomes, therefore this signature is unique. By symmetry, a phase error on \mathcal{S}_P will give a unique $+1$ measurement signature on \mathcal{S}_P .

A phase error on \mathcal{S}_B will propagate to all the \mathcal{P}_k , where it will cause them all to give the $+1$ measurement outcome. As there are more than two \mathcal{P}_k , this will be a different signature from other errors considered previously,

which give signatures of either single or pairs of $+1$ measurement outcomes. By symmetry, a bit error on \mathcal{S}_P will give a unique signature of $+1$ measurement outcomes on all the \mathcal{B}_i .

Parity check qubits \mathcal{B} and \mathcal{P} . A bit error on a B_i will give a $+1$ outcome for measurements of that qubit. The only signatures previously considered that have a single $+1$ outcome are measured on \mathcal{S}_B and \mathcal{S}_P , neither of which are in \mathcal{B} . Therefore this is a unique signature. By symmetry, a phase error on a \mathcal{P}_k will also give a unique signature of a single $+1$ measurement of itself.

The final cases to consider are those that the original ring code failed under, (74) and (75).

Taking the case of (75) first, a bit error on the k -th phase-parity check qubit will now propagate to \mathcal{S}_B , and also to the \mathcal{B} as $C^T \mathbf{e}_k$. With C as given, this will then give a signature of a single $+1$ outcome on \mathcal{S}_B , and a single $+1$ outcome on a \mathcal{B}_i that is unique for each k . No previously-considered error gives this signature; it is unique.

For the case of (74), a phase error on the i -th bit-parity check qubit will both propagate to \mathcal{S}_P , and also transform as $B^T P \oplus C$ onto the phase-parity check qubits, where ‘ \oplus ’ stands for addition modulo 2 (two errors on the same qubit cancel out). In the case of the ring, $P = B$ and B is given by (39). We have therefore

$$B^T P = B^T B = \begin{pmatrix} 1 & 0 & 1 \\ 1 & 1 & 0 \\ 0 & 1 & 1 \end{pmatrix} \begin{pmatrix} 1 & 1 & 0 \\ 0 & 1 & 1 \\ 1 & 0 & 1 \end{pmatrix} = \begin{pmatrix} 0 & 1 & 1 \\ 1 & 0 & 1 \\ 1 & 1 & 0 \end{pmatrix} = \mathbf{1} \oplus \mathbf{1} \quad (81)$$

where $\mathbf{1}$ is the matrix of all 1s. With C as given by (80), we therefore have

$$B^T P \oplus C = \begin{pmatrix} 0 & 0 & 1 \\ 1 & 0 & 0 \\ 0 & 1 & 0 \end{pmatrix} \quad (82)$$

That is, a phase error on the i -th bit-parity check qubit gives a single $+1$ outcome on a phase-parity check qubit that is unique for each i , and a $+1$ outcome on \mathcal{S}_P . No other type of error previously considered gives this type of signature. It is therefore a unique signature.

Remark: Note that the situation of (74) by itself only needs the addition of \mathcal{S}_B to produce unique signatures. The addition of C is required to solve the situation of (75). While the matrix $C = \mathbf{1}$ is sufficient for the situation of (75), when then added into the case of (74) this matrix transforms the errors as $B^T P \oplus C = \mathbf{1} \oplus \mathbf{1} \oplus \mathbf{1} = \mathbf{1}$, which produces non-unique syndromes for error on different qubits. Hence the requirement for $C = M_p$ to satisfy both scenarios.

There are no other cases to consider so this concludes the proof as all single errors of both types are detectable and give rise to unique measurement signatures. \square

For completeness, we give an example of a full circuit corresponding to this set of cross-checks in Figure 6.

5.4.2 Cross checks for distance 3 codes Hamming codes

With a little work, we can extend this proof to a general construction for distance 3 quantum codes. Note that this is not the only way to produce $d = 3$ CPC codes (and in subsequent sections we will consider numerical search techniques); however, this construction is guaranteed to produce a valid quantum code, and gives a bound on the resources required. The result is encapsulated in the following theorem:

Theorem 2. *Let L be a classical Hamming code with parameters $[n, k, 3]$ and adjacency matrix A_L , where the adjacency matrix relates to the generator matrix as*

$$G = [\mathbf{1} | A'] = \left[\begin{array}{c|c} \mathbf{1} & \frac{A_L}{\mathbf{1}} \end{array} \right]$$

where $\mathbf{1}$ is a row of all 1s. For all such L , with $k > 2$, a valid quantum code may be constructed using the structure of (78) and (79), with $B = P = A_L$ and $C = M_P$, where M_P is the $(n - k) \times (n - k)$ permutation matrix with no fixed point (where $(n - k)$ is the number of parity check bits in the classical code L). This quantum code has parameters $[[2n - k + 1, k - 1, 3]]$.

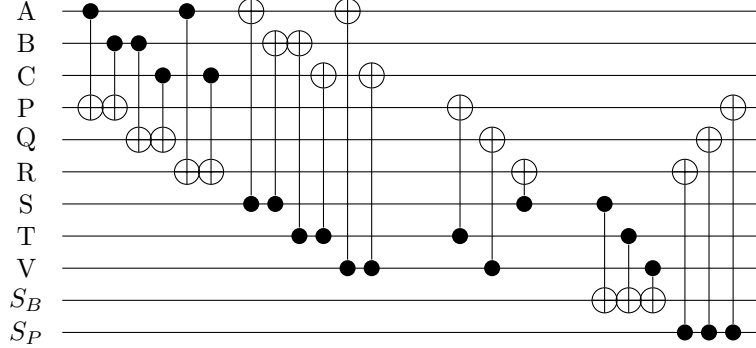


Figure 6: Circuit representation of encoder/decoder for the $[[11,3,3]]$ ring code given by (79) and (78). The three groups of circuits represent (B, P) , the cross-checks C , and the use of the overall parity check qubits S_B, S_P .

Proof. We parallel the proof for the ring code, and take each set of qubits in turn, showing that the construction gives unique signatures for each single-qubit error.

We note that the form of the Hamming code given in the definition of A_L above means that $G_S = [1|A_L]$ is the generator of the ‘shortened Hamming code’ L_s [36, §34-93]. This code is obtained from L by removing the data (qu)bit whose row in the original adjacency matrix A' is all 1s. Equivalently, this data (qu)bit may be considered as set to a fixed ‘zero’ state. By construction, the shortened Hamming code is a valid classical code; that is, A_L generates a valid classical code L_s with parameters $[n - 1, k - 1, 3]$.

Data qubits \mathcal{D} . A bit error on a \mathbf{D}_j is detected on the \mathcal{B}_i , as L_s is a valid classical code. Similarly, a phase error on a \mathbf{D}_j is located by the P_k as L_s is a valid classical code.

Overall parity check qubits S_B, S_P . A bit error on S_B will cause a $+1$ measurement result on S_B itself. All errors on data qubits cause pairs of $+1$ measurement outcomes, therefore this signature is unique. By symmetry, a phase error on S_P will give a unique $+1$ measurement signature on S_P .

A phase error on S_B will propagate to all the P_k , where it will cause them all to give the $+1$ measurement outcome. As the adjacency matrix of the shortened classical code A_L contains no row of all 1s (we have excluded this row by construction of A_L), then there is no single error on a data qubit that can give rise to this set of measurements. This will therefore be a unique signature in this case. By symmetry, a bit error on S_P will give a unique signature of $+1$ measurement outcomes on all the \mathcal{B}_i .

Parity check qubits \mathcal{B} and \mathcal{P} . As before, a bit error on a B_i will give a $+1$ outcome for measurements of that qubit. The only signatures previously considered that have a single $+1$ outcome are measured on S_B and S_P , neither of which are in \mathcal{B} . Therefore this is a unique signature. By symmetry, a phase error on a P_k will also give a unique signature of a single $+1$ measurement of itself.

We now consider the propagation of a bit error on the k -th phase-parity check qubit. As in the ring case and equation (75), in the general case this will propagate both to S_B directly, and to the \mathcal{B} as $C^T \mathbf{e}_k$. With C as given, this will then give a signature of a single $+1$ outcome on S_B , and a single $+1$ outcome on a \mathcal{B}_i that is unique for each k . No previously-considered error gives this signature; it is unique.

A phase error on the i -th bit-parity check qubit, the generalisation of (74), propagates to give a single $+1$ measurement outcome on the S_P , and also propagates to the phase-parity check qubits as $B^T P \oplus C$. We now prove the following lemma:

Lemma 3. *For classical shortened binary Hamming codes, $A_L^T A_L = \mathbf{1} \oplus \mathbf{1}$.*

Proof. If the generator matrix of a code L is $G = [1|A]$ then the generator of the dual code L^\perp is $H = [A^T|1]$. The dual code of a (non-shortened) Hamming code is a simplex code [36]. The generator of a simplex code is obtained by listing all k -digit binary strings and removing the all-zero string. We first show that simplex codes are self-orthogonal; that is $HH^T = 0$, for $k > 2$.

We first show that the $k = 2$ case is not self-orthogonal. The generator (not in standard form) is the list of 2-digit binary numbers as columns, without zero:

$$H_2 = \begin{bmatrix} 0 & 1 & 1 \\ 1 & 0 & 1 \end{bmatrix} \quad (83)$$

it is trivial to show that $H_2 H_2^T \neq 0$, either by direct computation or by noting that the elements of the matrix $H_2 H_2^T$ are the different dot-products of the code words (the rows). As addition is modulo 2, each code word product with itself gives 0 (as there are an even number of 1s in each word) but the off-diagonal elements will be 1 as the two code words share only a single 1.

We now prove self-orthogonality for simplex codes > 3 by induction. The base case is $k = 3$:

$$H_3 = \begin{bmatrix} 0 & 0 & 0 & 1 & 1 & 1 & 1 \\ 0 & 1 & 1 & 0 & 0 & 1 & 1 \\ 1 & 0 & 1 & 0 & 1 & 0 & 1 \end{bmatrix} = \left[\begin{array}{c|c|c} 0^{(3)} & 1 & 1^{(3)} \\ \hline H_2 & 0 & H_2 \end{array} \right] \quad (84)$$

By direct computation $H_3 H_3^T = 0$. All words have an even number of 1s, and each pair of words share an even number of 1s.

For the inductive step, we note that

$$H_k = \left[\begin{array}{c|c|c} 0^{(2^{k-1}-1)} & 1 & 1^{(2^{k-1}-1)} \\ \hline H_{k-1} & 0 & H_{k-1} \\ \hline 0 & 0 & 0 \end{array} \right] \quad (85)$$

The first row (word) contains an even number of 1s as $(2^{k-1} - 1)$ is necessarily odd. By the inductive hypothesis, $H_{k-1} H_{k-1}^T = 0$, therefore all other words also contain an even number of 1s. The diagonal of the matrix $H_k H_k^T$ is therefore all 0s. The first word (first row) also necessarily shares an even number of 1s with each other word. All other pairs of words are made up of two copies of the equivalent code words in H_{k-1} ; by the inductive hypothesis, they therefore share an even number of 1s. Therefore if $H_{k-1} H_{k-1}^T = 0$ then $H_k H_k^T = 0$. Combined with the base case, we can therefore conclude that $H_k H_k^T = 0$ for all $k > 3$.

To complete the proof of the lemma, we note that we can write the generator of a simplex code as $H = [A_L^T | \mathbf{1} | \mathbb{1}]$, by splitting off the column of all 1s. Note further that as a consequence, $[\mathbb{1} | A_L]$ is the generator of the shortened Hamming code. We therefore have

$$\begin{aligned} 0 &= H H^T \\ &= [A_L^T | \mathbf{1} | \mathbb{1}] \begin{bmatrix} A_L \\ \hline \mathbf{1} \\ \hline \mathbb{1} \end{bmatrix} \\ &= A_L^T A_L \oplus \mathbf{1} \oplus \mathbb{1} \\ &\Rightarrow A_L^T A_L = \mathbf{1} \oplus \mathbb{1} \end{aligned} \quad (86)$$

□

Using Lemma 3, for a code with $B = P = A_L$, when a phase error on a \mathcal{B}_i propagates to the \mathcal{P}_k under $B^T P \oplus C$, with C as given this is therefore $A_L^T A_L \oplus M_P = \mathbf{1} \oplus \mathbb{1} \oplus M_P = M'_P$; that is, a different permutation matrix with no fixed point. The phase error on the i -th bit-parity check qubit gives a single +1 outcome on a phase-parity check qubit that is unique for each i , and a +1 outcome on \mathcal{S}_P . No other type of error previously considered gives this type of signature. It is therefore a unique signature.

There are no other cases to consider. Therefore in all cases the construction given takes a classical $[n, k, 3]$ Hamming code and generates a valid distance 3 quantum code from two copies of the shortened form L_s s.t. $[n - 1, k - 1, 3]$. The number of data qubits is $k - 1$ and the number of parity check qubits is $n - k + 2$. Therefore the valid quantum code has parameters $[[2n - k + 1, k - 1, 3]]$. This concludes the proof.

□

We can now see that the $[[11,3,3]]$ ring is a special case of this more general Hamming code construction. The classical code used, with adjacency matrix (39), is the shortened form of the Hamming $[7,4,3]$ code, with the row of all 1 removed from the adjacency matrix. Explicitly, the generator of the dual simplex code (that is the parity check matrix of the $[7,4,3]$ Hamming code) is the list of all 3-digit binary numbers excluding zero:

$$G_d = \begin{bmatrix} 0 & 0 & 0 & 1 & 1 & 1 & 1 \\ 0 & 1 & 1 & 0 & 0 & 1 & 1 \\ 1 & 0 & 1 & 0 & 1 & 0 & 1 \end{bmatrix} = \left[\begin{array}{ccc|ccc} 1 & 0 & 0 & 1 & 1 & 0 & 1 \\ 0 & 1 & 0 & 0 & 1 & 1 & 1 \\ 0 & 0 & 1 & 1 & 0 & 1 & 1 \end{array} \right] = [\mathbb{1} | A_d] \quad (87)$$

in standard form. The adjacency matrix for the Hamming code is therefore

$$A = A_d^T = \begin{bmatrix} 0 & 1 & 1 \\ 1 & 0 & 1 \\ 1 & 1 & 0 \\ 1 & 1 & 1 \end{bmatrix} \quad (88)$$

by removing the row of all 1s, we recover the adjacency matrices for the ring code, (39).

5.4.3 Cross check matrices for general distance 3 codes

We now generalise this result further, for arbitrary distance 3 codes. We do not give a construction for the cross-check matrix, but prove the following theorem that tells us such a cross-check matrix can (almost) always be found.

Theorem 4. *For any pair of $d = 3$ classical codes L_1 and L_2 , with adjacency matrices A_1 and A_2 respectively, there exists a matrix C such that a valid quantum code may be constructed using the structure of (78) and (79), with $B = A_1$, $P = A_2$, and C , provided only that:*

1. L_1 and L_2 have the same number of parity-check (qu)bits, and
2. A_1 and A_2 do not contain a row of all 1s

Proof. The proof is the same as for theorem 2, except that we are replacing the pair of Hamming codes with the arbitrary distance 3 codes L_1 and L_2 . Most elements of the proof go through exactly as before. The requirement that A_1 and A_2 do not contain a row of all 1s eliminates repeated syndromes in the case of a phase error on \mathcal{S}_B , which will propagate to all the \mathcal{P}_k . We are left then with the two types of error propagation that depend most clearly on C : a bit error on the k -th phase-parity check qubit, and a phase error on the i -th bit-parity check qubit.

As before, a bit error on the k -th phase-parity check qubit will propagate both to \mathcal{S}_B directly, and to the \mathcal{B} as $C^T \mathbf{e}_k$. We therefore require that C^T is a valid code matrix: that is, that it has unique columns. C must therefore have unique rows.

Also as before, a phase error on the i -th bit-parity check qubit propagates to give a single +1 measurement outcome on the \mathcal{S}_P , and also propagates to the phase-parity check qubits as $B^T P \oplus C$. We therefore require $B^T P \oplus C$ to be a valid code; that is, it must have unique columns.

We now use the theorem of linear algebra, that any square matrix M may be written $M = N_1 + N_2$ where N_1 and N_2 are invertible [29]. If L_1 and L_2 share the same number of parity (qu)bits, then $B^T P$ will be a square matrix. Therefore restricting to codes L_1 and L_2 with the same number of parity (qu)bits, we have

$$\begin{aligned} B^T P &= N_1 \oplus N_2 \\ B^T P \oplus N_1 &= N_2 \end{aligned} \quad (89)$$

(recalling addition modulo 2). Let $N_1 = C$. We may therefore conclude the following:

1. $C = N_1$ is invertible. It will therefore have unique rows, as required.
2. $B^T P \oplus C = N_2$ is invertible. It will therefore have unique columns, as required.

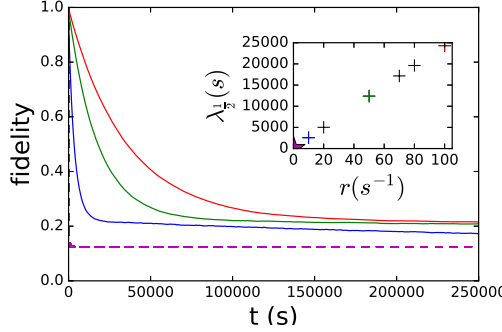


Figure 7: Numerical results for the $[[11, 3, 3]]$ CPC code using a bit-flip error rate of $\epsilon_{\text{bit}} = 0.007 \text{ s}^{-1}$ and a phase error rate $\epsilon_{\text{phase}} = 0.0007 \text{ s}^{-1}$, sampled over random states drawn from the Haar measure. Shown are the same fidelities for $r = 10 \text{ s}^{-1}$ (blue), $r = 50 \text{ s}^{-1}$ (green), and $r = 100 \text{ s}^{-1}$ (red). The unprotected fidelity appears as a dashed magenta line. Inset: Numerical fit of the half life of the fidelity, $\lambda_{\frac{1}{2}}$ versus cycle rate r for the three lines in the main figure plus others. The unprotected ($r = 0$) value of $\lambda_{\frac{1}{2}}$ is represented as a magenta star. Error-bars due to statistical fluctuations are smaller than the depicted lines.

As N_1 and N_2 are known always to exist, C will always exist with the relevant properties for a full quantum code. This concludes the proof. \square

We now prove our final theorem for these general distance 3 codes:

Theorem 5. *For any classical $[n, k, d \geq 3]$ code L with adjacency matrix A_L , a valid quantum code may be constructed using the structure of (78) and (79), with $B = A_L$, $P = A_L$, and some C , provided only that A_L does not contain a row of all 1s. Such a quantum code will have parameters $[[2n - k + 2, k, 3]]$.*

Proof. We use theorem 4, which guarantees the existence of C . Note that any $d \geq 3$ code is also a valid code for correcting a single error, so may be used in this construction. To use theorem 4 here we have $A_1 = A_L$ and $A_2 = A_L$. The structure of (78) and (79) means that the two copies of L give a total of k data qubits, and $2(n - k) + 2$ parity check qubits. The total number of qubits is therefore $2(n - k) + 2 + k = 2n - k + 2$. The overall distance of the quantum code is 3. This concludes the proof. \square

5.5 Numerical test of the $[[11, 3, 3]]$ code

We finish this section by demonstrating the $[[11, 3, 3]]$ ring code in use in a numerical simulation of a real-world example. To do this we choose bit-flip and phase error rates for an existing ion trap system (see [22] and related work), $\epsilon_{\text{bit}} = 0.007 \text{ s}^{-1}$ and $\epsilon_{\text{phase}} = 0.0007 \text{ s}^{-1}$.

We consider the protection of a random three qubit state, drawn from a distribution which obeys the Haar measure. We model the code as performing encoding and decoding with a rate r such that the circuit depicted in Figure 6 is applied $\frac{1}{r}$ times a second. We assume that all gates are fast and therefore errors can only occur within the window E , and we assume that all gates are perfect. Since the effective error rate which each instance of the code sees in this setup is inversely proportional to r , a code which is able to correct single errors will lead to an error rate per cycle which goes like $\frac{1}{r^2}$. The lifetime of a state should go as this error rate divided by the cycle rate r , implying that in this simple model a code which corrects single errors should yield state lifetimes which are proportional to r . We measure state lifetimes by extracting a half-life of the fidelity $\lambda_{\frac{1}{2}}$ by numerically fitting fidelity data with an exponential decay model.

Figure 7 presents numerical results for the $[[11, 3, 3]]$ code. The lifetimes are able to be extended well beyond the limitation of the unprotected lifetime of a single qubit due to bit-flip errors ($\frac{1}{\epsilon_{\text{bit}}} \approx 142 \text{ s}$) and even well beyond those due to the less probable phase errors ($\frac{1}{\epsilon_{\text{phase}}} \approx 1,420 \text{ s}$). Moreover, the lifetime scales linearly with r , confirming that the codes are able to correct arbitrary single qubit errors.

6 Tripartite CPC codes

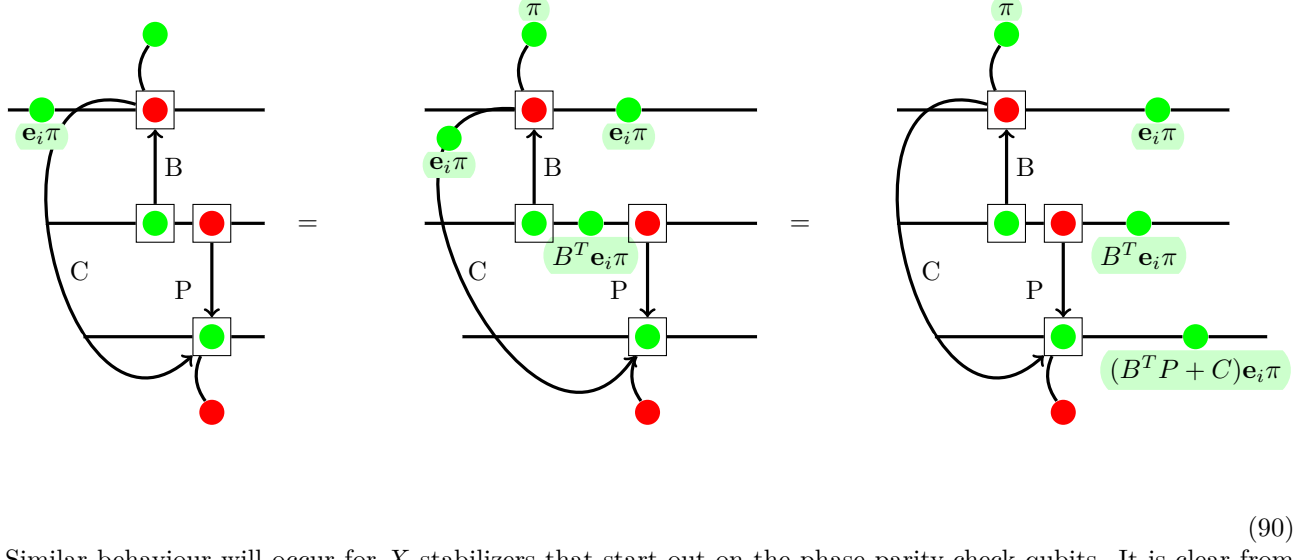
While we considered in the previous section distance 3 codes in detail, the structure of a CPC given in (78) is general for greater distances: the qubits are divided into data, bit-parity check, phase-parity check, and overall parity checks. This structure enables us to use the associated ZX toolkit to build, verify, and analyse new codes. We will also see in later section how this structure enables us to automate a search for codes that returns large numbers of codes that can then be subject to further optimisation based on required characteristics. We also note that the CPC formalism can be easily generalized to use whatever entangling gate a device implements natively and gain a significant improvement in efficiency [39].

In this section, we demonstrate that this framework and graphical toolkit works not only for codes that are encoded and decoded at every cycle, but is also capable of constructing codes in the standard model of quantum error correction. We look first at the dual roles of logical operators and stabilizers, and of error propagation. We then demonstrate how CPC codes using an encode-decode framework correspond to the standard code method of measuring stabilizers. We end the section by showing how CSS codes thereby are shown to be part of the set of CPC codes.

6.1 Stabilizers and logical operators

The CPC construction gives us dual ways of looking at an error correction code, in terms of stabilizers, logical operators, and error propagation. The first was initially hinted at in §4 when we demonstrated how a single coherent parity check element constructs a known stabilizer. We can view a CPC code as starting out with two sets of qubits, data and parity check; the data qubits are in an arbitrary state so have no guaranteed stabilizers; however, the parity-check qubits are in known states ($|+\rangle, |0\rangle$) with known stabilizers. The action of the encoder spreads the support of the stabilizer operators across both data and parity-check qubits. The CPC construction can therefore be seen as using the encoder to construct stabilizers of the code.

We can see directly how stabilizers are formed by considering their ZX representation. Taking (78) as representing an encoder, and assuming that the bit parity qubits are incorporated into the encoder before the phase ones, a stabilizer Z_{B_i} on a bit-parity check qubit is encoded to



Similar behaviour will occur for X stabilizers that start out on the phase parity-check qubits. It is clear from this structure of the encoder that there are no ‘mixed’ stabilizers. Z stabilizers on a bit check qubit encode to strings of Z stabilizers only, and equivalently for X . We can read off these stabilizers from the diagram by recalling that an empty wire is equivalent to the identity operator $\mathbb{1}$, and a green(red) π on a wire is equivalent to a $Z(X)$ operator. Z stabilizers can be written in terms of the adjacency matrices, indexed by the bit-parity check qubit B_i from which it originates:

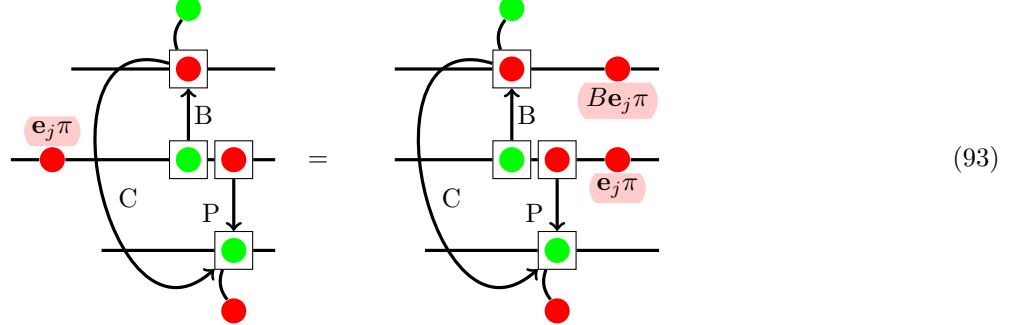
$$Z_{B_i} \rightarrow Z_{B_i} \otimes Z_{S_P} \bigotimes_j (\mathbb{1} + B_{ij}^T (Z_{D_j} - \mathbb{1})) \bigotimes_k (\mathbb{1} + (B^T P + C)_{ik} (Z_{P_k} - \mathbb{1})) \quad (91)$$

where j indexes the data qubits D_j , and k the phase-parity check qubits P_k . Note that, as desired, this expression is structured such that the final two elements each reduce to the identity when the adjacency matrices give zero components in the product (equivalent to a ZX diagram empty rail).

For the X stabilizers, as we are assuming that P happens after B , there will be no propagation through the data qubits to the bit-parity qubits, so

$$X_{P_k} \rightarrow X_{P_k} \otimes X_{S_B} \bigotimes_j (1 + P_{kj}^T (X_{D_j} - 1)) \bigotimes_i (1 + C_{ki}^T (X_{B_i} - 1)) \quad (92)$$

We now turn to the logical operators. The data qubits are not in known stabilizer states; however, we can track a logical operator through the encoder by ZX re-writing in exactly the same way as we can for stabilizers. For example, a X operator on a data qubit D_j transforms through the encoder to a logical operator across the space:

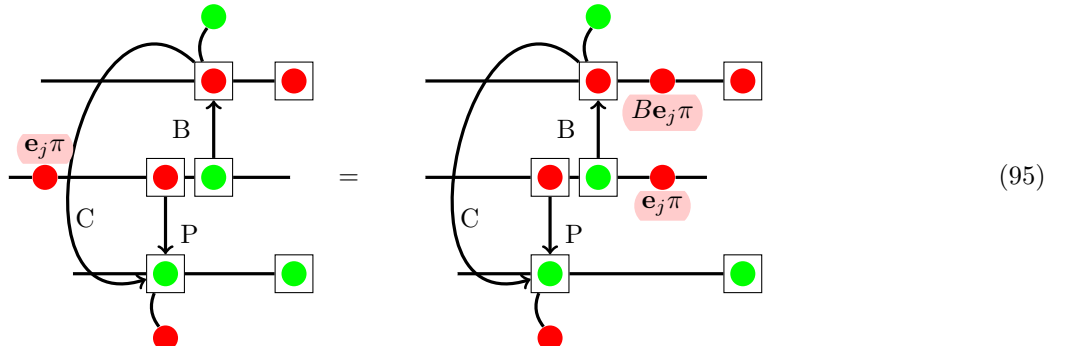


A Z logical operator will propagate to the P_i by symmetry. In operator terms, we therefore have the logical operators in the encoded space:

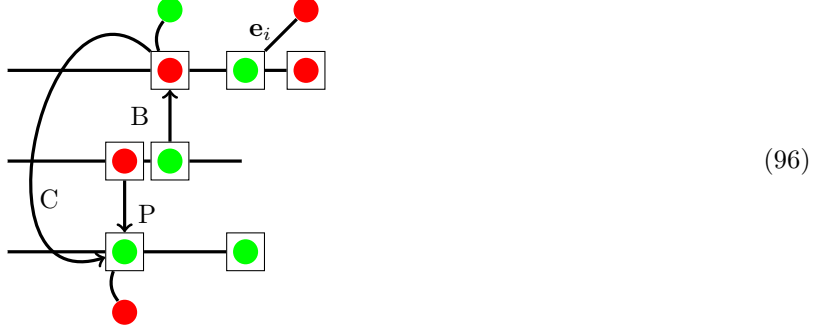
$$\begin{aligned} X_{D_j} &\rightarrow X_{D_j} \bigotimes_k (1 + B_{ji} (X_{B_i} - 1)) \\ Z_{D_j} &\rightarrow Z_{D_j} \bigotimes_j (1 + P_{jk} (Z_{P_k} - 1)) \end{aligned} \quad (94)$$

We now note the first duality, that the code can be viewed as encoding both the logical operators of the data qubits, and the known stabilizers of the parity-check qubits. The data qubits are encoded through the classical codes B and P , whereas the stabilizers are encoded through their inverses combined with the cross checks C . The reversibility of the basic CPC operation means that these operators all preserve their orthogonality: the encoded operators will all be orthogonal as the original ones are.

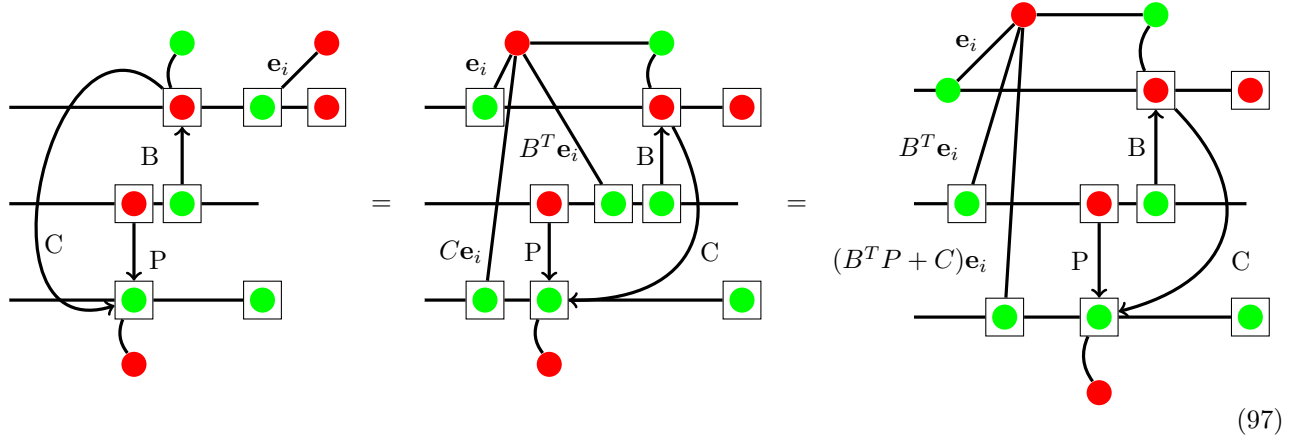
We get our second duality by considering equations (70)–(75), and recalling that the encoder is the time-reversal of the decoder. We can see that errors propagate through the decoder in the time-reversal of the way that logical operators and stabilizers propagate through the encoder. Consider now a decoder, and a single error in the encoded space, for example on an encoded data qubit, a D_i . We make explicit that this is a decoder by putting in the post-decode measurements of the parity qubits:



The measurement in the computational basis of the relevant \mathcal{B}_i (top rail measurement) will now pick up this error. However, let us now consider this measurement from a corresponding point of view where it happens before the decoder. What (set of) measurement(s) before the decoder corresponds to a measurement of a \mathcal{B}_i after the decoder? To find this, we first extract out a single measurement on the i -th output bit-parity qubit. Recall that definition (53)) gives us a way to do this by connecting a single node to a spider box with the unit vector corresponding to i :



We now re-write so that it pulls ‘backwards’ through the decoder:



This measurement of the Z operator on \mathcal{B}_i after the decoder then maps to a measurement of a composite Z operator before the decoder. The adjacency vectors \mathbf{e}_i , $B^T \mathbf{e}_i$, $(B^T P + C)\mathbf{e}_i$, describe the collection of nodes in their respective target spider boxes. The mapping between the diagram and the composite Z operator is then an identity on each empty wire, and a Z operator whenever the adjacency vectors give a node on a wire. That is,

$$Z_{B_i} \rightarrow Z_{B_i} \otimes Z_{S_P} \bigotimes_j (\mathbb{1} + B_{ij}^T (Z_{D_j} - \mathbb{1})) \bigotimes_k (\mathbb{1} + (B^T P + C)_{ik} (Z_{P_k} - \mathbb{1})) \quad (98)$$

We notice that this is exactly the same expression as that for the encoded stabilizer that originated at \mathcal{B}_i . This can also be seen directly from the diagrams: the positioning of π phases on spider nodes in (90) are determined by identical expressions to the adjacency vectors of the transformed measurement in (97). We can therefore conclude that a bit value measurement on a \mathcal{B}_i after the decoder is identical with a bit value measurement of the corresponding stabilizer (91) before the encoder. The corresponding statement for X operators on the \mathcal{P}_i follows by symmetric arguments.

We now have a full set of these dualities. A logical operator of a data qubit transforms through the encoder in the same way as an error on that data qubit in the encoded space transforms through the decoder, equations (93) and (95). An error on a parity-check qubit does **not** transform like a stabilizer (as the encode and decode are not identical); however, a measurement of an operator on a parity-check qubit after the decoder does. That is, a parity measurement after the decoder transforms through the decoder in the same way as stabilizer on that parity-check qubit is mapped through the encoder into a stabilizer of the encoded space.

We can now use these correspondences to prove the following theorem:

Theorem 6. *A valid CPC code constructed using the encode-decode framework corresponds to a valid stabilizer code where stabilizers are measured on the encoded space. The stabilizers in such a model are exactly the stabilizers of the CPC code, and the decode tables are identical.*

Proof. To prove this, we need to show that measuring these stabilizers gives the same syndrome for any correctable error as does the equivalent measurement of the single parity qubits after decode in the encode-decode model. By construction, we assume we have a valid CPC code in an encode-decode framework. That is, for codes of distance d we can detect and locate up to $d/2$ errors by parity qubit measurements after the decoder.

Let us consider a particular set of errors $\Lambda = \{\lambda_i\}$ that is decoded to a unique syndrome $S_\Lambda = \{s_j\}$, where each s_j is the outcome of measuring operator M_j (either X on \mathcal{P}_j or Z on \mathcal{B}_j , depending on whether the j th parity check qubit is in \mathcal{P} or \mathcal{B}). An equivalent situation is found by not propagating the errors, but rather transforming the measurements backwards through the decoder. Measuring the single operator M_j in the unencoded space is equivalent to measuring the set of operators $\{M_k\}_j$ in the encoded space.

If the subspace spanned by the $\{M_k\}_j$ is orthogonal to the other subspaces spanned by $\{M_k\}_{k \neq j}$, then by linearity the set of measurements $\{M_j\}$ on parity qubits after the decoder transforms to a set of measurements in the encoded space $\{\{M_k\}_j\}$ that span a subspace orthogonal to those spanned by $\{\{M_k\}_{l \neq j}\}$. That is, an error set $\Lambda = \{\lambda_i\}$ that has measurement syndrome $S_\Lambda = \{s_j\}$ on operators $\{M_j\}$ when decoded, will have measurement syndrome $S_\Lambda = \{s_j\}$ on operators $\{\{M_k\}_j\}$ on the encoded space. By equations (91), (92), (94), each M_j transforms backwards through the decoder to a stabilizer of the encoded state. Therefore the set $\{\{M_k\}_j\}$ is a set of measurements of stabilizers of the encoded state, and will give the same syndrome for an error set as measuring the corresponding operator after a decoder.

Therefore a CPC code constructed using the encode-decode framework can be viewed equivalently as a stabilizer code, with the same syndromes for errors. \square

For completeness, we note that the logical operators will also ‘pull back’ through the decoder in a similar way, to the same form as that given by pushing them forwards through the decoder, as in equations (94). Measuring the state of a data qubit is therefore done equivalently by measurement of the decoded qubit, or by measuring the encoded logical operators, as in standard practise with stabilizer codes.

6.2 CPC construction for CSS codes

The second way of considering the CPC framework comes directly from Theorem 6: as a theoretical structure for constructing stabilizer codes. The encoders and syndrome extraction can be either implemented directly, or else using standard fault-tolerant techniques such as entanglement via GHZ states [35]. The framework brings a number of advantages to the search and analysis of stabilizer error correction codes. The structure allows us to search for codes based on known classical codes, and (as we have demonstrated above) prove general results about how to construct them. The tripartite structure given so far for the codes is theoretically useful, but we will see that more generalised structures are possible, including generalised parity checks (not restricted to separate X -only and Z -only stabilizers). Furthermore, the ZX calculus machinery allows us to track errors and logical information flow, giving a powerful tool for the design and analysis of codes (including ones that can be tailored to match hardware). It also, as we will see in subsequent sections, gives us a necessary structure to search for codes – including using numerical discovery that can produce many thousands of possible codes for even implementations with a small number of qubits.

Theorem 6 therefore allows us to treat the CPC construction as a general quantum error correction framework. We now demonstrate a first example of this by giving the translation between CSS codes and one form of CPC construction. We can use the expressions for the set of stabilizers generated by the encoder, (91) and (92), to show this exact mapping for CPC codes with the tripartite structure we have been considering in this section.

A set of generators for a stabiliser subgroup (up to signs) can be written in symplectic notation as a matrix of the form:

$$G = (G_Z | G_X) \tag{99}$$

where G_X and G_Z are binary matrices where the (i, j) -th entry tells you whether a Z or an X is applied (for G_Z

and G_X respectively) to the j -th qubit of the i -th stabilizer [38]. In this form, standard CSS codes are written

$$G_{CSS} = \left(\begin{array}{c|c} G_Z & 0 \\ \hline 0 & G_X \end{array} \right) \quad (100)$$

(For example, for the Steane [[7,1,3]] code, $G_{X,Z}$ are both the parity check matrix of the classical [7,4,3] Hamming code.)

Let us now look at the tripartite CPC stabilizers given by (91) and (92). The Z stabilizer generators can be written

$$\begin{array}{ccccc} B_K & P_K & D_j & S_B & S_P \\ B_i & (\mathbb{1}_{ik} & (B^T P + C)_{ik} & B_{ij}^T & 1 \ 0) \end{array} \quad (101)$$

where they are indexed by the bit-parity check qubit B_i from which they originated. Similarly, the X stabilizer generators can be written

$$\begin{array}{ccccc} B_K & P_K & D_j & S_B & S_P \\ P_i & (C_{ik}^T & \mathbb{1}_{ik} & P_{ij}^T & 0 \ 1) \end{array} \quad (102)$$

The full set of generators for a tripartite CPC code can therefore be given by

$$G_{trip} = \left(\begin{array}{cccc|cccc} \mathbb{1}_{ik} & (B^T P + C)_{ik} & B_{ij}^T & 1 \ 0 & 0 & 0 & 0 & 0 \\ 0 & 0 & 0 & 0 & C_{ik}^T & \mathbb{1}_{ik} & P_{ij}^T & 0 \ 1 \end{array} \right) \quad (103)$$

We can conclude two things immediately. First, tripartite CPC codes are CSS codes – and *vice versa*. For any CSS code, given by (100), we can perform Gauss-Jordan elimination (and possibly re-shuffle some columns) to obtain a new set of generators of the form:

$$G_{CSS} = \left(\begin{array}{cccc|cccc} \mathbb{1} & G'_Z & G''_Z & 1 \ 0 & 0 & 0 & 0 & 0 \\ 0 & 0 & 0 & 0 & G'_X & \mathbb{1} & G''_X & 0 \ 1 \end{array} \right) \quad (104)$$

Then, letting $B := (G''_Z)^T$, $P := (G''_X)^T$, and $C := G'_X$, we obtain the equivalent CPC code, as long as this preserves $G'_Z = B^T P + C$.

Secondly, this means that the tripartite CPC framework gives a method by which CSS codes can be constructed from known classical codes that differ significantly from the usual CSS framework. Classical codes have previously had to be carefully chosen for CSS codes so that the generators will commute. This is one reason why the CSS framework is non-constructive: there is no way to start from a favourite classical code and turn it into a quantum one. Codes must be selected with care and simply tested to see if the generators commute. By contrast, in the CPC construction we can start from *any* classical code and create a quantum one, by finding the relevant cross check matrix C .

6.3 CPC codes and fault tolerance

Theorem 6 shows that the CPC framework can be considered in two equivalent ways, each with their separate use. Firstly it can be considered as a method of constructing small codes, with the encode and decode operations representing physical operations performed on the system. A ‘round’ of correction entails moving to and from the code space. Secondly, it can be used as a framework in which to construct, search, and analyse stabilizer codes for use with standard stabilizer measurement and syndrome extraction techniques. We now review the fault tolerance properties of CPC codes in this framework.

The first point we note is that the codes constructed tolerate errors on any of the data qubits and any of the parity-check qubits during the wait cycle. When it comes to decoding or syndrome extraction, when the CPC framework is used to construct standard stabilizer codes, then syndromes can be extracted using stabilizer measurements on syndrome qubits in standard fault-tolerant ways.

However, we can also see from the proofs of Theorems 1 and 2 that the codes are tolerant to faults when decoded directly. The cross-check matrices are constructed explicitly with two requirements:

- Single errors on *any* qubits (data or parity check) give unique syndromes of measurements of parity check qubits.
- Single errors on any qubits do not lead to undetectable errors on data qubits after corrections are applied.

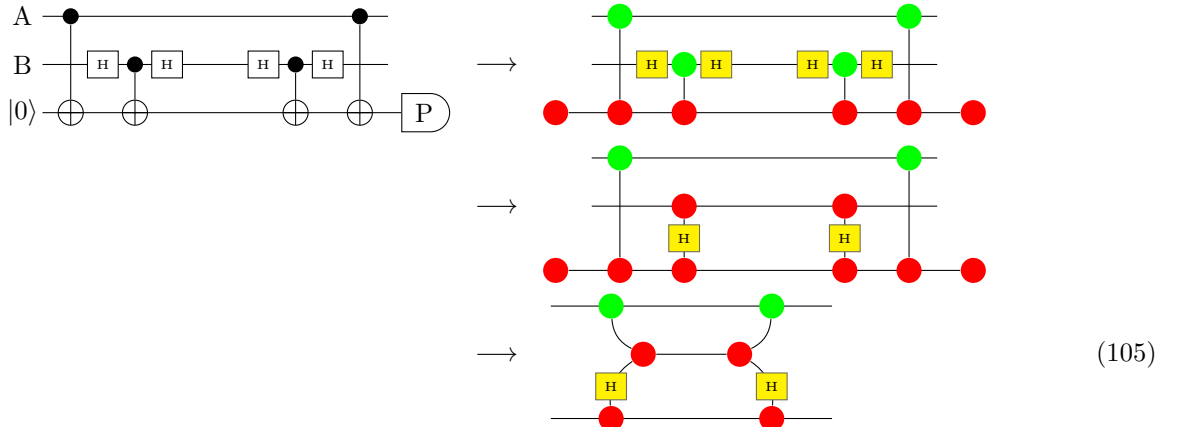
This satisfies what we want of a code, in the absence of formal fault tolerance. Although single errors can duplicate, the codes are constructed so that the patterns of multiple errors will be uniquely recognised and corrected. By tracking the individual error propagation routes, using the tools the *zx* calculus gives us, we produce low-overhead codes that are **de facto fault tolerant**. The difference with complete fault tolerance is that, for the codes and analysis presented in this paper, we have not considered errors occurring during the operation of the decoder; that is, between the different gates in the decoder (we have also not, of course, considered gate errors at all). The analysis in these cases will be further work.

7 Generalised CPC codes

We have considered up to now codes where X and Z errors are detected on separate sets of parity check qubits. This tripartite construction gives rise to codes with separation between stabilizers that are all X or all Z . We now complete the formalism by adding the ability to express general codes, by introducing a combined parity check gadget capable of determining combinations of both types of error.

7.1 Combined parity checking

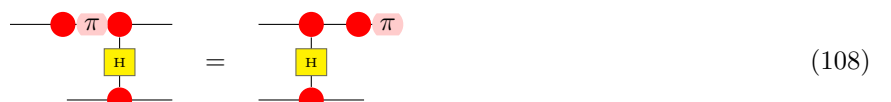
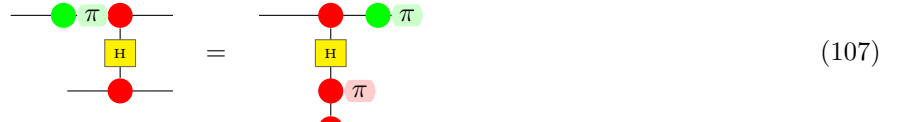
In order to construct a *generalised parity check*, we consider the following gadget that will compare the parity of the $Z \otimes X$ operator on qubits A and B at the beginning and end of the time in which errors occur:



We term the CNOT with Hadamards on the control leg the *conjugate propagator*:

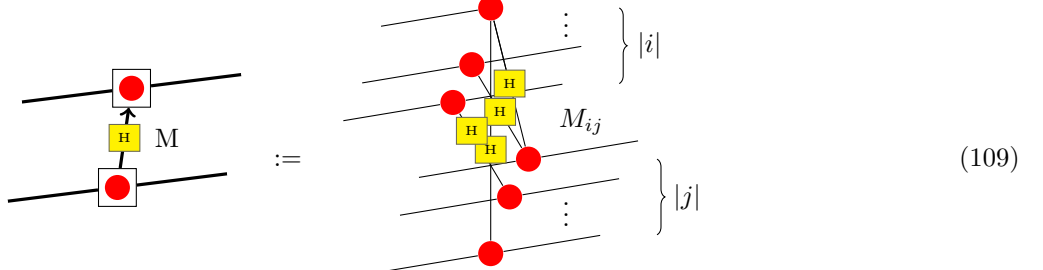


Error propagation through the conjugate propagator is easily seen:

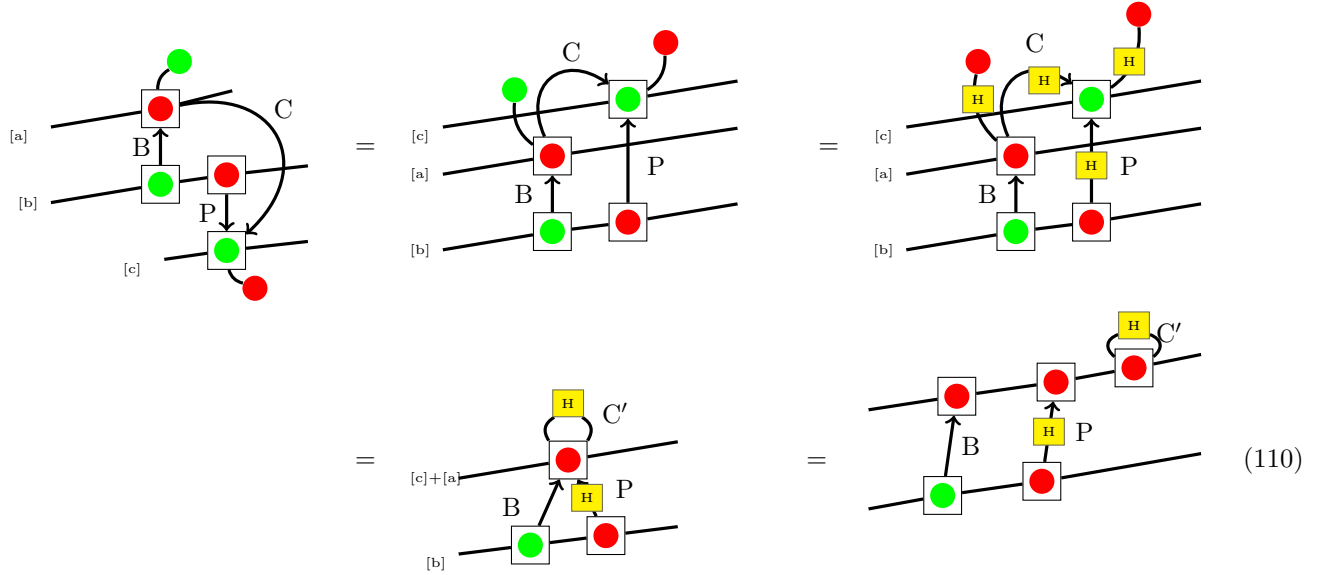


This shows its action as a NOT operation controlled on the parity of the X operator rather than Z (i.e. that the NOT is applied when the control is $|-\rangle$ rather than $|1\rangle$).

As with the bit and phase parity checks, (48), we can define new notation for a number of conjugate propagator actions determined by the matrix M . This can act interchangeably with a set of phase-parity checks (as long as the parity qubits are now initialised in $|+\rangle$ rather than $|0\rangle$).



The crucial difference with the phase-parity check defined by (48) is that the target parity qubits can be the same as those used by some bit-parity check matrix. The two together will determine a ‘mixed’ parity check, which translates to a stabilizer on the encoded space that is a combination of both X and Z operators. That is, combined bit- and phase- parities are stored on a single parity check qubit. By re-writing (78), we can give the normal form of these generalised CPC codes:



The final step is now the ‘block’ form for generalised codes. The penultimate re-write is simply the spider law, and then the final one splits out the cross-checks between parity-check qubits (combined top rail) again as the separate adjacency matrix C' . For tripartite codes, which we started with in this rewrite sequence, B and P act on distinct subsets of parity-check qubits. For the generalised codes, they can act on the same qubits; hence the final ‘block’ form in (110), where the single rail for all parity-check qubits shows that some of the target qubits of B and P are identical. The cross-checks C' (which we will re-label to C again hereafter) act between any combination of parity-check qubits.

The adjacency matrices that determine the checks are given as before by B , P , and C ; however, the full adjacency matrix will not have the same form as (79) as we have combined parity-check qubits. The full matrix for this case is also more complicated as the bit and phase checks can act on the same data qubits. With a possible abuse of notation, we use a complex adjacency matrix where real components are bit checks (through CNOTs) and imaginary components check phase information through the conjugate propagator:

$$\begin{array}{cc} \mathcal{D} & \text{Check} \\ \mathcal{D} & \begin{pmatrix} 0 & B^T + iP^T \\ B + iP & iC \end{pmatrix} \end{array} \quad (111)$$

This full adjacency matrix is given for illustrative purposes only; we will use the individual B, P, C matrices from here on.

The CPC formalism is now capable of constructing generalised stabilizer codes. We now turn to searching the space of these codes defined in this full formalism.

7.2 Automated design and search

This generalised CPC formalism gives a framework in which a large number of codes can be constructed. This is ripe for search by automated techniques. This will enable us to find, for instance, codes that give the greatest number of logical qubits for a given availability of physical qubits. This is one of the key issues in current quantum computing technology. The automated techniques outlined in this section are also capable of being combined with more sophisticated search and optimization strategies, in order to produce codes to order based on hardware and desired optimality conditions.

7.2.1 Matrix representation of errors

To design codes in an automated way, we need a representation which can be efficiently processed by a computer. We now translate the block-check formalism of (110) into matrix manipulation. In addition to the matrices for bit- and phase- checking, we also need a matrix-algebraic representation of errors, and the way in which they propagate, as seen from the ZX diagrams.

Assuming an $[[n, k, d]]$ code (where d is initially not known), we represent the different types of errors as four boolean column vectors, where a 1 represents an error and 0 represents no error. The first vector, $\vec{\mathcal{E}}_{b,d}$, is a vector of bit flip errors on the data qubits, and therefore of length k (the number of data qubits). The second vector, $\vec{\mathcal{E}}_{p,d}$, represents phase errors on the data qubits and is therefore also of length k . The second two vectors $\vec{\mathcal{E}}_{b,c}$ and $\vec{\mathcal{E}}_{p,c}$ are both of length $n - k$ (the total number of parity-check qubits) and represent bit and phase errors respectively on the parity-check qubits. The parity check matrices B and P are both of size $(n - k) \times k$, and C is a symmetric $(n - k) \times (n - k)$ matrix, $C = C_u + C_u^T$ where C_u is a strictly upper triangular matrix.

7.2.2 Matrix representation for syndrome extraction

An important point to note about the generalised formalism is that all parity check qubits are measured out in the computational basis. Both bit- and phase- errors convert to bit error syndromes on the parity check qubits (the latter via the action of the conjugate propagator), and we now give a way of representing these syndromes in matrix form.

Firstly, we must consider direct propagation of bit flip error information from the data qubits. This can be represented by the dot product $B \cdot \vec{\mathcal{E}}_{b,d}$ (recalling that \mathcal{E} are column vectors). Similarly, propagation of phase error information can be represented by $P \cdot \vec{\mathcal{E}}_{p,d}$.

Bit errors on the parity check qubits are directly represented by the vector $\vec{\mathcal{E}}_{b,c}$. Phase errors on the parity check qubits propagate to bit errors through the cross checks, as $C \cdot \vec{\mathcal{E}}_{p,c}$. We also need to consider indirect propagation of phase errors on the parity check qubits. This information is first propagated to the data qubits via the phase checks (the conjugate propagator acts symmetrically) and then propagated back via the bit checks. This indirect propagation is represented as $(P^T \cdot B) \cdot \vec{\mathcal{E}}_{p,c}$.

We now recall that bit flips on the parity check qubits will sum modulo 2, so the vector of measured syndrome values \vec{S} is

$$\vec{S} = [B \cdot \vec{\mathcal{E}}_{b,d}] \oplus [P \cdot \vec{\mathcal{E}}_{p,d}] \oplus [\vec{\mathcal{E}}_{b,c}] \oplus [(C \oplus P^T \cdot B) \cdot \vec{\mathcal{E}}_{p,c}] \quad (112)$$

where \oplus again represents the addition modulo 2.

Equipped with the ability to calculate syndromes, the task of determining how many errors a code can tolerate is a matter of testing how many errors can be included while still preserving unique syndromes. Because \vec{S} can be calculated efficiently, it is therefore straightforward to test the code distance of any code numerically, giving a powerful tool for automated code design.

7.2.3 Small codes from random search

The simplest method for automated code design is to randomly search the CPC code space. This is done by populating the matrices B , P and C_u randomly, and then checking all the syndromes for each code. We keep codes for which the desired code distance is achieved. For simplicity we use an error model comprising Pauli X and Z errors only (so a Pauli Y error is produced only by two simultaneous errors).

Using these methods, we found the following $[[9, 4, 3]]$ code:

$$B = \begin{pmatrix} 1 & 0 & 0 & 1 \\ 1 & 1 & 0 & 1 \\ 0 & 0 & 1 & 0 \\ 1 & 0 & 0 & 0 \\ 1 & 1 & 1 & 1 \end{pmatrix}, \quad (113)$$

$$P = \begin{pmatrix} 0 & 1 & 1 & 1 \\ 0 & 0 & 0 & 0 \\ 0 & 0 & 1 & 0 \\ 1 & 1 & 0 & 0 \\ 1 & 0 & 1 & 1 \end{pmatrix}, \quad (114)$$

$$C_u = \begin{pmatrix} 0 & 0 & 0 & 0 & 1 \\ 0 & 0 & 1 & 1 & 0 \\ 0 & 0 & 0 & 1 & 0 \\ 0 & 0 & 0 & 0 & 0 \\ 0 & 0 & 0 & 0 & 0 \end{pmatrix}. \quad (115)$$

This technique in fact finds many such codes. The search technique is straightforward. Therefore, rather than listing the codes, we instead give the GNU Octave program (less than 100 lines) in Appendix C. On a single core of a standard desktop computer, the given program generates around 2,500 $[[9, 4, 3]]$ codes in 10 minutes. Approximately 0.2% of all randomly generated $[[9, 4, d]]$ codes are able to correct single errors (d of at least 3). A Python version of this code is also available through [7].

This simple search technique for CPC codes is not confined to distance 3. In Appendix D we give the GNU Octave program which finds codes of arbitrary distance by random search. This program is also relatively simple, and again is less than 100 lines. In Appendix F we give the matrices for a $[[16, 4, 5]]$ code and $[[18, 4, 5]]$ code thus discovered (again using an error model consisting of elementary Pauli X and Z errors only). A Python version of this code is also available through [7].

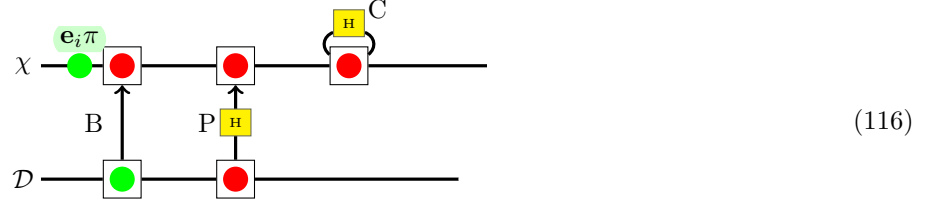
We would expect the methods given here to also interface well with more sophisticated search methods. These include simulated annealing [27] or some of its more advanced variants, parallel tempering [15, 43] and population annealing [25, 33, 44], or by genetic algorithms [18]. To try to increase code distance, the cost function used in these techniques could be chosen to be proportional to the number of error patterns with one more error than the code is currently able to correct (which yield non-unique syndromes). Penalties related to hardware constraints could also be added – for example penalties on gates based on the separation between the qubits on which they are performed.

7.3 Stabilizers for generalised codes

As in the case of tripartite codes, (91) and (92), we can extract lists of code stabilizers from the generalised code diagram (110). Given the search techniques outlined above, this also gives a method of finding stabilizer tables for the codes generated by searching.

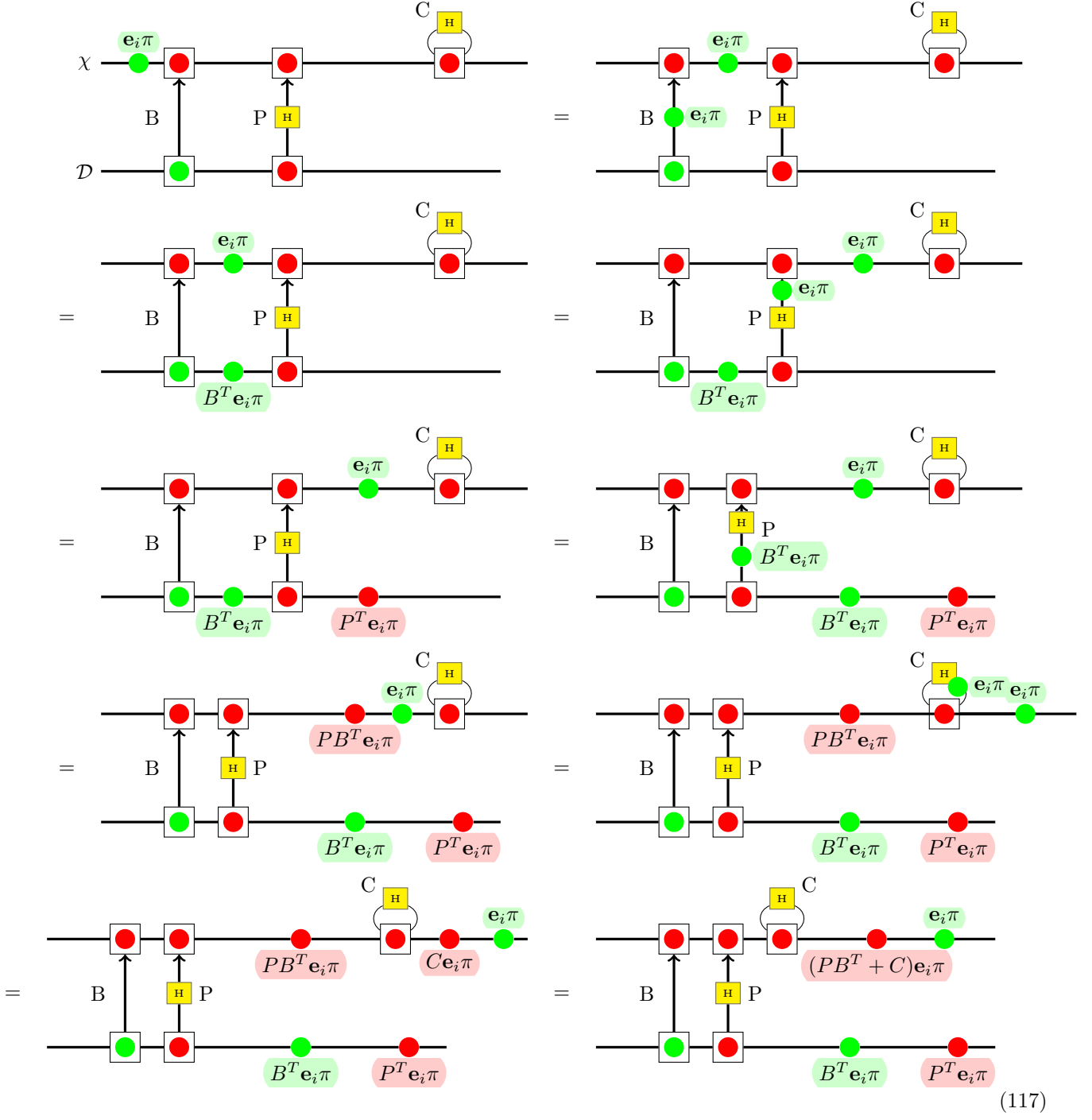
Code stabilizers in the generalised case are all transformations of Z_i stabilizers on the parity-check qubits, which we will denote χ_i , as in the generalised case all parity-check qubits are initialised and measured in the computational

basis. The i -th stabilizer is found by re-writing the diagram



(116)

Giving all steps in full, this re-write procedure is:



(117)

In full (c.f. the similar expressions in the case of tripartite codes (91),(92)), the resultant stabilizer is then

$$\begin{aligned} Z_{D_i} \rightarrow & (Z_{D_i}) \cdot \bigotimes_n (\mathbb{1} + C_{in}(X_{\chi_n} - \mathbb{1})) \cdot \bigotimes_k (\mathbb{1} + (B^T P)_{ik}(X_{\chi_k} - \mathbb{1})) \\ & \cdot \bigotimes_j (\mathbb{1} + P_{ij}^T(X_{D_j} - \mathbb{1})) \cdot \bigotimes_m (\mathbb{1} + B_{im}^T(Z_{D_m} - \mathbb{1})) \end{aligned} \quad (118)$$

where this is an operator on $\mathcal{H}_D \otimes \mathcal{H}_\chi$. The product “.” is used as the elements of the expression on \mathcal{H}_D and \mathcal{H}_χ will in general have overlapping support.

As a first use of this expression, we can directly calculate the stabilizers of the $[[9, 4, 3]]$ code discovered in the previous section:

$$\begin{array}{cccccccccc} Z & X & X & Y & Y & 1 & 1 & X & X \\ Z & Z & 1 & Z & 1 & Z & X & X & 1 \\ 1 & 1 & Y & 1 & X & X & Y & X & X \\ Y & X & 1 & 1 & 1 & X & X & Y & X \\ Y & Z & Y & Y & 1 & 1 & X & 1 & Y \end{array} . \quad (119)$$

The stabilizer tables for all codes presented here can be found in appendix F. We also provide a short GNU Octave program for converting matrices to stabilizers automatically in Appendix E. A Python version of this code is also available through [7].

8 Encoded computation

So far we have concentrated on generating the CPC framework for codes for quantum memory. We now look at the addition of computation to the formalism. Performing full quantum computation is a complex procedure; we concentrate here on outlining the formalism for Clifford operations only.

We have seen that the CPC framework covers (amongst others) CSS codes. It is therefore possible to perform encoded computation in the standard way. However, one major advantage of the CPC framework is that we have a great deal of control over structuring codes to deal with specific situations that we want to use them for. We can put this to use in finding efficient ways of performing encoded gates that will be particularly of use in small-scale scenarios, where resource optimization is the overriding concern.

8.1 Modifying the encoder

The key element to our new procedure for encoded computation is the modification of the encoding circuit to prepare the qubits for the Clifford operation. This then permits the procedure to be used in either the encode-wait-decode scenario, or else the standard encode-stabilizer measurement one. By changing the encoder, the procedure simultaneously sets up the code space and prepares it for the operation. The subsequent decoder (which is not changed) determines errors in the same way as when the code is used for memory.

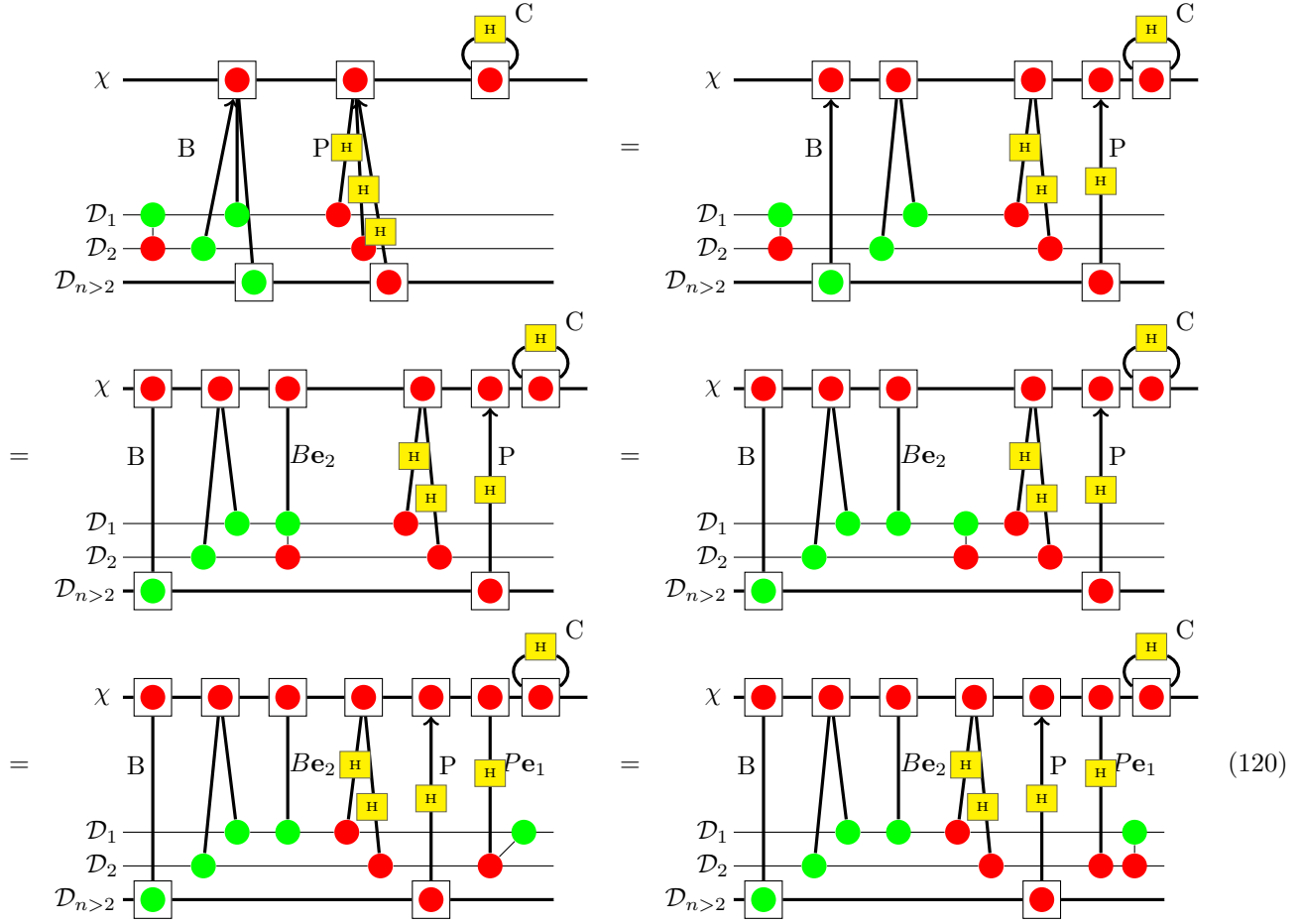
In Appendix G we perform such a modification of the encoder explicitly in Quantomatic for the ring code. In order to generalise this to a procedure for Clifford unitaries on any CPC code, we prove the following theorem:

Theorem 7. *Any unitary operation belonging to the Clifford group can be performed in the logical space between two data qubits in a CPC code by modifying the preparation state of the parity-check qubits and the B, P, C matrices that define the encoder only. Specifically, the decoder is not modified.*

Proof. The generators of the Clifford group are the Hadamard, CNOT and phase gate $S = \text{diag}(1, i)$ [21]. It is sufficient then to show that each generator passes through a CPC encoder modifying only the B , P , and C matrices, and retaining its own structure.

CNOT gate. The operation of a logical CNOT in the encoded space must be equivalent to the action of a single CNOT between the raw, unencoded qubits. We can therefore find the encoded procedure by ‘pushing’ the CNOT operation on data qubits D_i and D_j through the encoder as re-writes. Using (67), we split out the data

qubits that the CNOT operates on (here, without loss of generality we take them to be the first two in the spider box) from the rest of the data qubits, giving

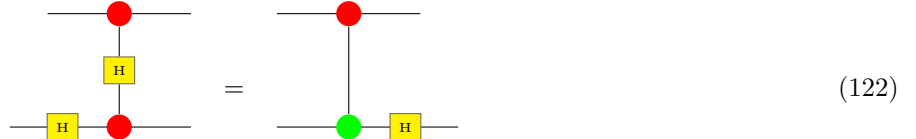


The modified encoder that prepares for the CNOT is therefore given by transforming the bit and phase parity check matrices as

$$B_{k1} \rightarrow B_{k1} \oplus B_{k2}, \forall k ; \quad P_{l2} \rightarrow P_{l2} \oplus P_{l1}, \forall l \quad (121)$$

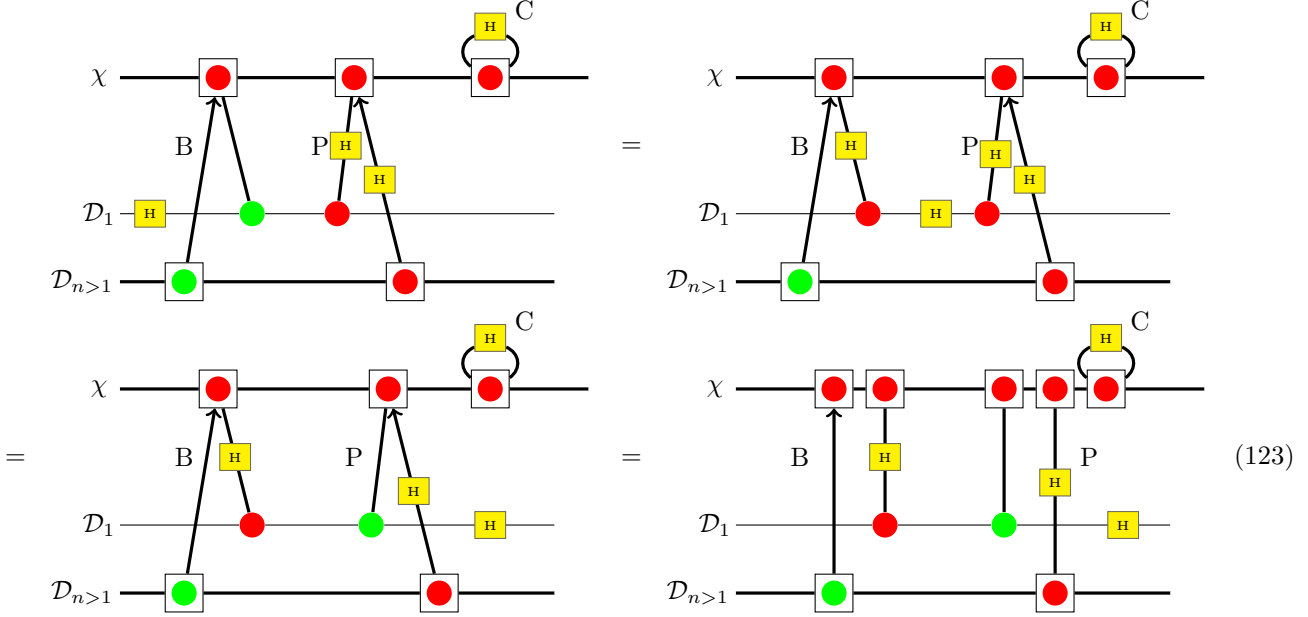
where k, l run over all the parity-check qubits χ . Again \oplus denotes addition modulo 2 in the components of the P and B matrices.

Hadamard gate. Pushing a Hadamard gate through the encoder changes a conjugate propagator to a CNOT and vice versa:

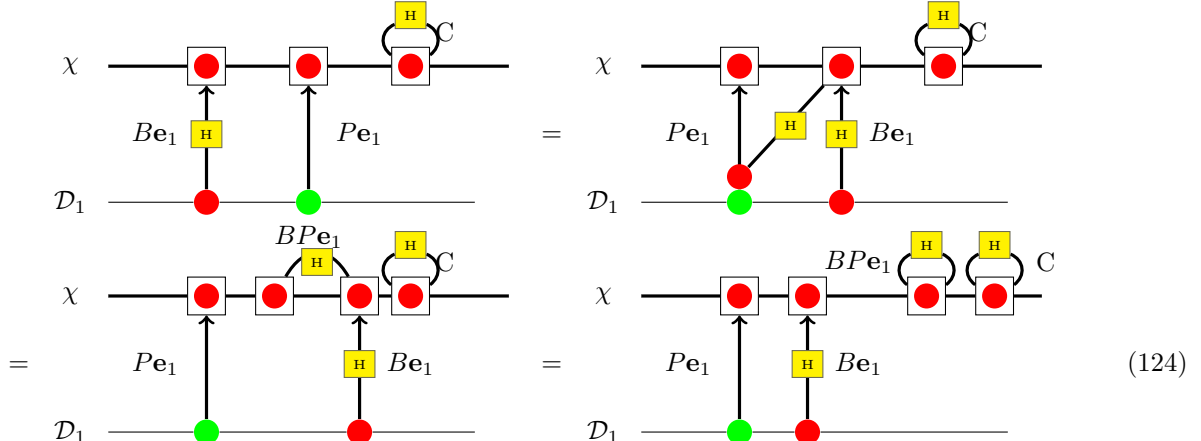


The Hadamard therefore modifies the encoder as (extracting out a single data qubit, w.l.o.g. the first, this

time):



Let us re-write the inner two (sets of) gates in detail separately:



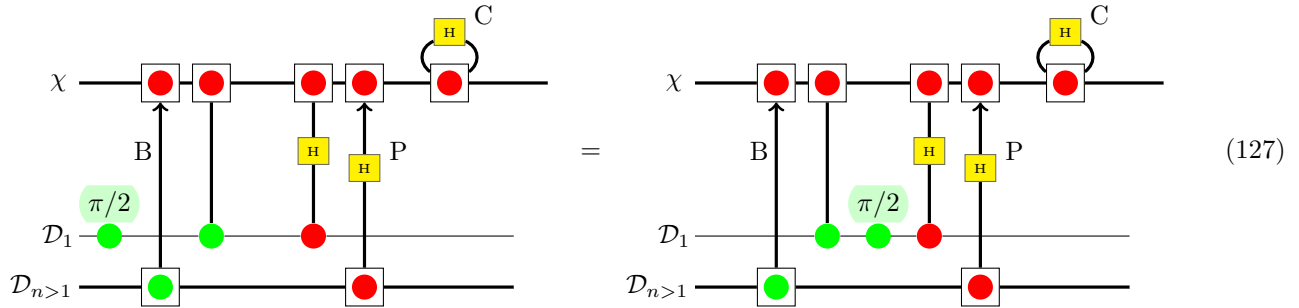
The modified encoder for a Hadamard on the first data qubit is therefore given by transforming the cross check matrix as

$$C_{kl} \rightarrow C_{kl} \oplus B_{k1}P_{l1} \quad \forall k, l \quad (125)$$

where again k, l indices run over all parity-check qubits χ . The bit-check and phase-check matrices also have their components that include the first data qubit interchanged:

$$B_{i1} \leftrightarrow P_{i1} \quad \forall i \quad (126)$$

Phase gate. Passing a phase gate (again, w.l.o.g. specified on the first data qubit) through the encoder rewrites as



To pass the $\pi/2$ phase through the red node we use the following identity (for any α):

(128)

where the first re-write is simply re-arranging the upper nodes, the second uses the bialgebra rule [9, 9.3], and the third an application of the spider rule.

Using this set of equations in reverse we can now push the green phase through the conjugate propagator:

(129)

where the final step uses the fact that the green $\pi/2$ state is the $+Y$ eigenstate, and the red $\pi/2$ is the $-Y$ eigenstate [9, 9.4.2]. We can now re-write the central rail of the new gate using an Euler decomposition of the Hadamard gate (5) in the following way:

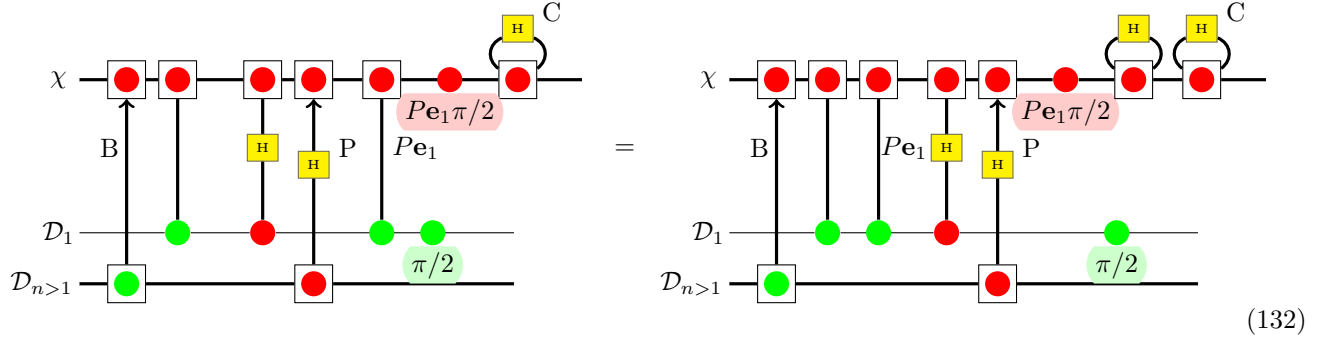
(130)

We therefore have

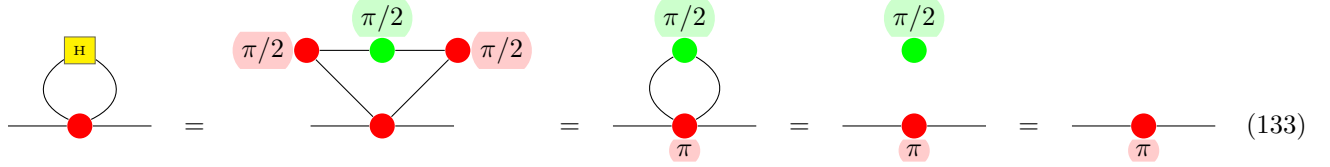
(131)

where there is no sum over i on the upper rail as it ranges only over a single value (that of the data qubit where the phase gate originated).

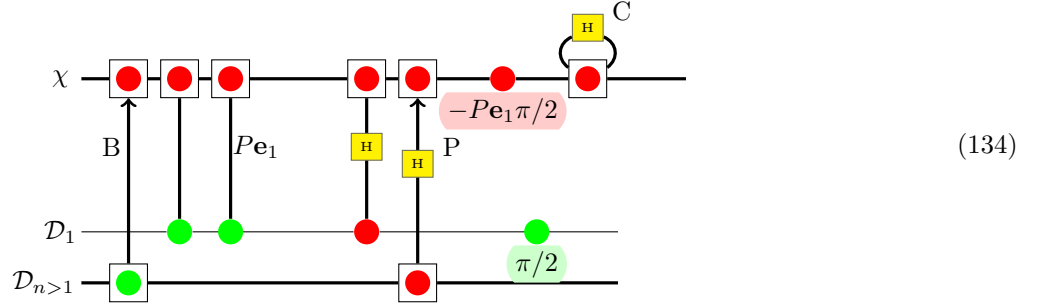
We now swap the order of the new CNOT gate(s) and the conjugate propagator, using the commutation relation found previously (124):



This time, however, the additional conjugate propagators on the parity-check qubits that are picked up by commuting these gates have their control and targets on the same qubits. They therefore reduce as follows:



The final state of the encoder after passing the phase gate through it is therefore



The modified encoder for the phase gate S on the i -th data qubit is therefore given by transforming the components of the bit-parity check matrix as (recalling that the CNOT is self-inverse)

$$B_{i1} \rightarrow B_{i1} \oplus P_{i1} \quad \forall i \quad (135)$$

where again i index runs over all parity-check qubits χ . The addition of the set of red $-\pi/2$ phases on the parity-check qubits can be seen as a modification of any of the operations, a separate set of single-qubit operations, or as a modification of the states in which the parity-check qubits are prepared.

Therefore the set of gates comprising the phase gate, the CNOT gate, and Hadamard pass through the encoder modifying only the matrices B , P , C , or the state preparation of the parity-check qubits. This concludes the proof. \square

8.2 Error propagation through the decoder or stabilizer measurement

Theorem 7 states that the decode circuit is unmodified when a Clifford unitary is encoded. Error information will therefore be detected in exactly the same way as if there had been no computation. This means that the only effect on how the code is decoded will come from the behaviour of that unitary, U_{Cliff} , itself.

The first of these additional complications is that the syndromes may be different. If U_{Cliff} contains any Pauli X or Z operations, these operations will be detected on the parity check qubits as if they were errors. Fortunately, this will happen in a completely predictable fashion, and the syndromes can be redefined appropriately, leading to no loss in code performance.

In addition to this, we also have the possibility that errors may be transformed. An error passing through U_{Cliff} may be transformed to a different type of error. For instance a Pauli X error may be transformed into a Y . This isn't a problem for codes that correct X and Z errors independently, but may decrease the code distance otherwise. This decrease in code distance may be avoided by guaranteeing that error patterns including Y errors also produce unique syndromes.

A final issue is that two qubit gates may propagate single qubit errors to multiple qubits. In principle error correction can still be performed (albeit at reduced performance) if a single error cannot be propagated into a larger number of errors than the code can handle. For instance a single CNOT can only propagate one error into two errors, so a distance 5 code would still perform some error correction if U_{Cliff} were a single CNOT gate. However, it would act as an effective distance 3 code. A better way to cope with this issue is to take advantage of the fact that we know how errors will propagate in U_{Cliff} , so we can make sure that these specific error patterns produce unique syndromes. We refer to this process as *local hardening* of a code.

To finish, we give an example of a numerically discovered $[[11, 3, 3]]$ code which is locally hardened against the errors propagated by a CNOT gate, where the first data qubit acts as the control and the second as the target:

$$B = \begin{pmatrix} 0 & 1 & 1 \\ 0 & 0 & 1 \\ 1 & 0 & 0 \\ 1 & 1 & 0 \\ 0 & 0 & 0 \\ 0 & 0 & 0 \\ 0 & 0 & 0 \\ 0 & 0 & 0 \end{pmatrix} \quad P = \begin{pmatrix} 0 & 0 & 0 \\ 0 & 0 & 0 \\ 0 & 0 & 0 \\ 0 & 0 & 0 \\ 0 & 1 & 1 \\ 0 & 0 & 1 \\ 1 & 0 & 0 \\ 1 & 1 & 0 \end{pmatrix}$$

$$C_u = \begin{pmatrix} 0 & 0 & 0 & 0 & 1 & 0 & 1 & 1 \\ 0 & 0 & 0 & 0 & 0 & 1 & 1 & 1 \\ 0 & 0 & 0 & 0 & 1 & 1 & 1 & 0 \\ 0 & 0 & 0 & 0 & 1 & 1 & 0 & 1 \\ 0 & 0 & 0 & 0 & 0 & 0 & 0 & 0 \\ 0 & 0 & 0 & 0 & 0 & 0 & 0 & 0 \\ 0 & 0 & 0 & 0 & 0 & 0 & 0 & 0 \\ 0 & 0 & 0 & 0 & 0 & 0 & 0 & 0 \end{pmatrix}. \quad (136)$$

9 Outlook and conclusions

We have seen how CPC codes enable the use of the zx-calculus as a high-level language for designing and verifying a (potentially large) class of stabilizer codes. We have seen how the construction gives structure to quantum codes and how that is reflected in the graphical representation. By using the graphical methods as a reasoning tool, we have taken classical codes and created quantum ones from them in ways that have not been done before. We have shown how pairs of classical codes can be combined to form quantum codes, without onerous restrictions on which codes we can use. In the case of classical distance 3 Hamming codes, we have an explicit construction for turning any one into a quantum code. ZX tools can be used to characterise any discovered code in terms of its stabilizers in a straightforward way.

A major result of the CPC construction is that large numbers of valid codes can be generated very quickly from the basic structural template, and generally have a significantly large ratio of logical qubits to physical qubits. We have given a number of new small (< 20 qubits) codes, and shown the simple search program that was used to find them. It is worth noting that while we have chosen to focus on small codes for presentation reasons, there is no reason that our search program would not work for much larger codes. As well as increasing the efficiency of the codes that are available to the first generations of quantum devices, CPC codes can also be performed in two different modes: either as single-shot codes that are encoded and decoded at each round, or else as standard stabilizer codes where syndromes are gathered through non-disturbing stabilizer measurements. In both cases, the graphical tools and structures are the same.

Finally, we have shown how in principle computation can be performed efficiently in the encoded space between logical qubits in the same code block. Rather than explicit operations, gates are performed by changing the encoder and/or stabilizer measurements. This has the potential to reduce significantly the overhead of physical operations for performing logical gates. It is also another tool to add to the performance of computation in error corrected systems, along with standard methods (braiding, transversal gates, and lattice surgery).

The CPC construction opens up the use of the ZX -calculus for rigorous and intuitive reasoning about stabilizer codes, with significant practical and theoretical benefits. It gives both a new structural understanding of quantum codes and their relation to classical, and an important new tool for the design and analysis of quantum error correcting codes which are capable of being uniquely tailored to the resources and error profile of target hardware.

We conclude by outlining a selection of future directions for this work.

Scaling for CPC codes

The examples we have demonstrated here are for small codes. It is, however, generally understood in classical error correction that the performance of codes dramatically improves for larger codes. In fact, the Shannon limit can only be reached in the limit of code size approaching infinity. While it is not clear whether the structure of the parity codes constructed in the CPC formalism will allow them to approach the Shannon limit, it is likely that larger codes will perform better than smaller codes. This is in direct contrast to many quantum error correction models which derive relatively little benefit from encoding more data qubits.

Low-density parity check (LDPC) codes are known to be state-of-the-art codes. This is both due to their performance close to the Shannon limit when their size becomes large, as well as due to the fact that there exist very fast (approximate) inference algorithms to decode them (cf. [31]). It will be important to discover how far those properties translate over to the coherent parity code construction. The main inference algorithm for LDPCs is based on belief propagation on graphical models. While such an algorithm is only exact for graphs which are trees, the algorithm is known to perform very well in practice for graphs which have not many small loops. Such properties can usually be achieved in practice. Furthermore, for given static codes one can also create decode tables. Our prime concern is thus the encoding level.

The main reason why LDPCs have such good performance is their large minimum code size. This is achieved through their random construction. In particular, for LDPCs the minus code size scales linearly with the size of the code. The behaviour is essential to achieve performance which approaches the Shannon limit. Given the various constraints in the construction of our codes it is likely that for large codes we will not be able to achieve a minimum code which scales linearly. The situation would thus be similar to that of the quantum error correction codes derived in [32]. However, as was shown in [32], as long as such a codes have bounded code distance, they perform well in practice. Linearly growing minimal distance is only required formally when the noise level is taken to zero. For any small but finite noise level, a code with bounded distance will perform well in practice.

Thresholds

In the context of quantum error correction codes as they are traditionally formulated, the threshold (defined as the error rate for which the encoding propagates more errors than it corrects) is an important quantity. For such codes, encoding is always a losing strategy if the error rate is above the threshold. The threshold is especially important for families of codes where the threshold is independent of the code's size (as is the case with, for example, toric codes).

For codes constructed within the CPC formalism, on the other hand, there is no reason to believe that for a given code, smaller codes which have the same threshold can be found. Therefore, while the threshold of any given code is a well defined mathematical quantity, an error rate being above the threshold of a code has no bearing on whether or not other codes can be found which can perform error correction at that error rate. The question of whether codes constructed in the CPC formalism can perform valid error correction at arbitrarily high error rates is open, but it cannot be answered by finding the threshold of individual codes.

Future directions

The quantum code framework presented here can in principle be applied to many different types of classical codes. One interesting future direction is to consider constructing quantum codes based on classical turbo codes

[2, 3], which have been used, for example, in 3G and 4G mobile transmissions. While turbo codes fall into the class of so-called convolutional codes, they are very closely related to LDPCs [30], and it is reasonable to consider that quantum error correction schemes based on turbo codes can be constructed using our coherent parity check formalism.

The CPC construction of codes marks a significant step forward for the use of quantum error correction on deployable hardware in both the immediate and longer terms. It allows informationally-dense codes to be constructed for memory, communication, and computation, either based on any previously known classical code, or directly without using such a code as a starting point. The suite of graphical and automated tools can be used by anyone without requiring a background in quantum theory or quantum error correction.

This paves the way for software design tools for quantum computers that give codes for specific hardware layouts and specifications. We have demonstrated automated design based on random search, but more powerful design tools could be constructed using more sophisticated algorithms such as evolutionary algorithms or those within the Monte Carlo ‘family’ of techniques (such as simulated annealing or parallel tempering). The CPC formalism also enables high-performance classical codes to be imported for use on quantum devices, closing the gap between the tools that have been developed in classical computer science and the theoretical structures of quantum error correction.

Acknowledgments

The authors would like to thank Viv Kendon for many useful discussions and comments on the text. We would also like to thank Samson Abramsky, Niel de Beaudrap, Ross Duncan, Earl Campbell, Elham Kashefi, and Tim Proctor for useful discussions of various aspects of these codes, and an anonymous referee for constructive comments.

DH and NC were funded by the UK EPSRC grant EP/L022303/1. AK is supported by the ERC under the European Union’s Seventh Framework Programme (FP7/2007-2013) / ERC grant n° 320571. SZ was funded by Nokia Technologies, Lockheed Martin and the University of Oxford through the Quantum Optimisation and Machine Learning (QuOpaL) project. JR was supported by a Durham Doctoral Studentship (Faculty of Science).

A Fidelity analysis of an elementary three-qubit CPC gadget

The CPC gadget is one of the simplest possible detection codes for the identification of bit-flip errors in a quantum computer. Whilst the ultimate aim is to build full quantum error correction codes capable of identifying and localising errors, detection codes remain of interest as they can be simple enough to implement on current hardware. Such experiments will adopt a *repeat-until-success* style approach with a detection code dictating which runs should be discarded. For example, in the case of the CPC gadget, only runs which return a 0 syndrome would be accepted. We demonstrate in this Appendix that, assuming the 0 syndrome is measured, the fidelity of qubits encoded via the CPC gadget is greater than that for unprotected qubits.

In our analysis, we will assume that, over the time of an error cycle t_c , a single qubit Q is subject to an error process of the form

$$E_Q = e^{-i\epsilon X} = \cos(\epsilon)I_Q - i\sin(\epsilon)X_Q, \quad (137)$$

where ϵ is proportional to the error probability in the time-frame t_c . Applying this error model to an unprotected data register of two raw qubits $|\psi_{\text{reg}}(0)\rangle = |\psi_A\psi_B\rangle$ yields the following state

$$\begin{aligned} |\psi_{\text{reg}}(t_c)\rangle &= E_A E_B |\psi_A\psi_B\rangle \\ &= \cos^4(\epsilon)I_A I_B |\psi_A\psi_B\rangle - i\sin(\epsilon)\cos(\epsilon)(X_A I_B + I_A X_B) |\psi_A\psi_B\rangle - \sin^2(\epsilon)X_A X_B |\psi_A\psi_B\rangle. \end{aligned} \quad (138)$$

It is convenient to quantify the overlap of the evolved state, $|\psi_{\text{reg}}(t_c)\rangle$, with the original state, $|\psi_{\text{reg}}(0)\rangle$, in terms of the fidelity $F_{\text{unprotected}}$. This yields

$$F_{\text{unprotected}} = |\langle\psi_{\text{reg}}(t_c)|\psi_{\text{reg}}(0)|\rangle|^2 = \cos^4(\epsilon) \approx 1 - 2\epsilon^2, \quad (139)$$

where we have made a Taylor expansion under the assumption that ϵ is small. In order to show that the CPC gadget suppresses the error rate, we need to show that when the 0 syndrome is measured the CPC gadget outputs a state with higher fidelity than the unprotected case, such that $F_{\text{CPC}|S=0} > F_{\text{unprotected}}$. The error operator across three qubits of the CPC gadget $|\psi_A\psi_B\rangle|0_P\rangle$ is

$$\begin{aligned} E_A E_B E_P &= e^{i\epsilon(X_A + X_B + X_P)} = \\ &\cos^3(\epsilon)I_A I_B I_P - i\sin(\epsilon)\cos^2(\epsilon)(X_A I_B I_P + I_A X_B I_P + I_A I_B X_P) \\ &- \sin^2(\epsilon)\cos(\epsilon)(X_A X_B I_P + I_A X_B X_P + X_A I_B X_P) - i\sin^3(\epsilon)X_A X_B X_P. \end{aligned} \quad (140)$$

Table A shows syndromes for the CPC gadget under the above error model. A 0 syndrome measurement will most likely indicate that no error has occurred. However, with lower probability, the two-qubit errors $\{X_A X_B, X_A X_P, X_B X_P\}$ could also result in a 0 syndrome. A 0 syndrome measurement therefore projects the output of the CPC gadget onto the state

$$|\psi_{\text{CPC}}(t_c)\rangle_{S=0} = \frac{\cos^3(\epsilon)I_A I_B I_P - \sin^2(\epsilon)\cos(\epsilon)(X_A X_B + X_B X_P + X_A X_P)}{\sqrt{|\cos^3(\epsilon)|^2 + 3|\sin^2(\epsilon)\cos(\epsilon)|^2}} |\psi_A\psi_B\rangle|0_P\rangle, \quad (141)$$

where the numerator represents the superposition of all the possible errors, weighted by their respective probabilities, that will result in a 0 syndrome. The denominator is the renormalisation factor. The conditional fidelity after a single cycle is now given by

$$F_{\text{CPC}|S=0} = |\langle\psi_{\text{reg}}(t_c)|\psi_{\text{reg}}(0)|\rangle|^2 = \frac{\cos^6(\epsilon)}{\cos^6(\epsilon) + \sin^4(\epsilon)\cos^2(\epsilon)} = \frac{1}{3\tan^4(\epsilon) + 1} \approx 1 - 3\epsilon^4, \quad (142)$$

where we have again assumed that ϵ is small. We have now demonstrated that $F_{\text{CPC}|S=0} > F_{\text{unprotected}}$. The bit-flip error rate of qubits encoded via a CPC gadget is therefore lower than that for unprotected qubits.

B Verification and analysis of the ring code

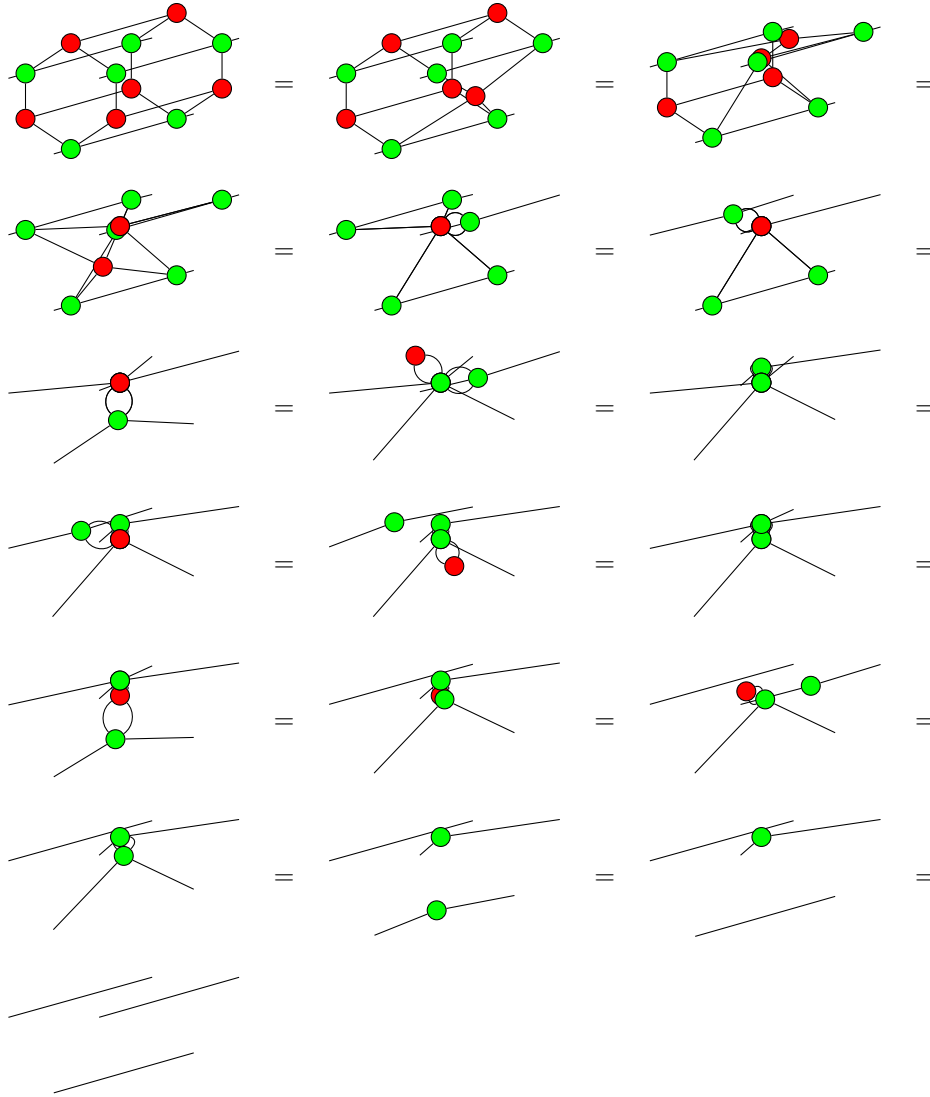
We give here the full derivation for equation (33) in §4.6, demonstrating that the ring code on six qubits rewrites to the identity operation on three data qubits. We then demonstrate analytically the error suppression power of the code, and finish with numerical results for encoded fidelity based on error rates in an ion trap quantum device.

Error, \mathcal{E}	Probability amplitude , p_A	Syndrome, S
No error	I	$\cos^3(\epsilon)$
1-qubit error	X_A	1
	X_B	$-\text{i} \sin(\epsilon) \cos^2(\epsilon)$
	X_P	1
2-qubit error	$X_A X_B$	0
	$X_A X_P$	$-\sin^2(\epsilon) \cos(\epsilon)$
	$X_B X_P$	0
3-qubit error	$X_A X_B X_P$	$-\text{i} \sin^3(\epsilon)$

Table 1: The syndrome table for the CPC gadget

B.1 Verification

The following is automated output from Quantomatic.



B.2 Fidelity analysis

It is convenient to use $E = \cos(\epsilon)\mathbf{1} + i\sin(\epsilon)X$ as our error operator, where X is the Pauli- x operator. The error operator on all six qubits is thus

$$\begin{aligned} E = & \cos^6(\epsilon)\mathbf{1} + i\sin(\epsilon)\cos^5(\epsilon)\left(\sum_{j \in \{\text{qubits}\}} X_j\right) - \sin^2(\epsilon)\cos^4(\epsilon)\left(\sum_{(j \neq k) \in \{\text{qubits}\}} X_j X_k\right) \\ & - i\sin^3(\epsilon)\cos^3(\epsilon)\left(\sum_{(j \neq k \neq l) \in \{\text{qubits}\}} X_j X_k X_l\right) + \sin^4(\epsilon)\cos^2(\epsilon)\left(\prod_{l \in \{\text{qubits}\}} X_l \sum_{(j \neq k) \in \{\text{qubits}\}} X_j X_k\right) \\ & + i\sin^5(\epsilon)\cos(\epsilon)\left(\prod_{l \in \{\text{qubits}\}} X_l \sum_{j \in \{\text{qubits}\}} X_j\right) - \sin^6(\epsilon)\left(\prod_{l \in \{\text{qubits}\}} X_l\right), \end{aligned}$$

which can be written more compactly as:

$$E = \sum_{n=1}^6 (i^n) \sin^n(\epsilon) \cos^{6-n}(\epsilon) \sum_{\{j_1 \dots j_n\} \in \{\text{qubits}\}} |\epsilon_{j_1 \dots j_n}| \prod_{k \in j_1 \dots j_n} X_k + \cos^6(\epsilon)\mathbf{1}$$

where $\epsilon_{j_1 \dots j_n}$ is the Levi-Civita symbol. For unencoded qubits and $\epsilon \ll 1$, it is easily shown that the fidelity of the uncorrected data qubits after a single bit-flip error is $F_{(\text{no corr})} = |\langle \psi | E | \psi \rangle|^2 \propto 1 - \epsilon^2$. The fidelity of encoded data qubits is

$$F_{[[6,3,1]]} = \sum_i p_{s_i} |\langle \psi | O_{s_i} | \psi'_{s_i} \rangle|^2,$$

where $|\psi'_{s_i}\rangle$ is the state after implementing the code depicted in (33), for parity bit measurements s_i with p_{s_i} the probability of measuring s_i , and O_{s_i} is an operator which performs relevant corrections based on the syndromes. To demonstrate error correction, we must show that $F_{[[6,3,1]]} \propto 1 - \epsilon^\eta$ with $\eta > 2$.

Starting from an initial state of the data qubits $|\psi\rangle = \sum_{ijk \in \{0,1\}} c_{ijk} |ijk\rangle$ and the parity qubits in state $|000\rangle$, applying the first set of CNOTs to encode the qubits gives the intermediate state

$$\begin{aligned} |\psi_{\text{enc}}\rangle = & (c_{000} |000\rangle + c_{111} |111\rangle) |000\rangle + (c_{001} |001\rangle + c_{110} |110\rangle) |110\rangle \\ & + (c_{010} |010\rangle + c_{101} |101\rangle) |011\rangle + (c_{100} |100\rangle + c_{110} |110\rangle) |101\rangle, \end{aligned} \quad (143)$$

We then apply the error operator followed by the second set of CNOT gated, measure the parity qubits and apply correction bit-flips as required. We consider each possible set of parity qubit measurement outcomes s_i in turn. To calculate the fidelity of each of these, we first re-normalize each of the conditional wavefunctions such that $|\langle \psi'_{ijk} | \psi'_{ijk} \rangle|^2 = 1$ and then calculate the sum of each of these conditional fidelities multiplied by the probability of a the associated syndrome measurement, $F = \sum_{ijk \in \{0,1\}} p_{ijk} |\langle \psi | \psi'_{ijk} \rangle|^2$.

Parity measurements $s_i = 000$: The most likely event leading to this outcome is that no error has occurred, so no corrective bit-flip will be applied. The final state of the data qubits is

$$\begin{aligned} |\psi'_{000}\rangle = & \{\cos^6(\epsilon) - i\cos^3(\epsilon)\sin^3(\epsilon)(X_A X_B X_C + X_A + X_B + X_C) \\ & + \cos^2(\epsilon)\sin^4(\epsilon)(X_A X_B + X_B X_C + X_A X_C)\} |\psi\rangle \end{aligned} \quad (144)$$

Because no correction has been applied, the fidelity for $s_i = 000$ is $|\langle \psi | \psi'_{000} \rangle|^2 = 1 - O(\epsilon^6)$.

Parity measurements $s_i = 001$: The most likely events leading to this outcome is that an error has occurred on a parity bit, so no correction is performed, and the final state of the data qubits is

$$\begin{aligned} |\psi'_{001}\rangle = & \{i\cos^5(\epsilon)\sin(\epsilon) - \cos^4(\epsilon)\sin^2(\epsilon)(X_A + X_C) - i\cos^3(\epsilon)\sin^3(\epsilon)(X_A X_B + X_B X_C) \\ & + \cos^2(\epsilon)\sin^4(\epsilon)X_B + i\cos(\epsilon)\sin^5(\epsilon)X_A X_C\} |\psi\rangle. \end{aligned} \quad (145)$$

The resultant fidelity is $|\langle \psi | \psi'_{001} \rangle|^2 = 1 - 2\epsilon^2 + \frac{2}{3}\epsilon^4 + O(\epsilon^5)$. Due to the symmetry of the code, $|\langle \psi | \psi'_{001} \rangle|^2 = |\langle \psi | \psi'_{010} \rangle|^2 = |\langle \psi | \psi'_{100} \rangle|^2$.

Parity measurements $s_i = 011$: The most likely events leading to this outcome is that a single error occurred on data qubit C

$$|\psi'_{011}\rangle = \{i \cos^5(\epsilon) \sin(\epsilon) X_C - \cos^4(\epsilon) \sin^2(\epsilon) (X_A X_B + \mathbf{1}) - i \cos^3(\epsilon) \sin^3(\epsilon) (X_B + X_A) + \cos^2(\epsilon) \sin^4(\epsilon) (X_A X_C + X_B X_C) + i \cos(\epsilon) \sin^5(\epsilon) X_A X_B X_C\} |\psi\rangle. \quad (146)$$

The fidelity is $|\langle\psi| X_C |\psi'_{011}\rangle|^2 = 1 - 2\epsilon^2 + \frac{2}{3}\epsilon^5 + O(\epsilon^5)$. By the symmetry of the code, $|\langle\psi| X_C |\psi'_{011}\rangle|^2 = |\langle\psi| X_B |\psi'_{101}\rangle|^2 = |\langle\psi| X_A |\psi'_{110}\rangle|^2$.

Parity measurements $s_i = 111$: In this case the decoding strategy is unclear, as there is no single most likely error. For simplicity, we will assume no correction, whence

$$|\psi'_{111}\rangle = \{i \cos^4(\epsilon) \sin^2(\epsilon) (X_A + X_B + X_C) - i \cos^3(\epsilon) \sin^3(\epsilon) (X_A X_B + X_B X_C + X_A X_C + \mathbf{1}) - \sin^6(\epsilon) X_A X_B X_C\} |\psi\rangle. \quad (147)$$

resulting in a code failure, with $|\langle\psi| \psi'_{111}\rangle|^2 = \frac{\epsilon^2}{3} - \frac{2}{9}\epsilon^4 + O(\epsilon^5)$. The probabilities of each of the measured results are as follow:

$$\begin{aligned} p_{000} &= 1 - 6\epsilon^2 + 17\epsilon^4 + O(\epsilon^5) \\ p_{001} = p_{010} = p_{100} = p_{011} = p_{101} = p_{110} &= \epsilon^2 - \frac{10}{3}\epsilon^4 + O(\epsilon^5) \\ p_{111} &= 3\epsilon^4 + O(\epsilon^5). \end{aligned} \quad (148)$$

The total fidelity is therefore

$$\begin{aligned} F_{[[6,3,1]]} &= p_{000} |\langle\psi| \psi'_{000}\rangle|^2 + 3p_{001} |\langle\psi| \psi'_{001}\rangle|^2 \\ &\quad + 3p_{011} |\langle\psi| X_C |\psi'_{011}\rangle|^2 + p_{111} |\langle\psi| \psi'_{111}\rangle|^2 = 1 - 15\epsilon^4 + O(\epsilon^5). \end{aligned} \quad (149)$$

The error scales as ϵ^4 compared with ϵ^2 for the uncorrected data qubits, hence this code improves the error rate for bit-flip errors on qubits in an arbitrary pure state.

Just as with repetition codes, instead of correcting bit-flips, the same parity check codes can be used to protect the qubits from phase errors. This is accomplished by rotating the basis of all the qubits such that the parity check qubits are now initialized in the $|+\rangle = \frac{|1\rangle + |0\rangle}{\sqrt{2}}$ state and are the control rather than the target in the CNOTs. Before we discuss codes that can correct both bit-flip and phase errors, it is instructive to characterise the performance of the $[[6, 3, 1]]$ code numerically for a specific hardware for which is is suitable (fast gates).

B.3 Numerical performance of the code in ion traps

To numerically model error correction, we must specify some of the device parameters. Motivated by ion trap systems [22], we choose a realistic bit-flip error rate³, of $\epsilon_{\text{bit}} = 0.007 \text{ s}^{-1}$. Since this code is only able to correct one type of error at a time, for the purposes of illustration we set $\epsilon_{\text{phase}} = 0 \text{ s}^{-1}$. We must also choose an appropriate fidelity metric. This is non-trivial because unlike with codes that protect a single qubit, we should fix a metric that accurately reflects how well we protect multiple qubits simultaneously. We therefore introduce three fidelity metrics.

Firstly, to compare with other codes, we examine the ability of the code to protect single qubits by performing a numerical experiment: We prepare the data qubits all in a bit (phase) eigenstate $|000\rangle$ ($|+++ \rangle$). We then define the fidelity of a single qubit initialized in the appropriate eigenstate to be either

$$F_0 = \sum_{ij \in \{0,1\}} |\langle 0ij | U_{\text{corr}}(\tau) |000\rangle|^2, \quad (150)$$

or

$$F_+ = \sum_{ij \in \{+, -\}} |\langle +ij | U_{\text{corr}}(\tau) |+++ \rangle|^2, \quad (151)$$

³Note that the error rate ϵ used in the calculations in section 4.6 is *not* the same as ϵ_{bit} and ϵ_{phase} in figures 7 and 8. Specifically, ϵ_{bit} and ϵ_{phase} are defined as the probability rate for errors of their respective type, with units of s^{-1} , while ϵ is a unit-less probability amplitude for an error: $\epsilon \propto \sqrt{\epsilon_{\text{bit}}}$.

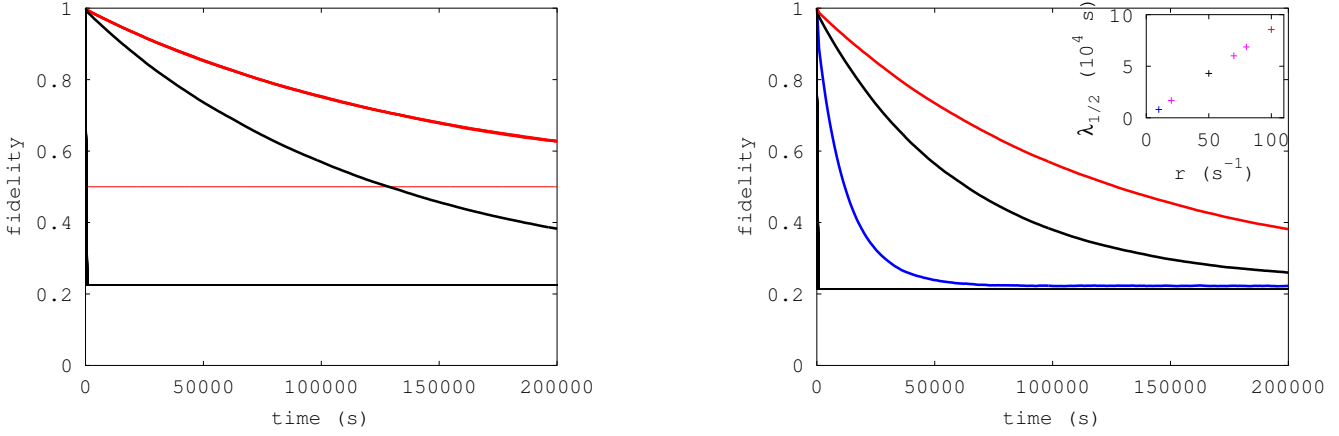


Figure 8: Numerical study of the $[[6, 3, 1]]$ code (cf. (33)) using a bit error rate of $\epsilon_{\text{bit}} = 0.007 \text{ s}^{-1}$ and a phase error rate $\epsilon_{\text{phase}} = 0 \text{ s}^{-1}$. Left: Fidelity versus time for a correction cycle rate of $r = 100 \text{ s}^{-1}$ showing F_{rand} (black) from equation (152) and F_0 from equation (150) (red). F_+ from equation (151) remains 1 for all times (not shown). Right: F_{rand} for $r = 10 \text{ s}^{-1}$ (blue), $r = 50 \text{ s}^{-1}$ (black), and $r = 100 \text{ s}^{-1}$ (red). Inset: Numerical fit of $\lambda_{1/2}$ versus cycle rate r for the three times in the main figure plus others. Thin lines represent curves for unprotected qubits with the same error rate. Error-bars due to statistical fluctuations are smaller than the depicted lines.

where $U_{\text{corr}}(\tau)$ is a unitary representing the action of the error correction from time 0 to time τ .

Secondly, to characterise the ability to protect a highly entangled multi-body state, we use the following fidelity metric

$$F_{\text{rand}} = \frac{1}{|R|} \sum_{\psi \in R} |\langle \psi | U_{\text{corr}}(\tau) | \psi \rangle|^2, \quad (152)$$

where we define R to be a set of randomly generated states drawn from the Haar distribution.

Thirdly, from these two fidelities we define the half life, $\lambda_{1/2}$ by numerically fitting the data to

$$F_{\text{fit}} = F_{\infty} + (1 - F_{\infty}) \exp \left(-\frac{\log(2)}{\lambda_{1/2}} \tau \right), \quad (153)$$

where F_{∞} is a fitting parameter corresponding to the expected value of the fidelity after a long period of time.

In order to run simulations, we also have to choose a correction cycle rate r appropriate for the system under study. For our error rate of $\epsilon_{\text{bit}} = 0.007 \text{ s}^{-1}$, values of r in the range 10 s^{-1} to 100 s^{-1} are reasonable. The numerical results are shown in figure 8.

As figure 8 (right) demonstrates, the $[[6, 3, 1]]$ code (depicted in (33)) is capable of protecting qubits for a far longer time than the unprotected lifetime of $\epsilon_{\text{bit}}^{-1} \approx 142 \text{ s}$, regardless of whether the qubits are entangled with each other. Furthermore, figure 8 (left) shows that state lifetimes scale linearly with r , indicating that, as the calculations in section 4.6 show, the protocol is capable of correcting single bit-flip errors on any of the qubits.

C Source code for finding distance 3 CPC codes

GNU Octave code for finding distance 3 CSS codes using random search in the CPC formalism. This program was used to find the matrices (113), (114), (115) in §7.2.3. Feel free to reuse/modify but please attribute the source and cite this paper in any published work. This code (along with a Python version) is available at the repository at [7] (file name ‘CPC_randSearch_simple’). Code written by Nicholas Chancellor.

```
n=9; % total number of qubits
k=4; % number of data qubits being protected

nCheck=10000; % number of random codes to checks
```

```

nKeep=10; % maximum number of successful codes to keep

MbCell=cell(nKeep,1); % cellular array of bit checks for successful codes
MpCell=cell(nKeep,1); % cellular array of phase checks for successful codes
McCell=cell(nKeep,1); % cellular array of cross checks for successful codes

nSuccess=0; % number codes successfully found

binConvert=2.^((0:(n-k-1))); % vector used later to convert binary numbers to integers

for iRand=1:nCheck % loop for generating random instances
    Mb=round(rand(k,n-k)); % random bit check matrix
    Mp=round(rand(k,n-k)); % random phase check matrix
    Mc=round(rand(n-k,n-k)); % random cross check matrix
    Mc=triu(Mc); % make cross check matrix upper triangular
    Mc=Mc-diag(diag(Mc)); % make cross check matrix strictly upper triangular
    syndromeList=zeros(n-k,2*n+1); % list for storing syndromes for all error patterns with up to
        % a single error
    iSyndrome=2; % leave first vector in list blank to signify case of no error

    for iBitData=1:k % syndromes for bit flip errors on data qubits
        bitErrVec=zeros(1,k); % vector listing bit errors
        bitErrVec(iBitData)=1; % add single bit error
        syndromeList(:,iSyndrome)=bitErrVec*Mb; % calculate syndrome
        iSyndrome=iSyndrome+1; % increment for storing in list
    end
    for iPhaseData=1:k % syndromes for phase errors on data qubits
        phaseErrVec=zeros(1,k); % vector listing phase errors
        phaseErrVec(iPhaseData)=1; % add single phase error
        syndromeList(:,iSyndrome)=phaseErrVec*Mp; % calculate syndrome
        iSyndrome=iSyndrome+1; % increment for storing in list
    end
    for iBitPar=1:(n-k) % syndromes for bit flip errors on parity check qubits
        bitErrVec=zeros(1,n-k); % vector listing bit errors
        bitErrVec(iBitPar)=1; % add single bit error
        syndromeList(:,iSyndrome)=bitErrVec; % calculate syndrome
        iSyndrome=iSyndrome+1; % increment for storing in list
    end
    for iPhasePar=1:(n-k) % syndromes for phase errors on parity check qubits
        phaseErrVec=zeros(1,n-k); % vector listing phase errors
        phaseErrVec(iPhasePar)=1; % add single phase error
        syndromeList(:,iSyndrome)=mod(phaseErrVec*(Mc+transpose(Mc)+transpose(Mp)*Mb),2); %
            % calculate syndrome
        iSyndrome=iSyndrome+1; % increment for storing in list
    end
    syndromeNums=binConvert*syndromeList; % treat as binary numbers and convert to decimal for
        % easier comparison
    if length(unique(syndromeNums))==length(syndromeNums) % check if syndromes are unique
        nSuccess=nSuccess+1; % another code successfully found!
    if nSuccess<(nKeep+1) % only keep so many codes to avoid memory issues
        MbCell{nSuccess}=transpose(Mb); % store bit check matrix, transpose to agree with
            % convention in paper
        MpCell{nSuccess}=transpose(Mp); % store phase check matrix, transpose to agree with
            % convention in paper
    end
end

```

```

    McCell{nSuccess}=Mc; % store cross check matrix
  end
end
end

```

D Source code for finding arbitrary distance CPC codes

GNU Octave code for finding tripartite CPC (CSS) codes of arbitrary distance using random search. This program was used to find the codes in Appendix F, and referenced in §7.2.3. Feel free to reuse/modify but please attribute the source and cite this paper in any published work.

Program to search codes that also correct for elementary Pauli Y errors (along with a Python version) is available at the repository at [7] (file name ‘CPC_randSearch_allDists_includeY’). Code written by Nicholas Chancellor.

```

n=16; % total number of qubits
k=4; % number of data qubits being protected
nErr=2; % number of errors code needs to be tolerant to (d=2*nErr+1 under most circumstances)

nCheck=1000; % number of random codes to checks
nKeep=10; % maximum number of successful codes to keep

MbCell=cell(nKeep,1); % cellular array of bit checks for successful codes
MpCell=cell(nKeep,1); % cellular array of phase checks for successful codes
McCell=cell(nKeep,1); % cellular array of cross checks for successful codes

nSuccess=0; % number codes successfully found

binConvert=2.^ (0:(n-k-1)); % vector used later to convert binary numbers to integers

for iRand=1:nCheck % loop for generating random instances
  Mb=round(rand(k,n-k)); % random bit check matrix
  Mp=round(rand(k,n-k)); % random phase check matrix
  Mc=round(rand(n-k,n-k)); % random cross check matrix
  Mc=triu(Mc); % make cross check matrix upper triangular
  Mc=Mc-diag(diag(Mc)); % make cross check matrix strictly upper triangular
  nSyndrome=0;
  for nErr1=0:nErr
    nSyndrome=nSyndrome+nchoosek(2*n,nErr1); % number of unique syndromes which need to be
    % checked
  end
  syndromeList=zeros(n-k,nSyndrome); % list for storing syndromes for all error patterns with
  % up nErr errors
  iSyndrome=2; % leave first vector in list blank to signify case of no error

  for inErr=1:nErr % loop over number of errors
    errList=zeros(2*n,1);
    errList(1:inErr)=1; % configuration of inErr errors which corresponds to the smallest
    % possible binary number
    for iConfig=1:nchoosek(2*n,inErr)
      % syndromes for bit flip errors on data qubits
      bitErrVec=errList(1:k)'; % vector listing bit errors
      syndromeList(:,iSyndrome)=syndromeList(:,iSyndrome)'+bitErrVec*Mb; % calculate syndrome
      % syndromes for phase errors on data qubits
      phaseErrVec=errList((k+1):(2*k))'; % vector listing phase errors
    end
  end
end

```

```

syndromeList(:,iSyndrome)=syndromeList(:,iSyndrome)'+phaseErrVec*Mp; % calculate syndrome
% syndromes for bit flip errors on parity check qubits
bitErrVecPar=errList((2*k+1):(k+n))'; % vector listing bit errors
syndromeList(:,iSyndrome)=syndromeList(:,iSyndrome)+bitErrVecPar'; % calculate syndrome
% syndromes for phase errors on parity check qubits
phaseErrVecPar=errList((k+n+1):end)'; % vector listing phase errors
syndromeList(:,iSyndrome)=syndromeList(:,iSyndrome)'+mod(phaseErrVecPar*(Mc+transpose(Mc)
    ↪ +transpose(Mp)*Mb),2); % calculate syndrome
syndromeList(:,iSyndrome)=mod(syndromeList(:,iSyndrome),2); % errors add mod 2
iSyndrome=iSyndrome+1; % increment for storing in list
for iIncr=1:(2*n-1) % increment error list
    if errList(iIncr)==1 && errList(iIncr+1)==0 % if error can be moved up by one slot
        errList(iIncr)=0;
        errList(iIncr+1)=1; % move error up
        nErrLess=nnz(errList(1:iIncr));
        errList(1:iIncr)=zeros(iIncr,1);
        errList(1:nErrLess)=1; % bits below moved bit reset to lowest value
        break % break loop after successfully incrementing
    end
end
end

syndromeNums=binConvert*syndromeList; % treat as binary numbers and convert to decimal for
    ↪ easier comparison
if length(unique(syndromeNums))==length(syndromeNums) % check if syndromes are unique
    nSuccess=nSuccess+1; % another code successfully found!
    if nSuccess<(nKeep+1) % only keep so many codes to avoid memory issues
        MbCell{nSuccess}=transpose(Mb); % store bit check matrix, transpose to agree with
            ↪ convention in paper
        MpCell{nSuccess}=transpose(Mp); % store phase check matrix, transpose to agree with
            ↪ convention in paper
        McCell{nSuccess}=Mc; % store cross check matrix
    end
end
end

```

E Source code for converting CPC matrices to stabilizer tables

GNU Octave code for converting CPC matrices to stabilizer tables in latex array form. Feel free to reuse/modify but please attribute the source and cite this paper in any published work. This code (along with a Python version) is available at the repository at [7] (file name ‘CPC_mats_2_stabalizers’). Code written by Nicholas Chancellor.

```

Mb=transpose(Mb); % convention in paper is transpose of what is used in code
Mp=transpose(Mp); % convention in paper is transpose of what is used in code

k=size(Mb,1); % number of logical qubits

n=size(Mb,1)+size(Mb,2); % number of total qubits

strCellLines=cell(n-k,1); % cellular array for storing lines of the latex array

```

```

indirectProp=Mp'*Mb; % indirectly propagated phase information

for i=1:(n-k) % iterate over stabilizers
    strCellChars=cell(n,1); % cell for storing (X, Z, Y or 1) elements of stabilizer row
    numZmultList=zeros(n,1); % number of times a Z stabilizer element is found on a given qubit
    numXmultList=zeros(n,1); % number of times an X stabilizer element is found on a given qubit
    % apply matrix formula to create stabilizers
    % Z stabilizers
    numZmultList(k+i)=numZmultList(k+i)+1; % bit information of measured qubit
    numZmultList(1:k)=numZmultList(1:k)+Mb(:,i); % bit information from measured qubits
    % X stabilizers
    numXmultList(1:k)=numXmultList(1:k)+Mp(:,i); % phase information from measured qubits
    numXmultList((k+1):end)=numXmultList((k+1):end)+Mc(:,i)+Mc(i,:); % phase information
        % propagated by cross checks
    numXmultList((k+1):end)=numXmultList((k+1):end)+indirectProp(:,i); % phase information
        % propagated indirectly
    % write stabilizer table
    for iWrite=1:n
        if mod(numZmultList(iWrite),2)==0 && mod(numXmultList(iWrite),2)==0 % if there are neither
            % X nor Z stabilizers
            strCellChars{iWrite}='1';
        elseif mod(numZmultList(iWrite),2)==1 && mod(numXmultList(iWrite),2)==0 % if there is only
            % a Z stabilizer
            strCellChars{iWrite}='Z';
        elseif mod(numZmultList(iWrite),2)==0 && mod(numXmultList(iWrite),2)==1 % if there is only
            % an X stabilizer
            strCellChars{iWrite}='X';
        elseif mod(numZmultList(iWrite),2)==1 && mod(numXmultList(iWrite),2)==1 % if there are both
            % X and Z stabilizers
            strCellChars{iWrite}='Y'; % X and Z combine to form Y
        end
    end
    strCellLines{i}=strjoin(strCellChars,'&');
    % latex formatted characters for line
end

latex_array=strjoin(strCellLines,'\\\\\\n'); % combine lines to make total latex array

% write latex array to file
fid = fopen (saveName, "w");
fputs (fid, latex_array);
fclose (fid);

```

F Additional Codes

In this Appendix we give examples of codes discovered using the CPC formalism. We characterise the codes by giving both the CPC matrices B , P , and C_u matrices, and the associated code stabilizer table. The GNU Octave program that generated these codes is given in Appendix D and in the repository at [7].

F.1 Numerically discovered codes

Numerically discovered $[[16, 4, 5]]$ code

Running on a single core of a standard desktop, our program will be able to find approximately one code in two hours. On running, we found that approximately 0.0012% (1.2×10^{-5}) of randomly generated matrices yielded a valid code. The following is an example of such a valid codes (note that transposes are shown to save space on the page):

$$B = \begin{pmatrix} 1 & 1 & 0 & 0 & 0 & 0 & 1 & 1 & 0 & 1 & 1 & 1 \\ 1 & 0 & 0 & 1 & 1 & 0 & 0 & 0 & 0 & 1 & 0 & 1 \\ 0 & 0 & 0 & 1 & 0 & 1 & 1 & 1 & 0 & 1 & 0 & 1 \\ 1 & 0 & 0 & 1 & 1 & 1 & 1 & 1 & 0 & 0 & 0 & 1 \end{pmatrix}^T \quad (154)$$

$$P = \begin{pmatrix} 1 & 0 & 1 & 0 & 0 & 1 & 0 & 0 & 0 & 0 & 1 & 0 \\ 0 & 1 & 1 & 1 & 1 & 0 & 0 & 0 & 1 & 0 & 1 & 1 \\ 0 & 0 & 1 & 1 & 0 & 0 & 0 & 1 & 1 & 0 & 0 & 0 \\ 1 & 1 & 1 & 1 & 1 & 1 & 1 & 1 & 0 & 0 & 1 & 0 \end{pmatrix}^T \quad (155)$$

$$C_u = \begin{pmatrix} 0 & 0 & 0 & 0 & 1 & 1 & 1 & 0 & 1 & 0 & 0 & 1 \\ 0 & 0 & 0 & 1 & 0 & 1 & 0 & 0 & 0 & 1 & 1 & 0 \\ 0 & 0 & 0 & 0 & 0 & 0 & 0 & 0 & 0 & 1 & 0 & 0 \\ 0 & 0 & 0 & 0 & 0 & 1 & 1 & 1 & 1 & 0 & 1 & 1 \\ 0 & 0 & 0 & 0 & 0 & 1 & 0 & 0 & 1 & 1 & 1 & 0 \\ 0 & 0 & 0 & 0 & 0 & 0 & 0 & 1 & 1 & 1 & 1 & 1 \\ 0 & 0 & 0 & 0 & 0 & 0 & 0 & 0 & 1 & 1 & 1 & 0 \\ 0 & 0 & 0 & 0 & 0 & 0 & 0 & 0 & 1 & 1 & 0 & 0 \\ 0 & 0 & 0 & 0 & 0 & 0 & 0 & 0 & 0 & 1 & 0 & 1 \\ 0 & 0 & 0 & 0 & 0 & 0 & 0 & 0 & 0 & 0 & 1 & 0 \\ 0 & 0 & 0 & 0 & 0 & 0 & 0 & 0 & 0 & 0 & 0 & 0 \end{pmatrix} \quad (156)$$

The stabilizer table for this code is

$$\begin{array}{cccccccccccccccc} Y & Z & 1 & Y & Z & 1 & X & 1 & X & X & 1 & X & X & 1 & 1 & X \\ Z & X & 1 & X & X & Z & X & X & 1 & 1 & 1 & 1 & X & X & X & X \\ X & X & X & X & 1 & 1 & Z & 1 & 1 & 1 & 1 & 1 & X & 1 & 1 & 1 \\ 1 & Y & Y & Y & X & X & X & Y & 1 & 1 & 1 & X & 1 & 1 & 1 & X \\ 1 & Y & 1 & Y & 1 & 1 & 1 & Z & 1 & X & X & X & X & 1 & 1 & 1 \\ X & 1 & Z & Y & 1 & 1 & 1 & X & 1 & Y & X & X & X & X & X & 1 \\ Z & 1 & Z & Y & X & X & X & X & X & 1 & Y & X & X & X & X & X \\ Z & 1 & Y & Y & 1 & X & X & X & X & X & 1 & Z & X & 1 & X & X \\ 1 & X & X & X & X & X & 1 & X & X & X & X & X & Z & X & 1 & X \\ Z & Z & Z & 1 & X & 1 & 1 & 1 & 1 & X & X & X & Z & X & X & X \\ Y & X & 1 & 1 & X & 1 & X & X & X & 1 & 1 & 1 & 1 & X & Y & 1 \\ Z & Y & Z & Y & X & X & 1 & 1 & 1 & X & X & 1 & 1 & 1 & 1 & Z \end{array} \quad (157)$$

Numerically discovered $[[18, 4, 5]]$ code

Running on a single core of a standard desktop, our program will be able to find approximately 64 working codes in 10 minutes. Approximately 1.5% of randomly generated matrices yielded a valid code. One example is:

$$B = \begin{pmatrix} 1 & 1 & 1 & 0 & 1 & 1 & 0 & 1 & 0 & 1 & 0 & 0 & 1 & 1 \\ 1 & 0 & 0 & 1 & 1 & 0 & 1 & 0 & 1 & 1 & 0 & 0 & 0 & 0 \\ 1 & 1 & 0 & 0 & 0 & 1 & 1 & 0 & 0 & 1 & 0 & 1 & 1 & 1 \\ 1 & 1 & 0 & 1 & 0 & 0 & 0 & 1 & 0 & 1 & 1 & 1 & 0 & 1 \end{pmatrix}^T \quad (158)$$

$$P = \begin{pmatrix} 0 & 1 & 1 & 0 & 0 & 1 & 1 & 1 & 1 & 0 & 1 & 0 & 1 & 1 \\ 0 & 0 & 1 & 1 & 1 & 1 & 1 & 1 & 0 & 1 & 0 & 1 & 1 & 0 \\ 1 & 0 & 1 & 1 & 1 & 0 & 1 & 1 & 1 & 1 & 0 & 0 & 0 & 1 \\ 0 & 0 & 1 & 1 & 1 & 1 & 1 & 0 & 0 & 1 & 1 & 0 & 1 & 1 \end{pmatrix}^T \quad (159)$$

$$C_u = \begin{pmatrix} 0 & 0 & 1 & 1 & 0 & 0 & 1 & 0 & 1 & 0 & 0 & 0 & 0 & 1 \\ 0 & 0 & 0 & 1 & 1 & 1 & 1 & 0 & 0 & 0 & 1 & 0 & 0 & 1 \\ 0 & 0 & 0 & 1 & 1 & 1 & 1 & 0 & 1 & 0 & 1 & 1 & 0 & 0 \\ 0 & 0 & 0 & 0 & 1 & 1 & 0 & 0 & 1 & 1 & 1 & 1 & 1 & 0 \\ 0 & 0 & 0 & 0 & 0 & 1 & 0 & 0 & 1 & 1 & 0 & 0 & 0 & 1 \\ 0 & 0 & 0 & 0 & 0 & 0 & 1 & 0 & 0 & 1 & 0 & 1 & 1 & 1 \\ 0 & 0 & 0 & 0 & 0 & 0 & 0 & 0 & 0 & 0 & 0 & 1 & 1 & 1 \\ 0 & 0 & 0 & 0 & 0 & 0 & 0 & 0 & 0 & 0 & 1 & 0 & 0 & 1 \\ 0 & 0 & 0 & 0 & 0 & 0 & 0 & 0 & 0 & 0 & 0 & 1 & 1 & 0 \\ 0 & 0 & 0 & 0 & 0 & 0 & 0 & 0 & 0 & 0 & 0 & 0 & 1 & 1 \\ 0 & 0 & 0 & 0 & 0 & 0 & 0 & 0 & 0 & 0 & 0 & 0 & 0 & 0 \\ 0 & 0 & 0 & 0 & 0 & 0 & 0 & 0 & 0 & 0 & 0 & 0 & 0 & 0 \\ 0 & 0 & 0 & 0 & 0 & 0 & 0 & 0 & 0 & 0 & 0 & 0 & 0 & 0 \end{pmatrix} \quad (160)$$

The stabilizer table for this code is

$$\begin{array}{cccccccccccccccccccc} Z & Z & Y & Z & Y & X & X & 1 & X & X & X & X & X & X & 1 & X & X & 1 \\ Y & 1 & Z & Z & X & Y & X & X & X & X & 1 & 1 & 1 & 1 & X & 1 & 1 & 1 \\ Y & X & X & X & X & Y & X & X & 1 & 1 & X & 1 & 1 & 1 & X & X & X \\ 1 & Y & X & Y & X & X & Z & X & X & 1 & X & X & X & X & 1 & 1 & X & X \\ Z & Y & X & X & 1 & 1 & X & 1 & Y & X & 1 & 1 & 1 & 1 & X & X & 1 & 1 \\ Y & X & Z & X & X & 1 & X & 1 & 1 & Y & X & 1 & 1 & 1 & X & X & 1 & X \\ X & Y & Y & X & 1 & X & X & 1 & 1 & 1 & Z & 1 & X & 1 & 1 & 1 & 1 & 1 \\ Y & X & X & Z & 1 & X & 1 & X & X & 1 & 1 & Y & 1 & X & 1 & 1 & 1 & X \\ X & Z & X & 1 & X & 1 & 1 & 1 & X & X & 1 & 1 & Z & X & X & 1 & X & X \\ Z & Y & Y & Y & X & X & 1 & 1 & 1 & 1 & 1 & X & 1 & Y & X & 1 & 1 & X \\ X & 1 & 1 & Y & 1 & X & 1 & 1 & X & X & X & 1 & X & 1 & Y & X & X & 1 \\ 1 & X & Z & Z & X & 1 & X & X & 1 & 1 & X & X & X & 1 & X & 1 & Z & X & X \\ Y & X & Z & X & X & X & 1 & 1 & X & 1 & X & 1 & 1 & 1 & X & 1 & Y & 1 \\ Y & 1 & Y & Y & 1 & 1 & X & 1 & X & X & 1 & X & X & 1 & X & X & 1 & Y \end{array} \quad (161)$$

F.2 Other codes

[[10, 3, 3]] code from combining checks for parity bit flips on the [[11, 3, 3]] code

A relatively straightforward design alteration to the [[11, 3, 3]] code is to have a single qubit check all parity check qubits for phase errors, rather than one for those which check for bit errors on the data qubits, and a separate one which checks for phase errors. The resulting parity check matrices for this code are:

$$B = \begin{pmatrix} 1 & 0 & 1 & 0 & 0 & 0 & 0 \\ 1 & 1 & 0 & 0 & 0 & 0 & 0 \\ 0 & 1 & 1 & 0 & 0 & 0 & 0 \end{pmatrix}^T \quad (162)$$

$$P = \begin{pmatrix} 0 & 0 & 0 & 1 & 0 & 1 & 0 \\ 0 & 0 & 0 & 1 & 1 & 0 & 0 \\ 0 & 0 & 0 & 0 & 1 & 1 & 0 \end{pmatrix}^T \quad (163)$$

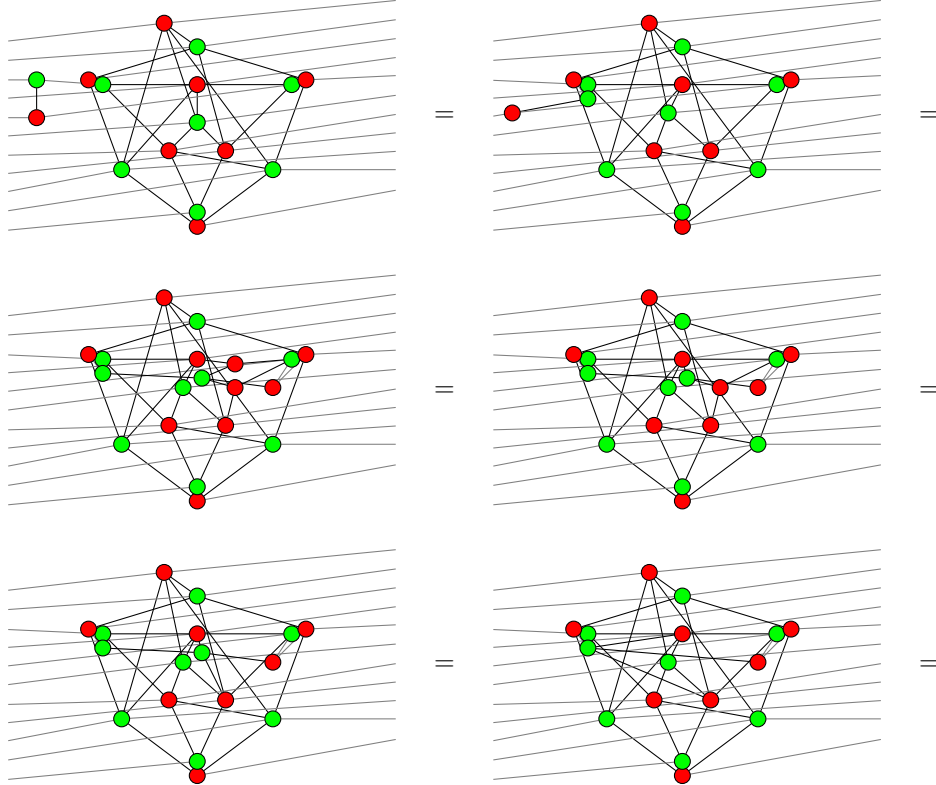
$$C_u = \begin{pmatrix} 0 & 0 & 0 & 0 & 0 & 1 & 1 \\ 0 & 0 & 0 & 1 & 0 & 0 & 1 \\ 0 & 0 & 0 & 0 & 1 & 0 & 1 \\ 0 & 0 & 0 & 0 & 0 & 0 & 1 \\ 0 & 0 & 0 & 0 & 0 & 0 & 1 \\ 0 & 0 & 0 & 0 & 0 & 0 & 1 \\ 0 & 0 & 0 & 0 & 0 & 0 & 0 \end{pmatrix}. \quad (164)$$

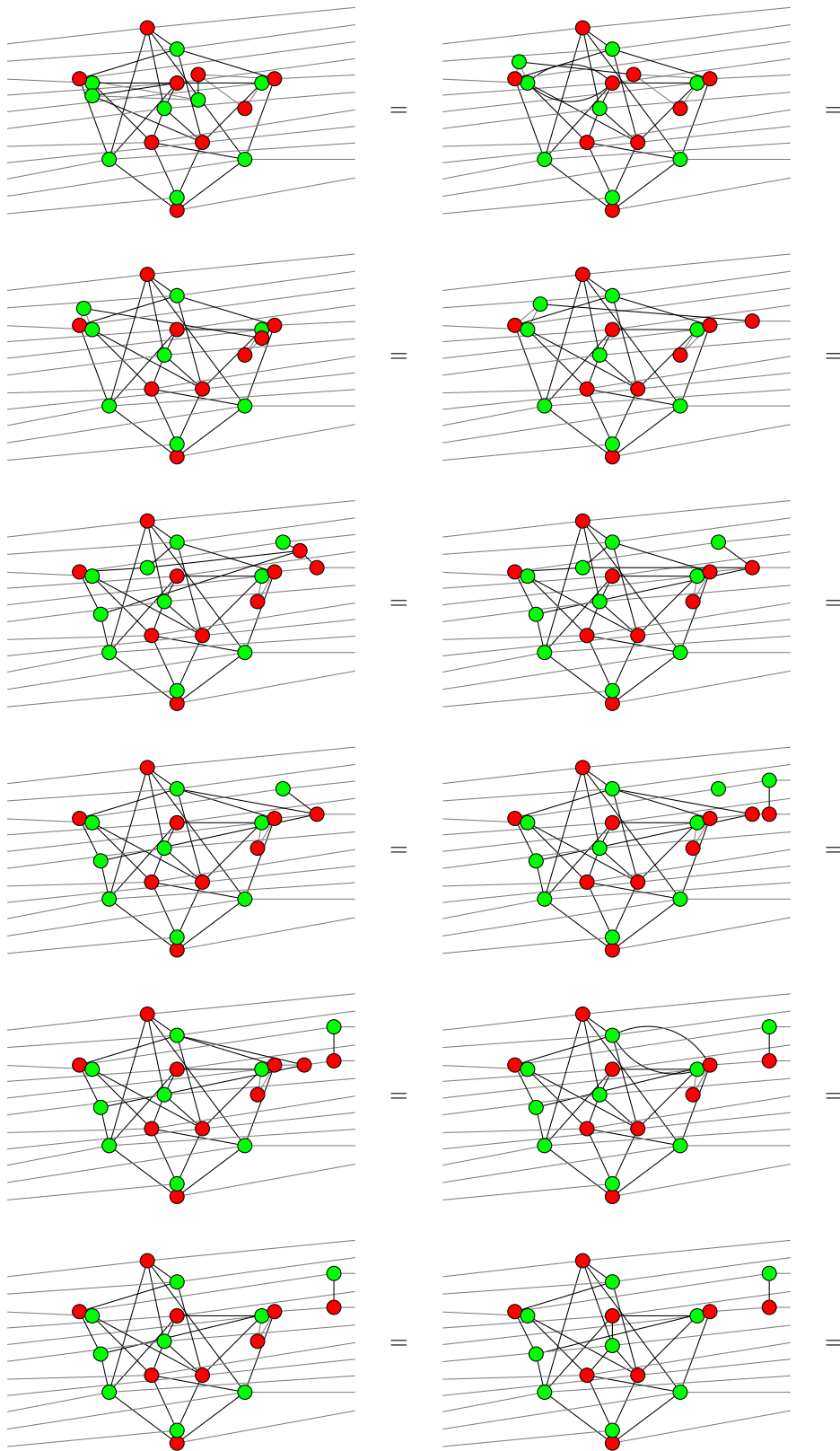
The corresponding stabilizer table is:

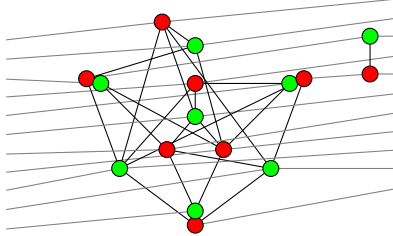
$$\begin{array}{cccccccccc} Z & Z & 1 & Z & 1 & 1 & 1 & X & 1 & X \\ 1 & Z & Z & 1 & Z & 1 & 1 & 1 & X & X \\ Z & 1 & Z & 1 & 1 & Z & X & 1 & 1 & X \\ X & X & 1 & 1 & X & 1 & Z & 1 & 1 & X \\ 1 & X & X & 1 & 1 & X & 1 & Z & 1 & X \\ X & 1 & X & X & 1 & 1 & 1 & 1 & Z & X \\ 1 & 1 & 1 & X & X & X & X & X & X & Z \end{array} \quad (165)$$

G Encoded CNOT with Quantomatic

We give the modification of the encoder for the $[[11,3,3]]$ ring code of Section 5 to perform a CNOT operation in the encoded space. The general solution for CPC codes is given in Section 8; this specific example is generated in Quantomatic by passing the CNOT operation through the encoder as follows:







This completes the modification.

References

- [1] Backens, M. [2014]. The ZX-calculus is complete for stabilizer quantum mechanics, *New Journal of Physics* **16**: 093021. arXiv:1307.7025.
- [2] Berrou, C. and Glavieux, A. [1996]. Near optimum error correcting coding and decoding: Turbo-codes., *IEEE Trans. on Communications* **44**: 1261.
- [3] Berrou, C., Glavieux, A. and Thitimajshima, P. [1993]. Near shannon limit error-correcting coding and decoding: Turbo-codes., *Proc. 1993 IEEE International Conf. on Communications, Geneva, Switzerland*, p. 1064.
- [4] Bravyi, S. B. and Kitaev, A. Y. [1998]. Quantum codes on a lattice with boundary, quant-ph/9811052. Translation of *Quantum Computers and Computing* 2 (1), pp. 43-48. (2001).
- [5] Calderbank, A. R. and Shor, P. W. [1996]. Good quantum error-correcting codes exist, *Phys. Rev. A* **54**: 1098–1106.
- [6] Campbell, E., Terhal, B. and Vuillot, C. [2016]. The steep road towards robust and universal quantum computation, *arXiv preprint arXiv:1612.07330*.
- [7] Chancellor, N. [2017]. CPC code creation software as presented at coherent parity check construction for quantum error correction, <https://doi.org/10.15128/r1bn999672k>. Durham University.
- [8] Coecke, B. and Duncan, R. [2011]. Interacting quantum observables: categorical algebra and diagrammatics, *New Journal of Physics* **13**(4): 043016.
- [9] Coecke, B. and Kissinger, A. [2017]. *Picturing Quantum Processes: A first course in quantum theory and diagrammatic reasoning*, Cambridge University Press.
- [10] de Beaudrap, N. and Horsman, D. [2017]. The zx calculus is a language for surface code lattice surgery. Accepted for QPL 2017.
- [11] Dennis, E., Kitaev, A., Landahl, A. and Preskill, J. [2002]. Topological quantum memory, *J. Math. Phys.* **43**: 4452.
- [12] Devitt, S. J., Munro, W. J. and Nemoto, K. [2013]. Quantum error correction for beginners, *Rep. Prog. Phys.* **076001**: 1–41.
- [13] Duncan, R. and Garvie, L. [2017]. Verifying the smallest interesting colour code with quantomatic. Accepted for QPL 2017.
- [14] Duncan, R. and Lucas, M. [2013]. Verifying the steane code with quantomatic, *EPTCS* **171**: 33–49.
- [15] Earl, D. and Deem, M. W. [2005]. Parallel tempering: Theory, applications, and new perspectives, *Phys. Chem. Chem. Phys* **7**: 3910–3916.
- [16] Emmanuel Jeandel, Simon Perdrix, R. V. [2017]. A complete axiomatisation of the zx-calculus for clifford+ t quantum mechanics, *arXiv:1705.11151 [quant-ph]*.
- [17] Feynman, R. [1985]. *QED: The Strange Theory of Light and Matter*, Princeton University Press.
- [18] Fogel, D. B. [1994]. An introduction to simulated evolutionary optimization, *IEEE Transactions on Neural Networks* **5**(1).
- [19] Fowler, A. G., Mariantoni, M., Martinis, J. M. and Cleland, A. N. [2012]. Surface codes: Towards practical large-scale quantum computation, *Physical Review A* **86**(3): 032324.
- [20] Fowler, A. G., Stephens, A. M. and Groszkowski, P. [2009]. High threshold universal quantum computation on the surface code, *Phys. Rev. A* **80**: 052312.
- [21] Gottesman, D. [1999]. The heisenberg representation of quantum computers, in S. P. Corney, R. Delbourgo and P. D. Jarvis (eds), *Proceedings of the XXII International Colloquium on Group Theoretical Methods in Physics*, pp. 32–43. arXiv:quant-ph/9807006.

[22] Harty, T. P., Allcock, D., Ballance, C., Guidoni, L., Janacek, H., Linke, N., Stacey, D. and Lucas, D. [2014]. High-fidelity preparation, gates, memory, and readout of a trapped-ion quantum bit, *Physical Review Letters* **113**: 220501.

[23] Horsman, C. [2011]. Quantum picturalism for topological cluster-state computing, *New J. Phys.* **13**: 095011.

[24] Horsman, C., Fowler, A., Devitt, S. and Van Meter, R. [2012]. Surface code quantum computing by lattice surgery, *New Journal of Physics* **14**(12): 123011.

[25] Iba, K. H. Y. [2003]. *THE MONTE CARLO METHOD IN THE PHYSICAL SCIENCES: Celebrating the 50th Anniversary of the Metropolis Algorithm*, Vol. 690, AIP.

[26] Joyal, A. and Street, R. [1991]. The geometry of tensor calculus, i, *Advances in mathematics* **88**(1): 55–112.

[27] Kirkpatrick, S., Gelatt, C. D. and Vecchi, M. P. [1983]. Optimization by simulated annealing, *Science* **220**(4598): 671–680.
URL: <http://science.sciencemag.org/content/220/4598/671>

[28] Kissinger, A. and Zamdzhev, V. [2015]. Quantomatic: A proof assistant for diagrammatic reasoning, *International Conference on Automated Deduction*, Springer, pp. 326–336.

[29] Lord, N. J. [1987]. Matrices as sums of invertible matrices, *Mathematics Magazine* **60**(1): 33–35.

[30] MacKay, D. J. C. [2002]. Turbo codes are low density parity check codes, <http://www.inference.eng.cam.ac.uk/mackay/turbo-ldpc.pdf>.

[31] MacKay, D. J. C. [2003]. *Information Theory, Inference, and Learning Algorithms*, Cambridge University Press.

[32] MacKay, D. J., Mitchison, G. and McFadden, P. L. [2004]. Sparse graph codes for quantum error-correction, *IEEE Transactions on Information Theory* **50**(10): 2315.

[33] Matcha, J. [2010]. Population annealing with weighted averages: A monte carlo method for rough free energy landscapes, *Phys. Rev. E* **82**: 026704.

[34] Ng, K. F. and Wang, Q. [2017]. A universal completion of the zx-calculus, *arXiv:1706.09877 [quant-ph]*.

[35] Nickerson, N. H., Li, Y. and Benjamin, S. C. [2013]. Topological quantum computing with a very noisy network and local error rates approaching one percent, *Nature communications* **4**: 1756.

[36] Oklobdzija, V. G. [2001]. *The Computer Engineering Handbook: Electrical Engineering Handbook*, CRC Press, Inc., Boca Raton, FL, USA.

[37] Penrose, R. [1971]. Applications of negative dimensional tensors, *Combinatorial Mathematics and its Applications*, Academic Press, pp. 221–244.

[38] Preskill, J. [2015]. Lecture notes for physics 229:quantum information and computation. Chapter 7 obtained at <https://www.lorentz.leidenuniv.nl/quantumcomputers/literature>.

[39] Roffe, J., Headley, D., Chancellor, N., Horsman, D. and Kendon, V. [2017]. Protecting quantum memories using coherent parity check codes, *arXiv:1709.01866*.

[40] Selinger, P. [2007]. Dagger compact closed categories and completely positive maps, *Electronic Notes in Theoretical computer science* **170**: 139–163.

[41] Steane, A. [1996]. Error correcting codes in quantum theory, *Phys. Rev. Lett.* **77**: 793–797.

[42] Stephens, A. M. [2014]. Fault-tolerant thresholds for quantum error correction with the surface code, *Phys. Rev. A* **89**: 022321.
URL: <https://link.aps.org/doi/10.1103/PhysRevA.89.022321>

[43] Swendsen, R. H. and Wang, J. S. [1968]. Replica monte carlo simulation of spin-glasses, *Phys. Rev. Lett.* **57**: 2607.

[44] Wang, W., Machta, J. and Katzgraber, H. G. [2015]. Population annealing: Theory and application in spin glasses, *Phys. Rev. E* **92**: 063307.